8-2014

Regulators of Bacterial Cell Division: Investigations of Min Oscillation and FtsA Activity

Jennifer R. Herricks

REGULATORS OF BACTERIAL CELL DIVISION: INVESTIGATIONS OF MIN OSCILLATION AND FTSA ACTIVITY

By

Jennifer Renee Juarez Herricks, B.S.

APPROVED:

_____
Supervisory Professor
William Margolin, Ph.D.

_____
Kevin Morano, Ph.D.

_____
Theresa Koehler, Ph.D.

_____
Peter Christie, Ph.D.

_____
Joseph Alcorn, Ph.D.

APPROVED:

_____
Dean, The University of Texas
Graduate School of Biomedical Sciences at Houston

REGULATORS OF BACTERIAL CELL DIVISION: INVESTIGATIONS OF MIN OSCILLATION AND FTSA ACTIVITY

A

DISSERTATION

Presented to the Faculty of The University of Texas Health Science Center at Houston and The University of Texas MD Anderson Cancer Center Graduate School of Biomedical Sciences in Partial Fulfillment of the Requirements for the Degree of

DOCTOR OF PHILOSOPHY

By

Jennifer Renee Juarez Herricks, B.S.

Houston, Texas

August 2014

DEDICATION

I dedicate this work to my nieces, Hailey Marie Lester Juarez and Katherine Anne Abraham, and to my goddaughter, Livy Ann Guidry. They bring me constant joy and love, and remind me of the things in life that are truly important.

ACKNOWLEDGEMENTS

First, I would like to thank my advisor, Bill, whose mentorship has made me a better scientist, as well as a better writer and communicator. I am thankful that Bill has always been supportive of my career goals and the many extracurricular activities I took on while in graduate school. Throughout the years, Bill has been a great teacher and scientific mentor.

I would also like to thank the members of my advisory, examining, and supervisory committees: Joe Alcorn, Kevin Morano, Peter Christie, Terri Koehler, Heidi Kaplan, Ambro van Hoof, Jade Wang, and Danielle Garsin. I especially appreciate their open doors and willingness to help me in any scientific endeavor. This was also true of the other MMG faculty, staff, and students. I would like to give special thanks to Kevin for his technical, scientific advice, as well as career advice and encouragement. In addition, the other GSBS faculty and staff have also provided a great support system.

I would like to acknowledge everyone who has been a part of the Margolin lab during my time as a graduate student. My time spent there would not have been the same without Kim Busiek. Kim and I spent most of our time in graduate school working across from each other and she became a valued coworker as well as a great friend. Veronica Rowlett has also been a supportive lab-mate and friend. Diep Nguyen has been an outstanding technician who has made valuable contributions to the research presented in this dissertation. I have enjoyed working with all of the students who have rotated through the Margolin lab, and I

would like to acknowledge Chris Evans, who also contributed to the work presented in this dissertation.

In addition, I want to thank all of my friends who have supported me over the years. Graduate school would not have been the same without the friends I have made here. In particular, Ale Klauer-King has been my peer mentor and one of my best friends. I also want to thank my best friends from home, who have been there for me since junior high and high school, Johanette Guidry and Mary Beth Maddox.

I could not have made it this far without all of the love and support I receive everyday from my family. I want to give very special thanks to my dad, because my love of science came from him. I also want to thank my mom, my brother, Nanny, Uncle Nel, and my grandparents. I want to thank Dee, Gary, Annie, and John for being the best in-laws that anyone could hope for. And finally, I want to thank my wonderful husband, Ben, who is incredibly understanding, loving, and supportive of me.

REGULATORS OF BACTERIAL CELL DIVISION: INVESTIGATIONS OF MIN OSCILLATION AND FTSA ACTIVITY

Jennifer Renee Juarez Herricks, B.S.

Supervisory Professor, William Margolin, Ph.D.

Cytokinesis is a fundamental process that is essential for bacterial proliferation. The cytokinetic machinery in bacteria is termed the “divisome”. The divisome is a complex of proteins that forms a ring at midcell over dividing nucleoids. In order for daughter cells to form, the divisome must constrict. As constriction occurs, two new cell poles are formed, one for each daughter cell. The first step in divisome formation is the assembly of FtsZ into a Z ring. The work presented in this dissertation focuses on two proteins that regulate the Z ring: MinD, which is a part of the Min system and important for positioning of the divisome; and FtsA, involved in early and late stages of divisome formation with a speculated role in regulating its constriction and disassembly. In *E. coli* the Min proteins oscillate from pole-to-pole to prevent Z ring formation at the cell poles. I found that MinD oscillation becomes irregular as cell length increases, and that it starts to pause frequently at each side of the developing septum. Eventually this irregular pattern switches to a doubled, regular pattern that is maintained in newly born daughter cells. I suggest this may be the mechanism by which Min proteins are equally distributed in daughter cells. My studies of FtsA show that ATP binding is important for its function *in vivo*, affecting its ability to interact with

FtsZ and possibly with itself and other division proteins. I also show for the first time that *E. coli* FtsA can hydrolyze ATP.

TABLE OF CONTENTS

Page No.

LIST OF FIGURES

Page No.

Chapter 4: Suppression of *ftsA27*, a thermosensitive *ftsA* mutant of *Escherichia coli*, suggests interplay between ATP binding and protein-protein interactions

Chapter 5: Other defects caused by FtsA active-site mutants

Chapter 6: Discussion

LIST OF TABLES

Page No.

Chapter 1: Introduction

SIGNIFICANCE

Cytokinesis is a fundamental process that is essential for bacterial proliferation. The cytokinetic machinery in bacteria is termed the “divisome”. The divisome is a complex of proteins that forms a ring at midcell over dividing nucleoids. The ring is composed of essential and non-essential proteins, most of which still have unknown functions. In order for cells to divide, the divisome must constrict. As constriction occurs two new cell poles are formed, one for each daughter cell. The cycle then repeats in each daughter cell, and so on. Figure 1.1 shows a general depiction of this process in the bacterium *Escherichia coli*.

There are many outstanding questions that need to be addressed before we can begin to fully comprehend the complexities of this process. What is the specific role of each protein that makes up the divisome? What molecular interactions are important for divisome formation? What controls the timing of divisome formation? How is the placement of the divisome regulated? How is the constriction and disassembly of the divisome controlled? How is cell wall and membrane synthesis coordinated with divisome constriction? Once these mechanisms are determined for one organism, how conserved are these mechanisms in other bacterial species? Many more questions exist and together are beyond the scope of any single study.

The work presented in this dissertation focuses on two proteins that regulate the divisome: MinD, which is a part of the Min system and important for positioning of the divisome; and FtsA, involved in early and late stages of

divisome formation with a speculated role in regulating its constriction and disassembly. Enhancing our understanding of bacterial cell division will undoubtedly add to our knowledge of molecular mechanisms that are critical to basic biology.

FIG 1.1

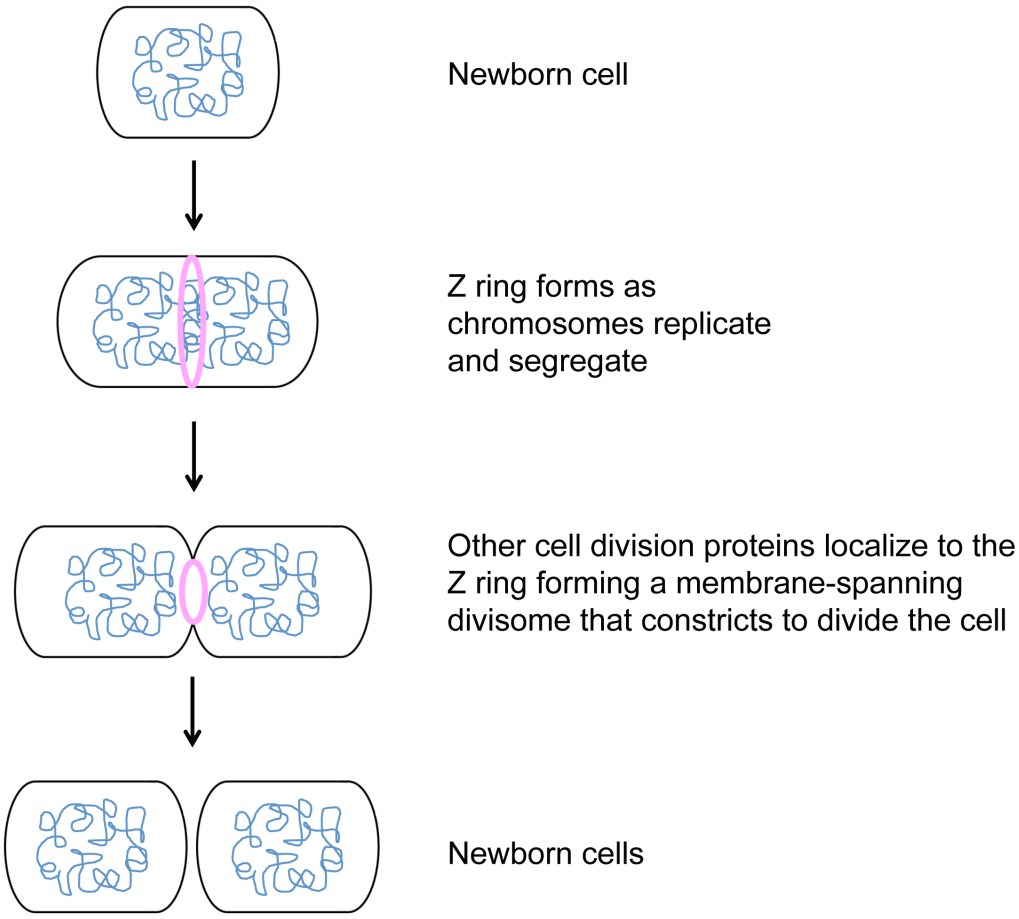

Figure 1.1: Cell division in *Escherichia coli*. A simplified model of *E. coli* cell division is depicted. The nucleoid is shown in blue and the Z ring/divisome that eventually divides the cell is in pink.

BACKGROUND

Cytokinesis and the cytoskeleton

All proliferating cell types must divide. In most organisms the cytoskeletal elements actin and tubulin play essential roles in this process. In eukaryotes, filamentous actin (F-actin), together with the motor protein myosin II, forms a cytokinetic actomyosin ring (Balasubramanian et al., 2004). Segregation of chromosomes during eukaryotic cell division is promoted by kinetochore microtubules composed of α and ß tubulin (Balasubramanian et al., 2004). Ancestral forms of actin and tubulin exist in most prokaryotes (Wickstead and Gull, 2011). In general, the major structural component of the prokaryotic cytokinetic ring (divisome) is the tubulin homolog FtsZ. A majority of bacteria also contain a cytokinetic actin homolog known as FtsA (Wickstead and Gull, 2011), but its role in cell division is less understood than that of FtsZ. Three classes of proteins are known to be involved in bacterial DNA segregation: actin-like ParM, tubulin-like TubZ, and the Walker-A ATPase ParA (Mierzejewska and Jagura-Burdzy, 2012). Over the course of evolution it seems that the prokaryotic and eukaryotic forms actin and tubulin have retained their overall functional and structural homology (Amos et al., 2004).

FtsZ and the formation of the bacterial divisome

In *Escherichia coli* and many other bacteria, assembly of the divisome is thought to begin with the polymerization of FtsZ into a ring-like structure called

the Z ring (Bi and Lutkenhaus, 1991). Recent studies with super-resolution microscopy techniques have revealed a more detailed picture of the molecular structure of the Z ring *in vivo.* Together this work suggests that the Z ring is a discontinuous assembly of short overlapping polymers (Biteen et al., 2012; Fu et al., 2010; Holden et al., 2014; Jennings et al., 2011; Rowlett and Margolin, submitted; Strauss et al., 2012). This structure is thought to act as a scaffold for the divisome (Adams and Errington, 2009; de Boer, 2010; Erickson et al., 2010; Lutkenhaus et al., 2012).

In addition to acting as a scaffold, it has been hypothesized that FtsZ can generate the force required for constriction of the Z ring (Allard and Cytrynbaum, 2009; Arumugam et al., 2012; Erickson, 2009; Hsin et al., 2012; Lan et al., 2009; Li et al., 2013; Osawa and Erickson, 2011; Osawa et al., 2008, 2009). FtsZ dynamics are thought to be important for generation of this force. Similar to its eukaryotic homolog tubulin, FtsZ displays dynamic polymerization and depolymerization regulated by GTP binding and hydrolysis (Mukherjee and Lutkenhaus, 1998). The Z ring is composed of approximately 30% of the total concentration of cellular FtsZ, and the FtsZ subunits within the ring are highly dynamic (Anderson et al., 2004). Fluorescence recovery after photobleaching (FRAP) experiments on FtsZ polymers at the Z ring have shown a recovery half time of tens of seconds that is correlated with the GTPase activity of FtsZ (Anderson et al., 2004; Stricker et al., 2002). A decrease in FtsZ GTPase activity caused by the *ftsZ* temperature sensitive allele, *ftsZ84*, has been shown to lead to a significant decrease in FtsZ polymer dynamics *in vivo* (Anderson et al., 2004;

Stricker et al., 2002). Although cells expressing *ftsZ84* survive with the slower dynamics of FtsZ polymers at low temperatures, viability is lost at high temperature (42˚C) (Addinall et al., 1997a). Other FtsZ mutants defective in polymerization, depolymerization, GTP binding, and GTP hydrolysis have been described and often affect cell viability (Addinall et al., 2005; Lu et al., 2001; Mukherjee et al., 2001; Redick et al., 2005), indicating that proper dynamics are important for FtsZ function.

Membrane anchors

FtsZ is a cytoplasmic protein, so to coordinate the invagination of the cell membrane and cell wall during cytokinesis, other proteins are needed to anchor FtsZ to the membrane. In *E. coli,* this is accomplished by two essential proteins, ZipA and FtsA (Hale and de Boer, 1997; Hale and de Boer, 1999; Liu et al., 1999; Pichoff and Lutkenhaus, 2002, 2005). FtsZ can be anchored to the membrane by either one of these proteins to form a Z ring, but both FtsA and ZipA are required for proper maturation of a functioning divisome (Busiek and Margolin, 2014; Busiek et al., 2012; Corbin et al., 2004; Hale and de Boer, 2002; Hale and de Boer, 1999; Liu et al., 1999; Pichoff and Lutkenhaus, 2002; Rico et al., 2004). Both FtsA and ZipA interact directly with adjacent residues on the carboxy-terminal tail of FtsZ, and likely compete for binding of FtsZ (Din et al., 1998; Hale et al., 2000; Haney et al., 2001; Liu et al., 1999; Ma and Margolin, 1999; Moreira et al., 2006; Mosyak et al., 2000; Shen and Lutkenhaus, 2009; Szwedziak et al., 2012). In addition to anchoring FtsZ to the membrane, FtsA

and ZipA may also help to stabilize the Z ring (Geissler et al., 2007; Kuchibhatla et al., 2011; Pazos et al., 2013; RayChaudhuri, 1999). For example, FtsZ is a known substrate for the ClpXP protease (Camberg et al., 2009, 2011; Dziedzic et al., 2010; Feng et al., 2013; Sass et al., 2011; Schiefer et al., 2013; Sugimoto et al., 2010; Weart et al., 2005). Recent work has identified the specific amino acid sequences on *E. coli* FtsZ that target it for ClpXP degradation, and one of the sequences partially overlaps with the FtsA and ZipA binding sites on the C-terminal tail of FtsZ (Camberg et al., 2014). These data suggest that FtsA and ZipA have overlapping roles in anchoring and stabilizing the Z ring at midcell. They also have several unique functions as described below.

ZipA is a biotopic integral inner membrane protein with a short amino-terminal periplasmic domain and large carboxy-terminal cytoplasmic domain (Hale and de Boer, 1997). The cytoplasmic domain can be further divided into several subdomains that include a charged region, followed by a proline/glutamine rich unstructured linker, and a globular domain at the carboxy terminus that is necessary and sufficient for interaction with FtsZ (Hale and de Boer, 1997; Hale et al., 2000). ZipA contains sequence elements that are similar to those of microtubule-stabilizing MAP-Tau proteins (RayChaudhuri, 1999). Like its eukaryotic counterparts, ZipA promotes FtsZ (tubulin) stability and induces bundling of FtsZ protofilaments (Hale et al., 2000; RayChaudhuri, 1999). The molecular mechanism by which ZipA is able to promote bundling of FtsZ protofilaments is unknown, but the globular domain of ZipA is sufficient for this activity (Hale et al., 2000).

ZipA is thought to be conserved only in gamma-proteobacteria, however, a potential structural homolog of ZipA has been described in the Gram-negative beta-proteobacterium *Neisseria gonorrhoeae* (Du and Arvidson, 2003). This suggests that ZipA may be more conserved than initially thought, but more studies are needed to determine if other structural homologs exist outside of the gamma-proteobacteria. In bacteria that lack ZipA, like the well-studied *B. subtilis* and *Caulobacter crescentus,* it is possible that other cell division proteins perform functions similar to ZipA, or that FtsZ protofilaments from these organisms can form stable bundles without the need for ZipA.

FtsA is widely conserved in bacteria, and the sequences that encode the *ftsZ* and *ftsA* genes are often found in tandem on bacterial chromosomes (Margolin, 2000). FtsA tethers the Z ring to the cytoplasmic membrane through a conserved carboxy-terminal amphipathic helix, which acts as a membrane targeting sequence (MTS) (Pichoff and Lutkenhaus, 2005). Although FtsA is non-functional without an MTS, the amphipathic helix of FtsA can be replaced with the amphipathic helix from MinD or the first integral membrane domain of the transmembrane protein MalF and still allow cell division (Pichoff and Lutkenhaus, 2005; Shiomi and Margolin, 2008). This suggests that FtsA must be bound to the membrane for functionality, but the specific sequence that allows interaction with the membrane is less important. Interestingly, an FtsA mutant with membrane targeting defects can still interact with FtsZ, localize to the Z ring, and recruit other essential division proteins to midcell, except for FtsN (Shiomi and Margolin, 2008).

FtsA has a canonical actin fold (Bork et al., 1992), and like actin, FtsA is comprised of four subdomains (FIG 1.2). To date there are only two crystal structures of FtsA available, one from *Thermotoga maritima* and the other from *Staphylococcus aureus* (van den Ent and Löwe, 2000; Fujita et al., 2014). Both of these structures reveal actin-like filaments formed by FtsA polymerization (Fujita et al., 2014; Szwedziak et al., 2012). However, one of the FtsA subdomains is structurally divergent from that of actin. Our group has shown that this unique subdomain, 1C, is important for recruiting downstream division proteins to the Z ring (Busiek et al., 2012; Corbin et al., 2004). Subdomain 2B of FtsA contains conserved residues that are important for FtsA-FtsZ interactions (Pichoff and Lutkenhaus, 2007; Szwedziak et al., 2012). The biochemical nature of these interactions is still not well understood.

FIG 1.2

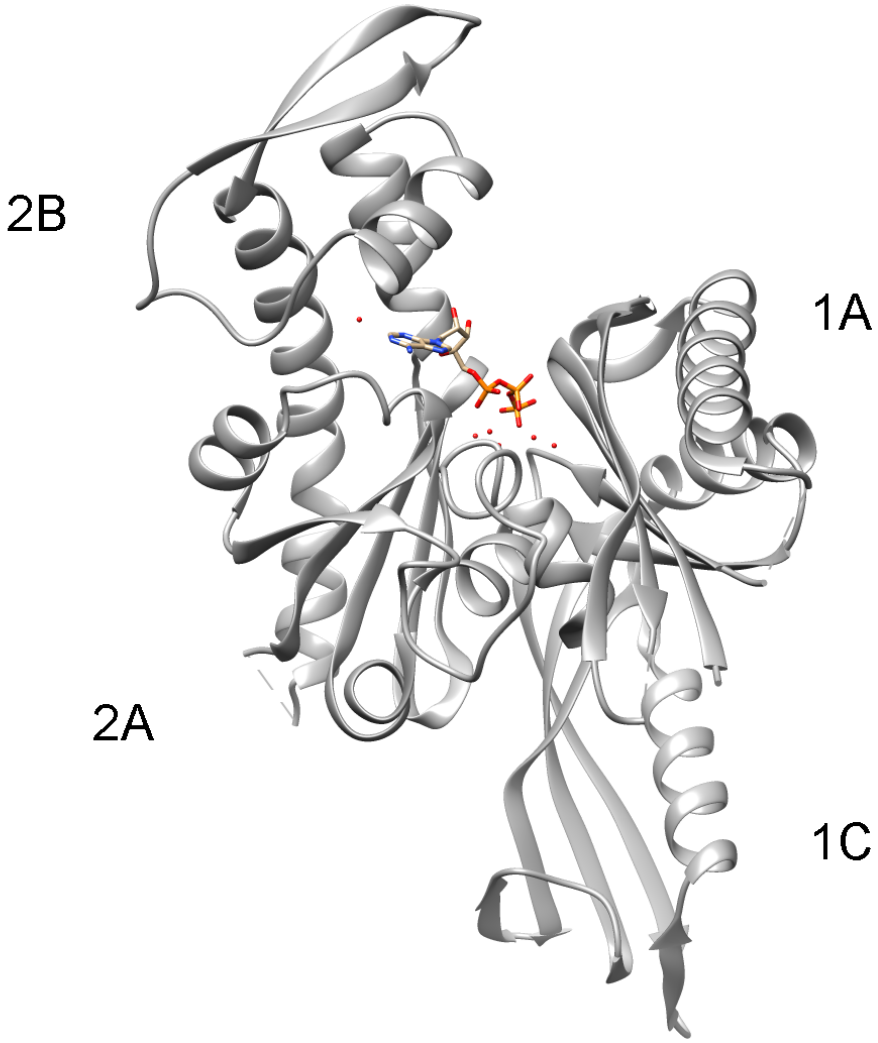

Figure 1.2: Structure of FtsA. Structural representation of FtsA from *Thermotoga maritima* with ATP bound. Subdomains are labeled. Red dots are water molecules.

Working with FtsA *in vitro* has historically been very difficult, and FtsA itself has been described as recalcitrant (Martos et al., 2012). Our group was the first to show that purified FtsA could interact with FtsZ polymers in an ATP dependent manner (Beuria et al., 2009). Since then, it was demonstrated *in vitro* that recruitment of FtsZ-YFP to liposomes by FtsA is enhanced in the presence of ATP (Osawa and Erickson, 2013). More recently, another group confirmed this observation using supported lipid bilayers and total internal reflection microscopy (Loose and Mitchison, 2014). In addition, Loose and Mitchison showed that FtsA-FtsZ interactions were highly dynamic on their supported lipid bilayer system, consistent with previous FRAP studies *in vivo* (Anderson et al., 2004; Geissler et al., 2007). The work presented in chapters 4 and 5 of this dissertation will address how FtsA interacts with other cell division proteins, especially FtsZ, and how ATP contributes to these interactions.

Recruitment and function of other division proteins

Maturation of the divisome requires the localization of many additional proteins to the Z ring, anchored by ZipA and FtsA. In *E. coli,* the essential downstream division proteins include FtsK, FtsQBL, FtsW, FtsI, and FtsN, all of which are integral membrane proteins. Major questions in the field include the function of the downstream proteins, how they interact with other division proteins, and how they are localized to the Z ring.

While some information exists about the activity of the downstream division proteins, more work is needed to understand how they are contributing to

divisome maturation. The essential function of FtsK in cell division, for example, remains unknown. For years it has been known that cells cannot survive without the N-terminal membrane-bound domain of FtsK, but that the C-terminal domain with double-stranded DNA translocase activity, involved in chromosome segregation and resolution of chromosome dimers, is dispensable (Aussel et al., 2002; Diagne et al., 2014; Draper et al., 1998; Liu et al., 1998; Wang and Lutkenhaus, 1998; Yu et al., 1998). Recent work suggests that the extreme N-terminus and linker domains of FtsK interact with other divisome proteins and may act as an essential checkpoint in cell division (Dubarry et al., 2010; Grenga et al., 2008). FtsQ, FtsB, and FtsL are bitopic integral membrane proteins known to exist as a complex, which is thought to bridge cell division events in the cytoplasm and periplasm (Buddelmeijer and Beckwith, 2004; Vicente and Rico, 2006). FtsW, a lipid II flippase, and FtsI, a transpeptidase, form a complex and are essential for the formation of septal peptidoglycan (Fraipont et al., 2011; Mohammadi et al., 2011). FtsN is the last essential cell division protein to localize to the divisome (Addinall et al., 1997b). FtsN recruits amidases, essential for peptidoglycan remodeling, and the Tol-Pal complex, required for proper invagination of the outer membrane in Gram-negative bacteria (Bernhardt and de Boer, 2003; Gerding et al., 2007; Peters et al., 2011). This suggests that FtsN plays an important role during the final stages of cytokinesis.

Previous data suggest that the essential division proteins are recruited to the Z ring in a linear order (Goehring and Beckwith, 2005; Vicente and Rico, 2006). However, more recent work suggests that although there is a genetic

dependence that determines the order of midcell localization (FtsZ, FtsA and ZipA, FtsK, FtsQBL, FtsW, FtsI, and then FtsN), protein-protein interactions among division proteins are intricate and complex (Goehring et al., 2005, 2006). For example, recent work has shown that interaction between FtsA and FtsN is required for proper FtsN localization (Busiek and Margolin, 2014; Goehring et al., 2006). More work is required to determine what interactions are required as well as the biological significance of each interaction between cell division proteins.

Regulation of the divisome by FtsA

For several reasons, it is thought that FtsA serves as the main Z ring membrane anchor (Pichoff and Lutkenhaus, 2005). Principal among these is the low conservation of *zipA* compared to the high conservation of the *ftsZ-ftsA* gene pair (Margolin, 2000). There is also direct and indirect evidence of FtsA directly recruiting downstream division proteins (Busiek and Margolin, 2014; Busiek et al., 2012; Corbin et al., 2004; Karimova et al., 2005), where no such evidence exists for ZipA. In addition, although ZipA has been shown to have unique functions (Johnson et al., 2004; Pichoff and Lutkenhaus, 2002; Potluri et al., 2012), a number of point mutations in *ftsA* have been identified that allow complete bypass of the requirement for *zipA* (Geissler et al., 2003; Goehring et al., 2007; Pichoff et al., 2012). Some of these point mutants, such as *ftsA** (R286W), can even bypass the requirement for some of the downstream cell division proteins (Bernard et al., 2007; Geissler and Margolin, 2005; Goehring et al., 2007).

Moreover, FtsA is the only essential cell division protein currently thought to act on the Z ring during early and late stages of cell division. In fact, before FtsA was known to anchor the Z ring to the membrane, mutations in *ftsA* were shown to cause cells to become long and filamentous with deep constrictions (Robinson et al., 1991; Tormo et al., 1980). This work suggests that FtsA continues to act after Z rings are formed and partially constricted, *i.e.*, that it acts late in the division process.

Recent work has also suggested that FtsA plays an important role in regulating and coordinating the final stages of cell division. In 2009 our group showed that the hypermorph FtsA* protein can shorten and bend FtsZ polymers *in vitro* in an ATP-dependent manner (Beuria et al., 2009). This type of activity could be critical for inducing divisome constriction. More recently our group showed that FtsA plays an important role in recruiting FtsN to the divisome (Busiek and Margolin, 2014). As described above, FtsN recruits amidases and the Tol-Pal complex, which are crucial for the final stages of cell division. It is possible that the interaction between FtsA and FtsN serves as a cell division checkpoint.

Taken together, the evidence suggests that FtsA is involved in (1) Z ring formation by anchoring FtsZ to the cytoplasmic membrane, (2) maturation of the divisome by recruiting downstream division proteins, and (3) constriction of the divisome by affecting the size of FtsZ polymers (FIG 1.3). But how is this multifaceted regulation of cell division coordinated? This question is explored in chapters 4 and 5 of this dissertation.

FIG 1.3

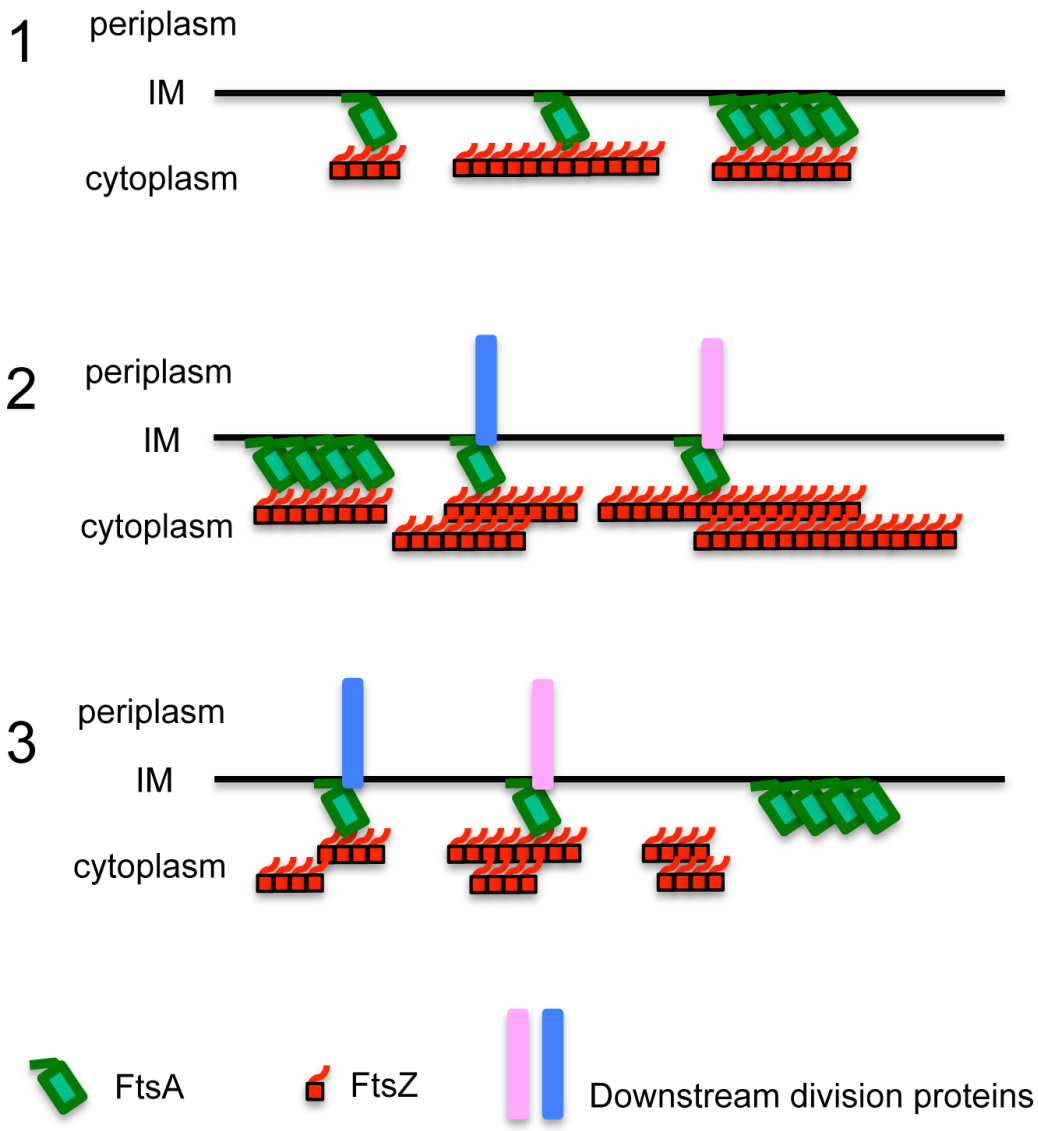

Figure 1.3: Predicted functions of FtsA. (1) FtsA anchors FtsZ to the cytoplasmic membrane, (2) FtsA allows maturation of the divisome by recruiting downstream division proteins, and (3) FtsA promotes constriction of the divisome by reducing the size of FtsZ polymers.

Positioning the divisome

Spatiotemporal control of the cytokinetic apparatus is critical for the production of healthy daughter cells. Improper regulation of this process can result in severed DNA if the cytokinetic ring constricts over chromosomes. If the ring is formed in the wrong cellular location, such as cell poles, daughter cells can be the wrong size and potentially have missing or extra copies of DNA. Known mechanisms for directing placement of the cytokinetic ring vary widely, but typically involve promotion of assembly at the site of division and inhibition of assembly at other cellular locations. In animal cells the small GTPase RhoA promotes formation of the actomyosin ring at the site of division, Rac1 inhibits its formation at the cell poles, and Cdc42 functions to maintain cell polarity (Jordan and Canman, 2012). In the budding yeast *Saccharomyces cerevisiae,* the site of cell division is determined by the previous division site, which is marked by a "bud scar" (Wloka and Bi, 2012). The actomyosin ring of *Schizosaccharomyces pombe*, the fission yeast, is positioned and anchored at midcell by Mid1 and Blt1 (Guzman-Vendrell et al., 2013). In contrast, Pom1 localizes to cell poles of *S. pombe* and creates an inhibitory gradient that prevents actomyosin ring formation at the poles (Bhatia et al., 2014). A similar group of diverse mechanisms exist to coordinate placement of the bacterial divisome.

Positive regulators of FtsZ placement in bacteria have only recently been identified, and include SsgAB of *Streptomyces coelicolor* (Willemse et al., 2011) and PomZ of *Myxococcus xanthus* (Treuner-Lange et al., 2013). These proteins localize to midcell prior to FtsZ and are required for Z ring formation and

positioning (Keijser et al., 2003; Treuner-Lange et al., 2013; van Wezel et al., 2000). Negative regulation of Z ring positioning in bacteria seems to be more common. However, in the absence of the two known systems that negatively regulate Z ring positioning in *B. subtilis* and *E. coli*, Z rings still form at midcell, although with less efficiency (Bernhardt and de Boer, 2005; Rodrigues and Harry, 2012; Wu and Errington, 2004). This suggests that there may be other positive regulators of Z ring placement yet to be identified.

Negative regulators of Z ring placement that are present in many bacteria include nucleoid occlusion (NO) and the Min system. NO is best characterized in *B. subtilis* and *E. coli* and involves the proteins Noc and SlmA, respectively (Bernhardt and de Boer, 2005; Wu and Errington, 2004). Although Noc is a member of the ParB family and SlmA is part of the TetR family, both Noc and SlmA bind to specific chromosomal DNA sequences that occur more frequently near the origin of replication, and less often near the terminus region (Cho et al., 2011; Tonthat et al., 2011; Wu et al., 2009). This pattern of localization allows Noc and SlmA to inhibit Z ring formation over unsegregated nucleoids. Recent studies have identified the molecular mechanism by which SlmA interacts with DNA and FtsZ to inhibit Z ring formation (Cho and Bernhardt, 2013; Tonthat et al., 2013), but direct interaction between Noc and FtsZ has yet to be demonstrated.

It is not yet understood how bacteria with no known Noc or SlmA homologs protect their DNA from severing by the divisome, and ensure daughter cells receive proper chromosome copy numbers. In the case of Actinobacteria

such as *Corynebacterium, Streptomyces,* and *Mycobacterium*, the DNA partitioning protein ParA (or a ParA homolog) coordinates chromosome segregation with cell division (Ditkowski et al., 2013; Donovan et al., 2010, 2013; Ginda et al., 2013). Proteins in the ParA family contain a characteristic P-loop ATPase domain and are widely involved in spatiotemporal positioning of both DNA and proteins in bacteria (Lutkenhaus, 2012).

Homologs of ParA involved in spatiotemporal regulation of cytokinesis include the positive regulator of Z ring positioning PomZ from *M. xanthus*, as well as negative regulators of Z ring positioning such as MipZ from *Caulobacter crescentus* and the well-conserved MinD protein. In *Caulobacter,* MipZ interacts with ParB, FtsZ and DNA (Thanbichler and Shapiro, 2006). Because ParB associates with *parS* sites on the chromosome that occur near the origin of replication, which is located near one cell pole prior to replication, ParB is positioned to one cell pole in pre-divisional cells (Mohl and Gober, 1997). As the chromosome replicates and segregates, another origin of replication moves to the opposite cell pole. This allows bipolar localization of ParB in cells undergoing cell division. MipZ forms ATP-bound dimers that nonspecifically interact with DNA (Kiekebusch et al., 2012). When ATP is hydrolyzed, MipZ becomes a monomer that preferentially associates with ParB (Kiekebusch et al., 2012). This cycle creates a MipZ gradient that extends from the cell poles where MipZ concentration is highest. MipZ directly inhibits FtsZ polymerization, and FtsZ localizes to the cellular location with the lowest concentration of MipZ (Thanbichler and Shapiro, 2006). When ParB, and by association MipZ, become

localized to both cell poles, the lowest concentration of MipZ occurs at midcell where FtsZ can polymerize into a Z ring to form a functional divisome (Thanbichler and Shapiro, 2006).

The Min system

The MipZ mechanism of Z ring positioning in *Caulobacter* is reminiscent of the more widely conserved Min system, which involves the ParA homolog, MinD (Monahan et al., 2014). The Min system prevents the formation of minicells (tiny cells devoid of DNA) by inhibiting Z ring formation at the DNA-free regions of the cell poles (de Boer et al., 1989). Studies of the Min system in *B. subtilis* and *E. coli* have resulted in two mechanistic models of Min system function (Figure 1.4). The effector protein of the Min system is MinC, which prevents FtsZ polymerization and is recruited to the membrane by binding to the membrane-associated MinD protein (de Boer et al., 1992; Dajkovic et al., 2008; Gregory et al., 2008; Hernandez-Rocamora et al., 2013; Hu and Lutkenhaus, 1999, 2000, 2003; Levin et al., 1998; Marston and Errington, 1999; Pichoff and Lutkenhaus, 2001; Shen and Lutkenhaus, 2010; Shiomi and Margolin, 2007a). The MinCD complex is localized to the cell poles via different mechanisms in each of the model organisms.

FIG 1.4

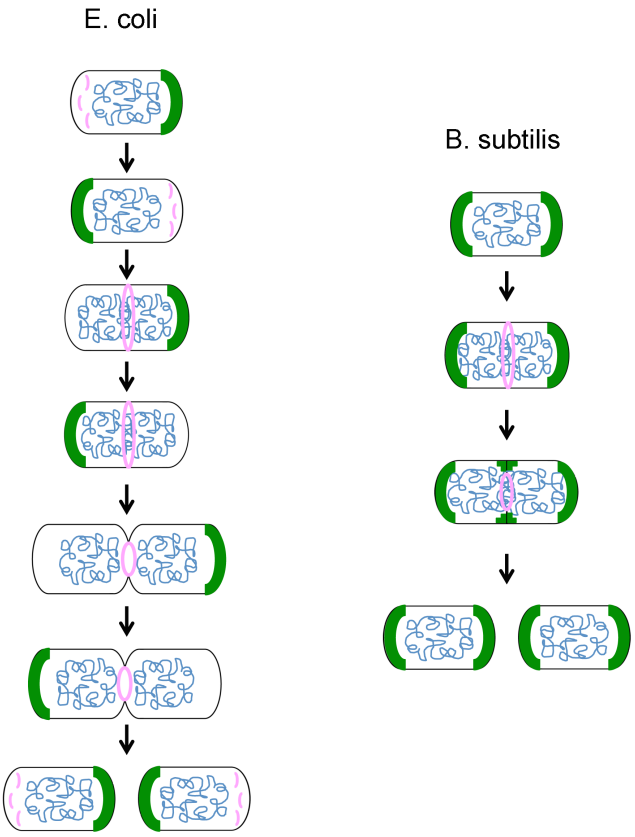

Figure 1.4: Spatial regulation of the divisome by Min and NO. A model of the Min system and NO in *E. coli* is presented on the left. As MinCD (green) oscillates from cell pole to cell pole, resulting from the action of MinE (not shown), FtsZ (pink) and FtsZ-associated proteins oscillate to opposite cell poles. NO prevents FtsZ from forming a ring over the nucleoid (blue) until the DNA begins to replicate and segregate. A model of the Min system and NO in vegetative *B. subtilis* is presented on the right. MinCD is anchored to the cell poles via MinJ and DivIVA (not shown). When septum formation begins the MinCDJ/DivIVA complex also localizes to the septum. NO, as in *E. coli*, prevents Z ring formation until the nucleoids begin to replicate and segregate.

In *B. subtilis,* the Min system is composed of MinCDJ and DivIVA (Bramkamp et al., 2008; Cha and Stewart, 1997; Edwards and Errington, 1997; Patrick and Kearns, 2008; Varley and Stewart, 1992). This system is present mostly in rod-shaped, endospore-forming, Gram-positive bacterial species (Barák, 2013). DivIVA localizes to the cell poles by recognizing negative membrane curvature (Lenarcic et al., 2009; Ramamurthi and Losick, 2009). MinJ associates with DivIVA and recruits MinCD to the cell poles (Bramkamp et al., 2008; Patrick and Kearns, 2008). The MinCDJ/DivIVA complex is also recruited to the vegetative septum where it is thought to prevent additional Z rings from forming adjacent to the midcell divisome (van Baarle and Bramkamp, 2010; Bramkamp et al., 2008; Gregory et al., 2008).

The oscillating Min system that is present in *E. coli* is functions differently, and exists mostly in non-endospore-forming, Gram-negative, rod-shaped bacteria and consists of three proteins, MinCDE (Barák, 2013; de Boer et al., 1989). MinE is the topological determinant for MinCD in this system (Hu and Lutkenhaus, 1999; Raskin and de Boer, 1999a). MinC dimers associate with ATP-bound MinD dimers that bind cooperatively to the cytoplasmic membrane via the MinD amphipathic helix (Szeto et al., 2003; Zhou and Lutkenhaus, 2003). MinE also interacts with the membrane, and forms a ring structure that moves toward membrane-bound MinD complexes (Hsieh et al., 2010; Renner and Weibel, 2012). MinE interaction with MinD disrupts MinD-MinC interaction and stimulates the ATPase activity of MinD, causing it to monomerize and dislodge from the membrane (Hu and Lutkenhaus, 2001; Hu et al., 2002; Ma et al., 2004;

Park et al., 2011, 2012). Nucleotide exchange and dimerization allow MinD to rebind the membrane away from areas of high MinE concentration (Lackner et al., 2003; Raskin and de Boer, 1999a). Together, these interactions form a pole-to-pole oscillation pattern that keeps MinC concentration highest at the cell poles, preventing Z ring assembly at the cell poles (Loose et al., 2011). Interestingly, until the nucleoid begins to replicate and segregate, allowing Z ring formation at midcell, FtsZ and FtsZ-associated proteins form an oscillatory pattern that is counter to Min protein oscillation (Bisicchia et al., 2013; Thanedar and Margolin, 2004). Chapter 3 of this dissertation will explore the oscillation patterns of the Min system in *E. coli* and focus on how the Min proteins become equally distributed in daughter cells after cell division (Juarez and Margolin, 2010).

Chapter 2: Materials and Methods

Some of the information from this chapter is based upon:

Juarez, J. R. and Margolin, W. 2010. Changes in the Min Oscillation Pattern before and after Cell Birth. Journal of Bacteriology. Volume 192, Issue 16, Pages 4134-4142. doi:10.1128/JB.00364-10 and is published with the permission of ASM Press, Copyright © 2010, American Society for Microbiology.

Strains and growth conditions

Except for where indicated, *E. coli* strains were grown in Luria-Bertani (LB) medium at 30°C, 37˚C or 42˚C as indicated and supplemented with tetracycline (10 μg ml^{-1}; Sigma-Aldrich), ampicillin (50 μg ml^{-1}; Fisher Scientific), kanamycin (25 μg ml^{-1}; Sigma-Aldrich), chloramphenicol (10-20 μg ml^{-1}; Acros Organics) and glucose (1%; Sigma-Aldrich), as needed. Cells were induced with 0.01 – 1 mM isopropyl- β -D-galactopyranoside (IPTG) or 1 – 10 μM sodium salicylate one hour prior to microscopic analysis or overnight on LB agar plates as indicated. Cloning was performed using *E. coli* strain XL1 Blue. *E. coli* strain C43 (BL21-DE3 derivative) was used for gene expression from pET28a.

All strains used in this study are listed in Table 2.1. Strain WM1264 (Corbin et al., 2002) is wild-type W3110 containing P*lac*, driving expression of a *gfp-minD* fusion, with *minE* downstream of *minD* in its native genetic context relative to *minE*. The entire construct is on a lambda InCh vector at the lambda attachment site (Boyd et al., 2000). To construct strain WM3149, WM1264 was transduced to Kan^R with P1 phage carrying Δ*minCDE::kan*; the resulting strain is functionally Min^-, despite the expression of *gfp-minD* and *minE*, because of the lack of *minC*. To shorten the longer cells of WM3149, we introduced plasmid pZAQ, a Tet^R pBR322 derivative carrying the *ftsQAZ* region from the *E. coli* chromosome (Ward Jr and Lutkenhaus, 1985). The medium copy number of this plasmid results in several fold-excess expression of the *ftsQ*, *ftsA*, and *ftsZ* genes. In WM3149, and especially in WM1264, where it was introduced as a control, pZAQ induces polar Z rings and minicells at a high frequency, as

expected. Importantly, this plasmid also induces more frequent midcell divisions (Begg et al., 1998), thus increasing the number of short cells in the population of WM3149.

WM4107 was constructed by transducing a P1 phage lysate grown on WM2965 (MCA27) into WM1074 and selecting for the tetracycline resistance linked to the *leu* locus. Resistant colonies were then screened for temperature sensitivity, which was observed at the expected cotransduction rate of 50%. The presence of the *ftsA27* allele was confirmed by sequencing *ftsA* genes that were polymerase chain reaction (PCR)-amplified from the genome. Using a similar method, I transduced the *ftsA* null allele from WM1281, which is 50% linked to *leu*+, into WM4107 derivatives containing various plasmids expressing *ftsA* alleles, selecting for Leu+ on M9 glucose medium, screening for tetracycline sensitivity, and confirming the presence of the null allele (a frameshift at the unique BglII site within *ftsA*) by restriction endonuclease digestion and gene sequencing.

Isolation of intragenic suppressors

Suppressors of *ftsA27* and *ftsA12* were isolated by growing cultures of WM4107 (*ftsA27*) and WM1115 (*ftsA12*) to early log phase at 30˚C. Cultures were then shifted to 42˚C for one hour. Serial dilutions of each culture were plated on LB agar at 30˚C to determine viability, and on pre-warmed LB agar incubated overnight at 42˚C to select for thermoresistant mutants. The *ftsA* alleles from colonies that could survive at 42˚C were PCR-amplified from the

chromosome using primers 822 and 823 (Table 2.2) and cloned as XbaI-PstI fragments into pWM2784. For plates that contained more than 4 colonies, only 4 were selected for PCR analysis. The constructs were then transformed into WM1115 (*ftsA12*) and tested for complementation at 42˚C. The *ftsA* genes from plasmid constructs that could complement were sequenced, and identified as either revertants or harboring intragenic suppressors of the original *ftsA27* or *ftsA12* mutation. Of ~20 alleles screen from each strain I obtained 7 intragenic suppressors for *ftsA27* and 6 intragenic suppressors for *ftsA12*.

DNA manipulation and analysis

Standard protocols or manufacturers' instructions were used to isolate and manipulate DNA, including preparation of plasmid DNA, restriction endonuclease digestion, DNA ligation, and PCR. Enzymes were purchased from New England BioLabs, Inc. (NEB). Plasmid DNA was purified using Wizard Plus SV miniprep DNA purification systems and DNA fragments were purified with Wizard SV gel and PCR clean-up systems from Promega. Phusion high-fidelity DNA polymerase from NEB and Kapa Biosystems High Fidelity Readymix from VWR International, LLC were used for PCR. DNA sequencing was performed by Genewiz, Inc. and SeqWright, Inc. Oligonucleotides were purchased from Sigma-Aldrich and Integrated DNA Technologies (IDT) and are listed in Table 2.2. The final versions of all relevant clones were sequenced to verify correct construction.

Plasmid Construction

All plasmids used in this study are listed in Table 2.1. For protein purification constructs, *ftsA* alleles were PCR amplified with primers 822 and 1514 and cloned as KpnI-EcoRI fragments into pWM1260 to replace the resident *ftsA* gene. Mutant *flag-ftsA* constructs in pDSW210 were made by PCR-amplifying the *ftsA* alleles with primers 822 and 823 and cloning the resulting products as XbaI-PstI fragments into pWM2784. For *flag-ftsA* constructs in pWM2060, I PCR-amplified *ftsA* alleles fused to *flag* using primers 888 and 823, and cloned the products as EcoRI-PstI fragments into pWM2060. Most *ftsA* alleles were PCR-amplified from chromosomal DNA using primers 822 and 823. Point mutations were created by site-directed mutagenesis with combinatorial PCR using 822 and 823 as "outside" primers (forward and reverse primers for *ftsA*). Forward and reverse overlapping, mutagenic, "inside" primers were created for each desired FtsA lesion and are listed in Table 2.2.

Protein Analysis

Crude extracts, eluates, and purified proteins were resuspended in 5X SDS loading buffer (0.2 M Tris-HCl (pH 6.8), 25% glycerol, 0.5 M DTT, 10% SDS, 0.05% bromophenol blue), boiled for 10 min, and separated by SDS-PAGE in a Mini PROTEAN Tetra Cell (Bio-Rad) using 12.5% polyacrylamide gels. Gels were stained with Coomassie protein stain for at least one hour followed by incubation in destaining solution.

For Western Blot analysis proteins were transferred from the polyacrylamide gels to nitrocellulose membranes using a Bio-Rad Mini Trans-Blot Cell. Mouse-derived, monoclonal anti-FLAG primary antibody (M2) was purchased from Sigma-Aldrich. Rabbit-derived, polyclonal anti-FtsA and anti-ZipA serums were affinity purified as described previously (Levin, 2002). Primary antibody dilutions of 1:2000, 1:5000, or 1:10000 were used. Goat-derived anti-mouse IgG and goat-derived anti-rabbit IgG secondary antibodies (Sigma-Aldrich) conjugated to horseradish peroxidase (HRP) were used at a 1:10000, 1:5000, or 1:2500 dilutions. Western Lightning ECL Pro kit (PerkinElmer) was used to detect chemiluminescence. Total protein on nitrocellulose membranes were stained using Swift Membrane Stain (G-Biosciences).

The Coomassie Plus (Bradford) Assay Kit and the BCA Protein Assay Kit (Reducing Agent Compatible), both from Pierce, were used to estimate protein concentrations. Molecular graphics and analyses were performed with the UCSF Chimera package (Resource for Biocomputing, Visualization, and Informatics at the University of California, San Francisco, supported by NIGMS P41-GM103311).

Microscopy

For microscopic analysis of GFP-MinD a single colony was inoculated in Luria-Bertani (LB) medium with 50 to 100 μM IPTG and grown at 30°C or 37°C until mid-logarithmic phase. Three microliters of culture was then placed on a cover glass on a glass-bottomed culture dish (MatTek Corp.) and overlaid with a

thin strip of 1.5% LB agarose. Time-lapse microscopy was done with a fully automated Olympus IX-71 microscope outfitted with a 100X objective (numerical aperture, 1.4) and filter wheels, with exposure intervals from 1.5 to 2 s and exposure times of 0.5 to 0.8 s with a 488-nm excitation light. The growth temperature on the slide was maintained at 32 to 33°C with a WeatherStation enclosure. Identical intervals and exposure times were used during any given time course. At these temperatures, the GFP-MinD oscillation period was often as fast as 10 s (Touhami et al., 2006), and cells grew significantly (0.5 to 1 μm) and sometimes divided during the time courses, which were mostly 6 to 8 min in length.

Images of GFP-MinD oscillation were captured and analyzed with SlideBook 5.0 software (Intelligent Imaging Innovations). Kymographs were obtained by drawing a linear mask region along the length of a cell, and then performing a smooth-curve analysis of that mask. Color intensity graphs were obtained by drawing four contiguous squares of identical sizes that encompassed the pole, left midcell, right midcell, and opposite pole and by quantitating total fluorescence in those squares over time. Midcell pausing data were compiled for each time course and analyzed in Microsoft Excel. To measure the frequency of GFP-MinD pausing at the midpoint of the cell, the number of midcell pauses for each cell was counted for the duration of the time course and then the number of pauses per 5 min was plotted versus cell length. Some cells divided during the time course, becoming two new cells. Therefore, only the length of time prior to cell division was used to normalize the frequency of GFP-MinD midcell pausing.

Cell lengths were measured at the beginning and end of each time course; for simplicity, only the starting lengths were used in the analysis. For comparison of partitionings into sister cells, the total intensities of GFP-MinD in 37 pairs of newborn cells were calculated with ImageJ software and analyzed with Microsoft Excel.

For immunofluorescence microscopy, cells were grown to mid-log phase at the indicated temperatures and fixed using paraformaldehyde and glutaraldehyde as previously described (Levin, 2002). Briefly, 500 µL of mid-log phase cells were fixed in paraformaldehyde and glutaraldehyde for 15 minutes at room temperature followed immediately by incubation for 30 minutes on ice. Cells were washed 3 times with 1X PBS and resuspended in 1X GTE. FtsA was stained using 1:500 anti-FtsA primary antibody and 1:200 anti-rabbit IgG secondary antibody conjugated to Alexa Fluor 488 (Life Technologies) or DyLight 550 (Pierce). Anti-FtsZ was stained with 1:2000 anti-FtsZ primary antibody and 1:200 of the Alexa Fluor 488 or DyLight 550 conjugated anti-rabbit IgG secondary antibody. DNA was stained by incubating 0.5 µg/mL 4',6-diamidino-2-phenylindole (DAPI) with cells for 5 minutes. Fluorescence images were captured using an Olympus BX60 microscope with a 100X oil immersion objective and a Hamamatsu C8484 digital camera with HCImage software. All non-fluorescence images were captured using differential interference contrast (DIC) microscopy with a 100X oil immersion objective. Images were compiled using Adobe Photoshop.

Protein purification

His_6-FtsA and its derivatives were expressed from pET28a in *E. coli* strain C43(DE3). Cells were grown to an optical density (OD_{600}) of 0.4 to 0.6 and induced with 1 mM IPTG for 3 hours at 30˚C. Cells were harvested by centrifugation and washed in buffer A (20 mM Tris-HCl (pH 7.4), 100 mM KCl, 25 mM potassium glutamate, and 5 mM $MgCl_2$). Cell pellets were stored at -80˚C. Prior to lysis, cell pellets were thawed and resuspended in lysis buffer (buffer A, 1 mM phenylmethylsulfonyl fluoride (PMSF, Sigma-Aldrich), cOmplete, EDTA-free cocktail protease inhibitor tablets (Roche Applied Science), and 5 mM imidazole). After homogenization, cells were lysed by 4 passages through a French pressure cell (SLM Aminco). Lysates were clarified by centrifugation at 23,000 X g for 30 minutes at 4˚C. Clarified lysates were incubated with equilibrated TALON Metal Affinity Resin (Clonetech Laboratories, Inc.) for 2 hours at 4˚C. Lysate-resin mixtures were then poured into gravity-flow columns and the lysates were allowed to flow through. The resin was washed with 200 ml each of buffer A containing 5 mM, 20 mM and 30 mM imidazole. His-tagged proteins were eluted from the resin with buffer A containing 150 mM imidazole. Eluate fractions containing protein were dialyzed two times at 4˚C for a total of at least 16 hours in buffer A with 1 mM DTT and 20% glycerol. Purified proteins were then distributed into 100 µL aliquots and stored at -20˚C. Purity was determined by Coomassie staining after SDS-PAGE and mass spectrometry (UTHealth Clinical and Translational Service Center).

ATP binding assays

To measure ATP binding by FtsA and FtsA mutants, 50 nM BodipyFL-ATP (Life Technologies) was incubated with 0.25 μM of the indicated purified protein in FtsA reaction buffer (50 mM Tris, pH 7.4, 100 mM KCl, 25 mM potassium glutamate, 5 mM $MgCl_2$, 1 mM EDTA, 1 mM DTT, and 20% glycerol) at 30˚C for 15 minutes. Samples were passed through a nitrocellulose membrane using a slot-blot apparatus (Hoefer Scientific Instruments). The membrane was presoaked in FtsA reaction buffer for at least 2 hours at 4˚C. The membrane was washed with 1 mL of FtsA buffer after protein samples were vacuumed through. Fluorescence retained on the membrane was imaged with a ChemiDoc MP System (BioRad) and staining intensities within an area of constant size for each sample were quantified using Image J software. For each experiment, three technical replicates of each sample were used. Fluorescent signal was averaged for each of the three replicates, and any background fluorescence was subtracted. The values displayed are relative to wild-type FtsA, which was normalized to one.

ATP hydrolysis assays

The EnzChek Phosphate Assay Kit from Life Technologies is very sensitive (lower detection limit of 2 μM phosphate) and was therefore used to detect phosphate release from low concentrations (0.1 – 1 μM) of FtsA and its derivatives. The manufacturer's instructions were modified for 96-well format. Briefly, FtsA or its derivative was diluted to 0.1-1 μM in FtsA reaction buffer.

Assay reagents, 2-amino-6-mercapto-7-methylpurine riboside (MESG) substrate and purine nucleoside phosphorylase, were added to 50 mM Tris-HCl, pH 7.4 with or without 1 mM ATP (Sigma-Aldrich). FtsA was mixed with the assay reagents in a clear, flat-bottom 96-well plate. OD_{360} was read using a Synergy MX Microplate Reader (BioTek) every 10-15 minutes for 1-4 hours at 37˚C unless otherwise indicated. Microsoft Excel was used to calculate and analyze the data. I initially detected a very low rate of phosphate release with wild-type FtsA (0.5 mol p_i/mol FtsA/minute) using the EnzChek assay. I then tested different buffers and protein concentrations to optimize conditions for FtsA ATP hydrolysis (optimal conditions described above). Figures and figure legends indicate any differences in buffer composition for given experiments.

Table 2.1 Strains and plasmids

Stain or plasmid	Genotype or description	Source or reference
***E. coli* strains**		
XL1-Blue	*recA1* cloning strain	Stratagene
C43(DE3)	F^- *ompT hsdSB (rB- mB-) gal dcm* (DE3)	Miroux and Walker, 1996
W3110	Wild-type strain	Laboratory collection
WM1074	MG1655 Δ*lacU169*	Laboratory collection
WM1115	WM1074 *ftsA12*(ts)	Laboratory collection
WM1264	P*trc*90-*gfp-minD-minE* inserted in chromosome at *attB*, in W3110	Corbin et al., 2002
WM1281	PB103 $ftsA^0$ *recA::Tn10*	Hale and de Boer, 1999
WM1659	WM1074 *ftsA(R286W)*	Geissler et al., 2003
WM2965	MCA27 [$MC4100_r$, *leu-260::Tn10, ftsA27*(ts)]	*E. coli* Genetic Stock Center
WM2991	W3110 *zipA1*(ts)	Pichoff and Lutkenhaus, 2002
WM3149	WM1264 *mincde::kan*	This study
WM4107	WM1074 *leu-260::Tn10, ftsA27*(ts)	This study
WM4585	WM4107 *ftsA(G213A, S195P)*	This study
WM4586	WM4107 *ftsA(G50E, S195P)*	This study
WM4587	WM4107 *ftsA(H159L, S195P)*	This study
WM4588	WM4107 *ftsA(T249M, S195P)*	This study
WM4589	WM4107 *ftsA(P250T, S195P)*	This study
WM4590	WM4107 *ftsA(P251L, S195P)*	This study
WM4591	WM4107 *ftsA(Y139D, S195P)*	This study
WM4631	WM1115 *ftsA(P299A, A188V)*	This study
WM4632	WM1115 *ftsA(G266V, A188V)*	This study
WM4633	WM1115 *ftsA(A18V, A188V)*	This study
WM4634	WM1115 *ftsA(A18S, A188V)*	This study
WM4635	WM1115 *ftsA(E102G, A188V)*	This study
WM4636	WM1115 *ftsA(V113L, A188V)*	This study

Plasmids

pDSW210	Derivative of pBR322 with P*trc* promoter	Novagen
pWM2060	pDSW210 without *gfp*	Geissler and Margolin 2005
pKG110	pACYC184 derivative with P*nahG* promoter	J. S. Parkinson
pET28a	Expression vector with P*T7* promoter	Novagen
pWM366	pZAQ (*E. coli ftsQAZ* in pBR322)	Ward Jr and Lutkenhaus, 1985
pWM1260	*his$_6$-ftsA* in pET28a	Geissler et al., 2003
pWM1609	*his$_6$-ftsA(R286W)* in pET28a	Geissler et al., 2003
pWM4327	*his$_6$-ftsA(S195P)* in pET28a	This study
pWM4522	*his$_6$-ftsA(G50E, S195P)* in pET28a	This study
pWM4523	*his$_6$-ftsA(G213A, S195P)* in pET28a	This study
pWM4760	*his$_6$-ftsA(G50E)* in pET28a	This study
pWM4819	*his$_6$-ftsA(G213A)* in pET28a	This study
pWM4678	*his$_6$-ftsA(K19M)* in pET28a	This study
pWM2784	*flag* in pDSW210	Shiomi and Margolin, 2007a
pWM2785	*flag-ftsA* in pDSW210	Shiomi and Margolin, 2007b
pWM2787	*flag-ftsA(R286W)* in pDSW210	Shiomi and Margolin, 2007b
pWM3073	*zipA* in pKG110	Shiomi and Margolin, 2007b
pWM3338	*flag-ftsA(A18S)* in pDSW210	This study
pWM3341	*flag-ftsA(G266V)* in pDSW210	This study
pWM3339	*flag-ftsA(A18V)* in pDSW210	This study
pWM3340	*flag-ftsA(V113L)* in pDSW210	This study
pWM3342	*flag-ftsA(P299A)* in pDSW210	This study
pWM3375	*flag-ftsA12*(ts) in pDSW210	This study
pWM3928	*flag-ftsA27*(ts) in pDSW210	This study
pWM3933	*flag-ftsA(A18V, A188V)* in pDSW210	This study
pWM3934	*flag-ftsA(V113L, A188V)* in pDSW210	This study
pWM3935	*flag-ftsA(P299A, A188V)* in pDSW210	This study
pWM3936	*flag-ftsA(A18V, S195P)* in pDSW210	This study

pWM3937	*flag-ftsA(V113L, S195P)* in pDSW210	This study
pWM3938	*flag-ftsA(P299A, S195P)* in pDSW210	This study
pWM4115	*flag-ftsA(G213A)* in pDSW210	This study
pWM4116	*flag-ftsA(T249M)* in pDSW210	This study
pWM4424	*flag-ftsA(G50E)* in pDSW210	This study
pWM4425	*flag-ftsA(Y139D)* in pDSW210	This study
pWM4426	*flag-ftsA(P250T)* in pDSW210	This study
pWM4427	*flag-ftsA(P251L)* in pDSW210	This study
pWM4428	*flag-ftsA(H159L)* in pDSW210	This study
pWM4537	*flag-ftsA(E14A)* in pDSW210	This study
pWM4538	*flag-ftsA(K19M) in pDSW210*	This study
pWM4653	*flag-ftsA* in pWM2060	This study
pWM4654	*flag-ftsA(R286W)* in pWM2060	This study
pWM4655	*flag-ftsA(R300E)* in pWM2060	This study
pWM4656	*flag-ftsA(R286W, R300E)* in pWM2060	This study
pWM4658	*flag-ftsA(G50E, R300E)* in pWM2060	This study
pWM4659	*flag-ftsA(G213A, R300E)* in pWM2060	This study
pWM4767	*flag-ftsA(Y139D, R300E)* in pWM2060	This study
pWM4868	*flag-ftsA(H159L, R300E)* in pWM2060	This study
pWM4869	*flag-ftsA(T249M, R300E)* in pWM2060	This study
pWM4870	*flag-ftsA(P250T, R300E)* in pWM2060	This study
pWM4871	*flag-ftsA(P251L, R300E)* in pWM2060	This study

Table 2.2 Oligonucleotides

Primer number	Sequence	Description
822	TATATATCTAGAATGATCAAG GCGACGGACAGA	*ftsA* forward with XbaI site
823	TATATACTGCAGTTAAAACTCT TTTCGCAGCCA	*ftsA* reverse with PstI site
888	CGGAATTCGACTACAAGGAC GACGATGACAAAGAGCTCGG TACCCGGGGATCC	pDSW-*flag* forward
1329	GCTCGGTATAGCGCGCCTCG ATCACC	*ftsA(P299A*) site-directed mutagenesis, inside, reverese
1330	GGTGATCGAGGCGCGCTATA CCGACG	*ftsA(P299A)* site-directed mutagenesis, inside, forward
1331	CGCGGTATGGAGGACGTTTT CCACATC	*ftsA(V113L)* site-directed mutagenesis, inside, reverse
1332	GATGTGGAAAACGTCCTCCAT ACCGCG	*ftsA(V113L)* site-directed mutagenesis, inside, forward
1337	GCGGCAACCTTCACGGTACC AATCTCCAG	*ftsA(A18V)* site-directed mutagenesis, inside, reverse
1338	CTGGAGATTGGTACCGTGAA CGTTGCCGC	*ftsA(A18V)* site-directed mutagenesis, inside, forward
1355	GAC TCT GGA GCG GCA GTA GGC	chromosomal *ftsA* forward for sequencing
1356	CGC AGC GCT TGT GCA TCG G	chromosomal *ftsA* reverse for sequencing
1514	CTATCGGAATTCTTAAAACTC TTTTCGCAGCC	*ftsA* reverse with EcoRI site
1533	GGTGATCGAGCCGGAGTATA CCGAGCTGC	*ftsA(R300E)* site-directed mutagenesis, inside, forward
1534	GCAGCTCGGTATACTCCGGC TCGATCACC	*ftsA(R300E)* site-directed mutagenesis, inside, reverse

1953	GCATCAAGTTATTCGGTATTGACG	*ftsA(S195)* site-directed mutagenesis, inside, forward
1945	CGTCAATACCGAATAACTTGATGC	*ftsA(S195)* site-directed mutagenesis, inside, reverse
2021	GAGATTGGTACCGCGATGGTTGCCGCTTTAGTAGG	*ftsA(K19M)* site-directed mutagenesis, inside, forward
2022	CCTACTAAAGCGGCAACCATCGCGGTACCAATCTC	*ftsA(K19M)* site-directed mutagenesis, inside, reverse
2027	CTGGTAGTAGGACTGGCGATTGGTACCGCGAAGG	*ftsA(E14A)* site-directed mutagenesis, inside, forward
2028	CCTTCGCGGTACCAATCGCCAGTCCTACTACCAG	*ftsA(E14A)* site-directed mutagenesis, inside, reverse

Chapter 3: Changing oscillations of the MinD protein before cell birth

This chapter is based upon Juarez, J. R. and Margolin, W. 2010. Changes in the Min Oscillation Pattern before and after Cell Birth. Journal of Bacteriology. Volume 192, Issue 16, Pages 4134-4142. doi:10.1128/JB.00364-10 and is published with the permission of ASM Press,

INTRODUCTION

Rod-shaped bacteria such as *Escherichia coli* divide by binary fission and thus assemble their cell division apparatus (the divisome) at the cell midpoint. Tubulin-like FtsZ is the major cytoskeletal protein of the divisome (Margolin, 2005) and assembles into a polymeric ring on the inner surface of the cytoplasmic membrane (the Z ring). Assembly and eventual constriction of the Z ring are crucial for divisome function, and thus it is not surprising that many regulatory factors control FtsZ assembly (Romberg and Levin, 2003). Notably, two negatively acting spatial regulatory systems, the Min system and nucleoid occlusion, ensure that the Z ring is located properly at the cell midpoint (Margolin, 2001). Whereas a major component of the nucleoid occlusion system can be deleted with no major effects on cell division (Bernhardt and de Boer, 2005), inactivation of the Min system causes cells to divide either at midcell or aberrantly at cell poles (Rothfield et al., 2005). The result of polar cell division is the formation of chromosome-free minicells and multinucleate, elongated cells.

The Min system in *E. coli* consists of three proteins, MinC, MinD, and MinE (de Boer et al., 1989). MinC has two separate domains, each of which binds to FtsZ and promotes disassembly of FtsZ polymers and polymer bundles (Dajkovic et al., 2008; Shen and Lutkenhaus, 2009; Shiomi and Margolin, 2007a). MinC also binds to MinD, an ATPase with a carboxy-terminal amphipathic helix that binds to the membrane only when the protein is bound to ATP (Hu and Lutkenhaus, 2003; Hu et al., 2002). MinD also forms polymers

(Suefuji et al., 2002). Finally, MinE is a small protein that binds to MinD and stimulates hydrolysis of its bound ATP in the presence of membranes. By doing so, MinE helps to dislodge MinD from the membrane, although MinE itself can bind to the membrane (Hsieh et al., 2010; Loose et al., 2011; Renner and Weibel, 2012). The result is that MinD and MinE form zones that oscillate from one cell pole to the other, with an oscillation period of seconds to minutes, depending on a number of factors, including temperature (Hale et al., 2001; Raskin and de Boer, 1997, 1999a; Touhami et al., 2006). In typical cells, MinD spends most of its time bound to the membrane at a cell pole, forming a U-shaped zone, and its transit to the opposite pole is rapid compared to its dwell time (Raskin and de Boer, 1999a). MinE typically forms a ring at the edge of the MinD zone (Raskin and de Boer, 1997, 1999b). The direction of the oscillation is determined strongly by cell geometry (Corbin et al., 2002; Varma et al., 2008). Other factors, such as membrane phospholipid composition, also influence MinD oscillation; MinD-ATP preferentially binds anionic phospholipids, such as cardiolipin, which is enriched at cell poles (Koppelman et al., 2001; Mileykovskaya et al., 2003; Mileykovskaya and Dowhan, 2000; Renner and Weibel, 2011, 2012; Szeto et al., 2003).

Because MinC binds to MinD, MinC oscillates in concert with MinD and therefore is present at the cell poles for longer times than anywhere else in the cell (Hu and Lutkenhaus, 1999; Raskin and de Boer, 1999b). This sets up a gradient of MinC, with the average smallest amount of MinC at midcell at any one time. The current model is that Z rings are most likely to assemble at the trough

of the MinC gradient and are discouraged from assembling at cell poles where the peak of the gradient exists (Huang et al., 2003). This is supported by the observation that non-ring FtsZ and FtsZ-associated proteins oscillate from pole-to-pole, presumably being chased back and forth by the alternating zones of high MinC concentration (Bisicchia et al., 2013; Thanedar and Margolin, 2004).

However, recent work in *Bacillus subtilis* has shed new light on the possible function of MinC on the Z ring and the divisome. *B. subtilis* lacks MinE and thus relies on a static MinC gradient. This is set up by the recruitment of MinCD to the Z ring during formation of the division septum (Marston and Errington, 1999; Marston et al., 1998). This seems paradoxical, as the presence of MinCD at the Z ring is predicted to destabilize it. However, in *B. subtilis*, Z rings containing MinCD remain functional. Therefore, MinCD seems to have an important role in preventing the immediate reassembly of Z rings at developing cell poles next to a recently used ring (Bramkamp et al., 2008; Gregory et al., 2008).

This recruitment of MinCD to the Z ring of *B. subtilis* prompted us to examine in more detail Min oscillations in *E. coli* cells undergoing septation. I hypothesized that MinCD binds to the Z ring at later stages of septation, perhaps helping the Z ring to function by stimulation of FtsZ disassembly. Previous results with green fluorescent protein (GFP)-MinC suggested that MinC could transiently localize to the Z ring during septation (Hu and Lutkenhaus, 1999). Consequently, I tested if MinD, the driving force of the oscillation, could also localize to the Z ring and if this localization was dependent on MinC. I also

hypothesized that a more central localization of MinCD during the time of septum formation would explain how Min proteins are partitioned equitably to both daughter cells.

RESULTS

MinD pauses often and asymmetrically at the septum in dividing cells

To study in detail the behavior of MinD during cell division, I used WM1264, a derivative of W3110 containing a *lac* promoter driving single-copy expression of *gfp-minD* along with the *minE* gene in its natural context downstream of *minD*. When expressed at low levels at 32 to 34°C on the surface of LB agarose, mobile, fluorescent zones of MinD were detectable at exposures of several hundred milliseconds. Most cells grew and divided normally over the time courses, which were typically 6 to 10 min, with time intervals of 1.5 to 2 s between exposures.

As expected, GFP-MinD alternately and repeatedly assembled into a U-shaped zone at each pole in nearly all, short (1.5 μm to ~3 μm in length) WM1264 cells that were not in the process of dividing. This regular oscillation is depicted as a kymograph, which plots fluorescence localization versus time (Figure 3.1A). Whereas about half of the cells in this size class displayed pole-to-pole oscillations only, the other half displayed a transient, membrane-bound collection, or pause, of GFP-MinD molecules at least once at midcell during the time course in addition to the polar zones. The time course of a cell displaying midcell pausing is shown as a kymograph (Figure 3.1B) and, for another cell undergoing septation, as a series of representative micrographs from a time course experiment (Figure 3.2, horizontal arrows).

FIG 3.1

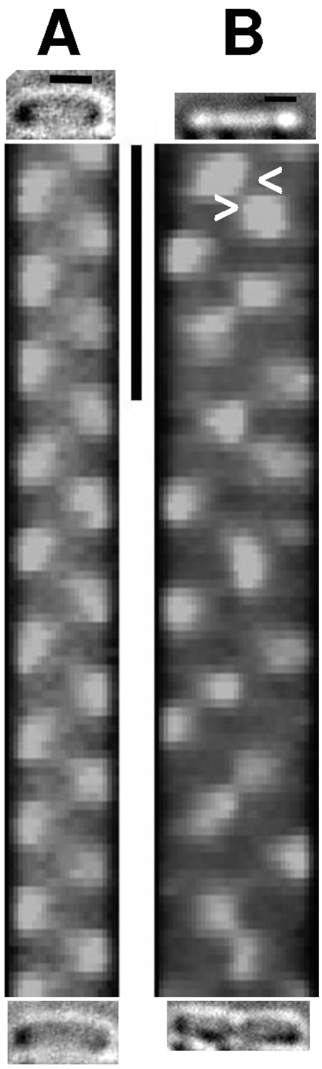

Figure 3.1: GFP-MinD pauses at midcell. Space-time kymographs and DIC images of representative cells of WM1264 are shown, with scale bars indicating cell length (1 μm, horizontal bar) and time (1 min, vertical bar). (A) Kymograph of a non-constricting cell exhibiting pole-to-pole oscillation of GFP-MinD without midcell pausing. The start time is at the top. (B) Kymograph of a constricting cell exhibiting GFP-MinD midcell pausing. Arrowheads indicate examples of two consecutive GFP-MinD midcell pausing events.

FIG 3.2

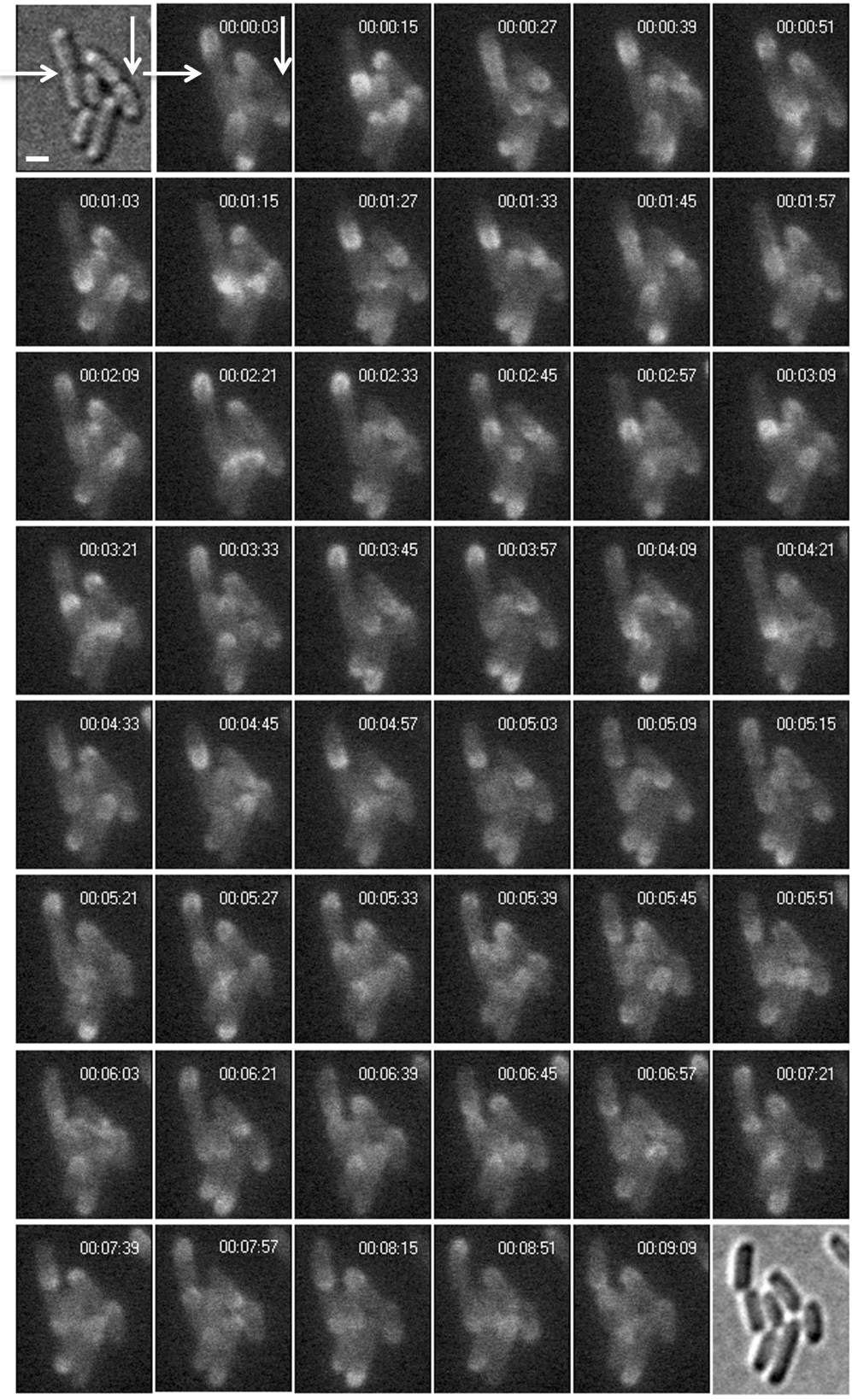
00:00:03
00:00:15
00:00:27
00:00:39
00:00:51
00:01:03
00:01:15
00:01:27
00:01:33
00:01:45
00:01:57
00:02:09
00:02:21
00:02:33
00:02:45
00:02:57
00:03:09
00:03:21
00:03:33
00:03:45
00:03:57
00:04:09
00:04:21
00:04:33
00:04:45
00:04:57
00:05:03
00:05:09
00:05:15
00:05:21
00:05:27
00:05:33
00:05:39
00:05:45
00:05:51
00:06:03
00:06:21
00:06:39
00:06:45
00:06:57
00:07:21
00:07:39
00:07:57
00:08:15
00:08:51
00:09:09

Figure 3.2: Micrographs of individual cells expressing GFP-MinD. The results of a 10-min time-lapse experiment are shown, with DIC images at the beginning and end. Horizontal arrows indicate a pre-divisional cell showing midcell pausing with eventual doubling and cell division, and vertical arrows indicate a post-divisional cell undergoing regular pole-to-pole oscillations. Images are shown at 12-s intervals (except between 1 min 27 s and 1 min 33 s) until 4 min 57 s, at which point the intervals are every 6 s until 5 min 51 s to highlight the initiation of GFP-MinD doubling in the dividing cell, and irregular intervals are shown afterward to maximize the visibility of the oscillation. Scale bar, 1 μm.

As cells increased in length (to ~3 μm) and developed visible constrictions at the division sites, the proportion of cells exhibiting at least one midcell pause of GFP-MinD during a time course increased until all cells examined showed some midcell pausing during the time course (Figure 3.3A). This midcell pausing usually involved a polar U-shaped zone that alternated with assembly of a U-shaped zone at the developing septum (Figure 3.1B, arrowheads, and Figure 3.2). Like the polar zones, these septal zones usually persisted for only a few seconds, but interestingly, they were usually asymmetric, appearing only at one side of the septum at a time.

While analyzing kymographs of numerous time-lapse movies of cells at late stages of septation, I asked if this septal localization of GFP-MinD was always followed by polar localization and whether consecutive localizations favored one side of the dividing cell over the other. One prediction was that if a GFP-MinD zone started at the left cell pole, then its next zone would more likely be the left side of the septum. However, I often observed zones that migrated from one side of the septum immediately to the opposite cell pole or to roughly the middle of the opposite cell, as well as zones that migrated from one side of the septum directly to the other side of the septum, bypassing an immediate return to a pole (Figure 3.1B and 3.2).

FIG 3.3

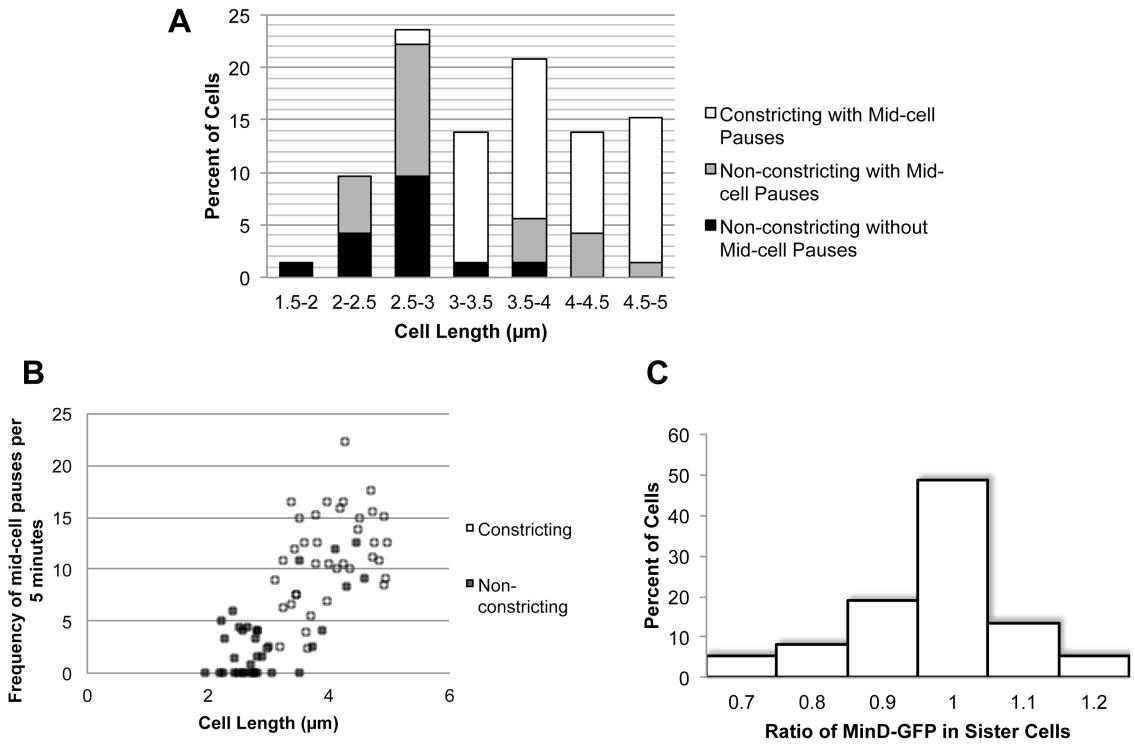

Figure 3.3: Increased GFP-MinD midcell pausing as septation approaches and equal distributions of GFP-MinD in daughter cells. (A) Frequencies of non-constricting or constricting cells displaying no midcell pausing or some midcell pausing are shown. (B) The frequencies of GFP-MinD pausing at midcell in either non-constricting or constricting cells are plotted. The frequencies were calculated from time-lapse experiments and normalized to midcell pauses at 5-min intervals. Open symbols represent cells that had visible constrictions in DIC images. Filled symbols represent cells that had no visible constrictions in DIC images. (C) Graph of the ratio of GFP-MinD intensities in each pair of recently divided sister cells.

Importantly, the frequency of pausing at the constricting septum steadily increased in the population as the cells elongated (Figure 3.3B). With an average of 6 total pauses per minute in constricting cells, the percentage of total midcell pauses reached ~50% (15 pauses per 5 min, or 3 pauses per min). Likewise, as cells approached division, the percentage of time that GFP-MinD dwelled at septal versus polar locations increased to about half of the total dwell time (data not shown).

GFP-MinD switches its oscillation pattern near the time of septum closure

To confirm the above observations, I tracked GFP-MinD movement in cells that seemed to complete their division septa during the several-minute time course. In cells with pronounced constrictions, there was frequent pausing of GFP-MinD at one side of the septum and occasional localization to other non-polar positions. Often, this irregular pattern switched to a transient, symmetric, doubled septum-to-pole pattern that then reverted to the previous single, irregular oscillation before switching again into a regular, stable, doubled septum-to-pole oscillation in each of the daughter cells. Two representative cells are shown in Figure 3.4, either as kymographs (Figure 3.4A and C) or as fluorescence intensity profiles (Figure 3.4B and D). Cells at this point had very deep constrictions, as viewed by DIC microscopy, consistent with full or almost complete daughter cell separation, and the cells could be seen pushing apart (Figure 3.4A and C). The transient splitting of septal MinD into two separate

polar zones can be clearly seen as an overlap between the two polar intensity peaks (green and blue waves, indicated by arrowheads in Figure 3.4B and D).

These results strongly suggest that in constricting cells, irregular oscillation with frequent midcell pauses is a precursor to a transient doubled oscillation between the two new and two old cell poles, which can revert to the irregular pattern but soon leads to regular, doubled oscillation around the time of septum closure. As described above, this pole-to-pole oscillation persisted for a while in short cells; GFP-MinD pausing at midcell was not observed in newborn cells (Figure 3.2, vertical arrows, and 3.3A and B). As newborn cells grew, GFP-MinD began to pause occasionally at the cell midpoint (Figure 3.4E).

FIG 3.4

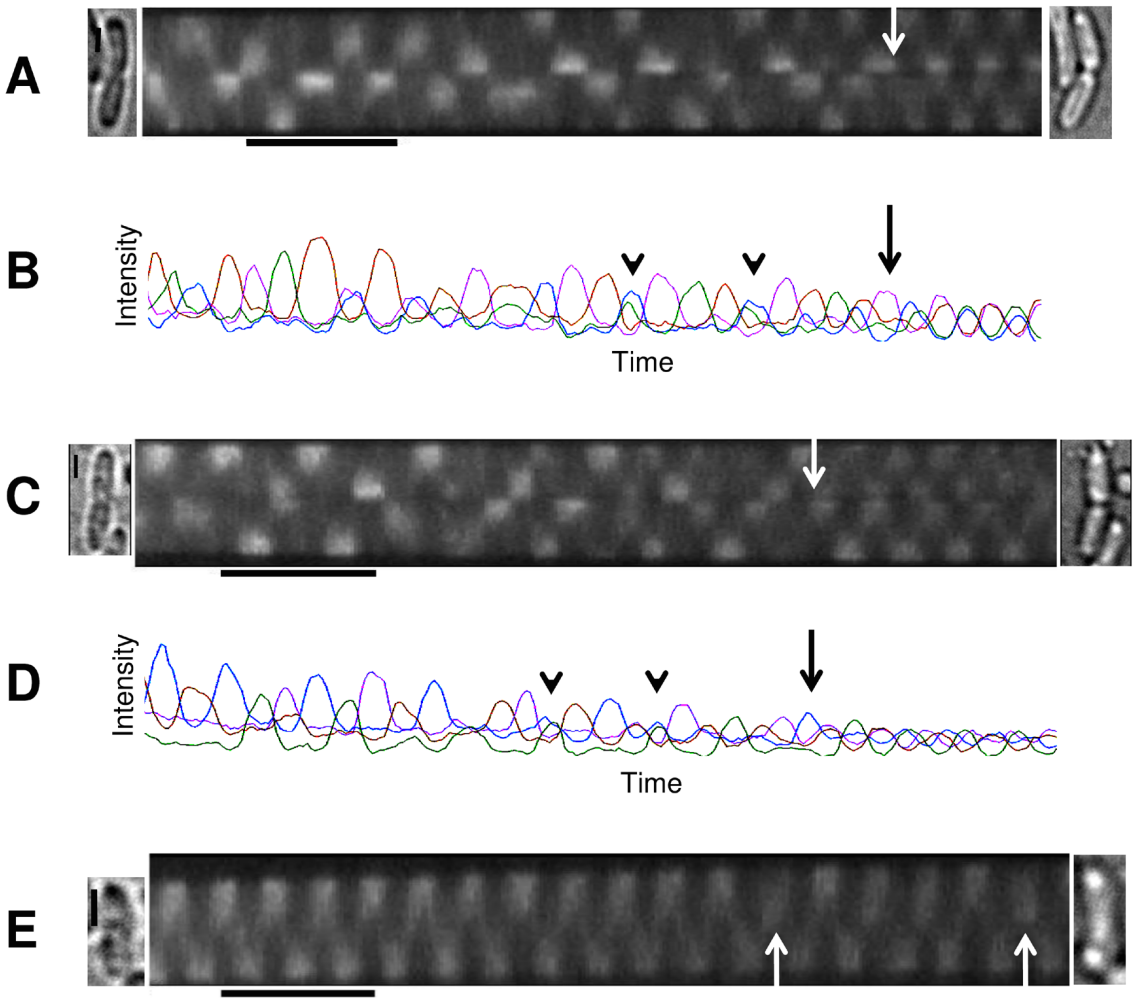

Figure 3.4: Switch in GFP-MinD oscillation patterns near the moment of septum closure. (A and C) Kymographs show GFP-MinD oscillation patterns in dividing cells. DIC images of cells before and after each time course are shown on each side of the kymographs. About the time of septation, the irregular oscillation pattern of GFP-MinD pausing at midcell switches to a double septum-to-pole pattern and then back to an irregular pattern with midcell pauses and again to a regular, doubled septum-to-pole pattern. Scale bars represent 1 μm (vertical) and 1 min (horizontal). (B and D) Corresponding graphs of GFP intensities in four regions of the cell versus time. Green, region 1, bottom cell pole; orange, region 2, lower side of the septum; purple, region 3, top side of the septum; blue, region 4, top cell pole. Near the time of complete septation, orange and purple waves synchronize, as do blue and green waves. Arrows indicate the switch to a regular, doubled pattern. Arrowheads indicate a transient doubled pattern before it becomes stable. (E) Kymograph and DIC images of a recently born cell that shows some GFP-MinD midcell pausing, indicated by the arrows. Scale bars are the same as in panels A and C.

Midcell pausing as a mechanism to distribute MinD to daughter cells

These data address the mechanism by which daughter cells receive equivalent amounts of the Min proteins. If cell separation were to occur when MinD is oscillating solely between poles of the mother cell, then the probability that one daughter cell would receive most or all of the Min proteins, at least MinD, would be high. For example, a MinD zone at the top cell pole at the moment of septum closure would result in the top daughter cell receiving most of the MinD, while the bottom daughter cell would theoretically receive little or none.

However, the absence of minicells in wild-type strains suggests that distribution of MinD must be generally symmetric. Consequently, if MinD oscillation doubled in the mother cell during the final seconds of septum closure, it would significantly increase the probability of both cells receiving MinD after septum closure. Intensity plots of the top poles, top septa, bottom septa, and bottom poles of the cells depicted in kymographs in Figure 3.4A and C indicate that equivalent amounts of GFP-MinD were indeed transferred to both daughter cells at about the time of septum closure (Figure 3.4B and D). I also determined that GFP-MinD fluorescence was partitioned roughly equally to daughter cells in a number of other cells that divided during time course experiments (Figure 3.3C).

If MinD is equally partitioned to daughter cells because of a divided population of MinD undergoing doubled oscillations during the moment of septum closure, then MinE would also be distributed and oscillations would precede the formation of daughter cells. Moreover, these oscillations should be in synchrony,

at least temporarily. The overlapping peaks to the right of the arrow in Figure 3.4B show that doubled oscillations were synchronous and remained so for the rest of the time course. I observed many other instances of the switch to stable pole-to-pole oscillations in daughter cells that continued after cell separation. One such cell is depicted in Figure 3.4D, although in this case synchrony was lost after a few oscillations. Figure 3.2 (horizontal arrows) shows another cell with similar MinD behavior that clearly divided during the time course (compare DIC images before and after the time course). These results demonstrate that MinD is distributed fairly equally to daughter cells upon septum closure and suggest that the same must be true for MinE.

MinC is not required for midcell pausing of GFP-MinD

A previous study of MinC localization in *E. coli* showed that GFP-MinC was sometimes observed oscillating from a cell pole to one side of the division septum during late stages of septation (Hu and Lutkenhaus, 1999), consistent with my observations for GFP-MinD. As MinC binds to FtsZ and to MinD, increased interactions between MinC and FtsZ at the constricting Z ring might be a mechanism to explain the visible pausing of MinC or MinD at the developing septum. In support of this idea, *B. subtilis* MinC, which does not oscillate, is recruited to closing cell division septa by DivIVA and MinJ (Bramkamp et al., 2008; Gregory et al., 2008). The presence of MinC at the septum in *B. subtilis* is thought to prevent immediate reassembly of adjacent Z rings, potentially acting as a licensing factor for new divisome formation.

It is not yet clear if MinC has a similar role in *E. coli*. However, if it does, then one might expect the pausing of GFP-MinD at invaginating septal membranes to be dependent on a transient population of MinC localized there. To test this idea, I repeated my time-lapse studies with GFP-MinD in WM3149, a derivative of WM1264 carrying a complete deletion of the *minCDE* locus. WM3149 (Δ*minCDE*) cells were a mixture of short filaments and minicells, typical of a Δ*min* mutant. This pattern results from the limited use of Z rings either for polar divisions, which generate chromosome-free minicells, or for nonpolar divisions, which generate two viable daughter cells.

The consequence of infrequent nonpolar division is that fewer cells actively divide at any given time, making it much more difficult to find cells at the proper late stage of septum formation. Furthermore, many of these cells were significantly longer than those of WM1264 because of deficiencies in nonpolar division. Therefore, it became much less likely that I would observe a cell of normal length with a simple pole-to-pole oscillation, because the oscillation wavelength of GFP-MinD (~7 μm) was often shorter than the cell length (Raskin and de Boer, 1999a). Indeed, many Δ*min* cells had three nodes of peak MinD accumulation—the two poles and midcell. Nonetheless, I was able to analyze a few dividing WM3149 (Δ*minCDE*) cells, and GFP-MinD still paused at invaginating division septa in these cells, with similar asymmetric patterns (data not shown). As MinC is completely lacking in these cells, this suggested that MinC is not required for midcell pausing of GFP-MinD.

To confirm this idea in a larger number of cells, I introduced pZAQ, a multicopy plasmid that expresses the native *ftsQAZ* gene cluster at levels several fold above native levels. The overproduction of FtsA and FtsZ from this plasmid partially overcomes the nonpolar division block in Δ*min* cells (Begg et al., 1998). As a result, cells of WM3149 (Δ*minCDE*) plus pZAQ (WM3454) were on average shorter than Δ*min* cells, although they still produced polar minicells at high frequency and were longer than *min*+ WM1264 cells.

Importantly, WM3454 (Δ*minCDE* +pZAQ) cells displayed the same types of oscillation patterns as WM1264 cells, including exclusively pole-to-pole oscillations in the shortest cells (Figure 3.5A) and midcell pausing in longer cells (Figure 3.5B). As with WM1264, the proportion of cells with GFP-MinD pausing at future midcell division sites in WM3454 (Δ*minCDE* +pZAQ) increased as cell length increased (Figure 3.5C), and the frequency of midcell pausing steadily increased as cells elongated and approached cytokinesis (Figure 3.5D). The pausing was not solely a result of the higher average lengths of these cells, because many cells in the normal range of 4 to 5 μm also exhibited midcell pausing. From these data, I conclude that pausing of GFP-MinD at midcell does not require MinC.

FIG 3.5

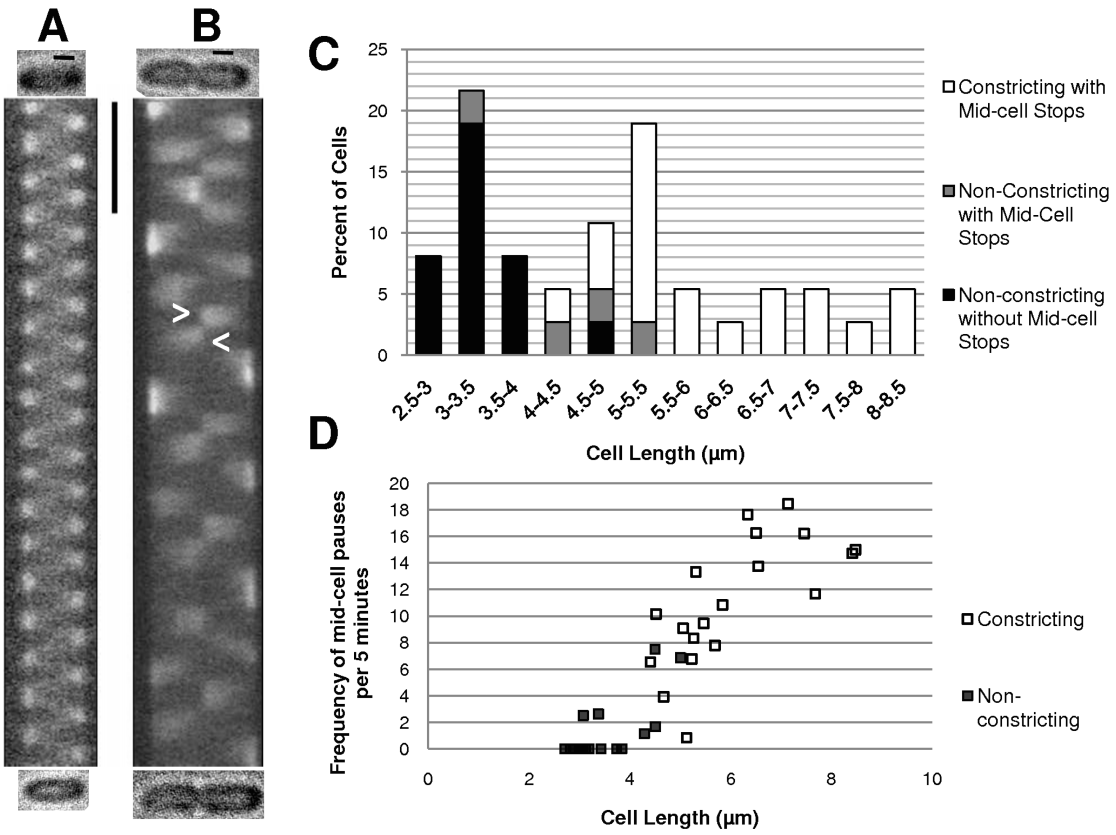
A
B
C
Percent of Cells
25
20
15
10
5
0
2.5-3
3-3.5
3.5-4
4-4.5
4.5-5
5-5.5
5.5-6
6-6.5
6.5-7
7-7.5
7.5-8
8-8.5
Cell Length (µm)
Constricting with Mid-cell Stops
Non-Constricting with Mid-Cell Stops
Non-constricting without Mid-cell Stops
D
Frequency of mid-cell pauses per 5 minutes
20
18
16
14
12
10
8
6
4
2
0
0
2
4
6
8
10
Cell Length (µm)
Constricting
Non-constricting

Figure 3.5: GFP-MinD oscillation in Δ*min* cells producing extra FtsQAZ.

(A and B) Kymographs of representative cells of WM3454 (Δ*minCDE* +pZAQ) are shown. Scale bars indicate 1 μm (horizontal) and 1 min (vertical). (A) Kymograph of a non-constricting cell exhibiting pole-to-pole oscillation of GFP-MinD without midcell pausing. (B) Kymograph of a constricting cell exhibiting GFP-MinD midcell pausing. Arrowheads indicate two consecutive GFP-MinD midcell pausing events. (C) Frequencies of non-constricting or constricting cells displaying no midcell pausing or some midcell pausing are shown. (D) The frequencies of GFP-MinD pausing at midcell in either non-constricting or constricting cells are plotted. The frequencies were calculated from time-lapse experiments and normalized per 5-min intervals. Open symbols represent cells that had visible constrictions in DIC images. Filled symbols represent cells that had no visible constrictions in DIC images.

MinD oscillation in minicells

The changes in the GFP-MinD oscillation pattern with cell length prompted us to ask if cells with very short lengths also exhibited pole-to-pole oscillations. In general, minicells formed by WM3149 (Δ*minCDE*)were quite symmetrical, and I did not detect a concerted motion of GFP-MinD in these minicells (data not shown). However, WM3149 (Δ*minCDE*) plus pZAQ and especially WM1264 plus pZAQ tended to generate minicells with diverse sizes and shapes, including double minicells. Although the mechanism behind this shape diversity is not known, it is well established that several fold overproduction of FtsZ increases polar divisions, both in *min* mutant and *min*$^+$ cells, because the excess FtsZ antagonizes the action of the Min proteins (Ward and Lutkenhaus, 1985).

Remarkably, many of these oblong or double minicells exhibited stable bidirectional oscillation (Figure 3.6). The direction of the oscillation was always along the long axis, consistent with our previous geometrical model for Min oscillation (Corbin et al., 2002). Long axes were generally between 1.5 and 2 μm in length. Therefore, the oscillation pattern in these minicells is similar to that in newborn cells with a normal rod shape. These results indicate not only that these minicells have sufficient ATP to drive the oscillation but also that pole-to-pole oscillation can be robust even over very short distances, provided there is a long axis.

FIG 3.6

Figure. 3.6: MinD oscillates along a long axis in minicells. Kymographs show GFP-MinD oscillation over time in representative minicells of WM1264 containing pZAQ, featuring either a double minicell (A) or an oblong minicell (B). DIC images of the minicells are shown to the left. The scale bar under the micrograph represents 1 μm, and the scale bar under the kymograph represents 1 min.

DISCUSSION

I show here that GFP-MinD, and by inference MinD itself, forms transient assemblies not only at cell poles but also at the developing division septum. The frequency of pausing at the septum steadily increased as the cells elongated and the septum matured. Although septal pausing of GFP-MinD rarely occurred in newborn cells, over the course of many oscillations, I detected at least one septal pause in approximately half of cells shorter than 3 μm in length. This argues against the idea that the septal pausing is simply a result of longer distances that allow a doubling of the oscillation wave, because the wavelength interval between MinD segments in filamentous cells lacking division septa generally exceeds 7 μm (Raskin and de Boer, 1999a).

Moreover, the morphology of the septal pausing suggests that MinD recognizes a specific cue at the septum. In cells with deep constrictions, GFP-MinD often localized at a U-shaped zone corresponding to one side of the division septum. This was followed either by reassembly at a cell pole or by migration to the other side of the septum, forming a corresponding inverse U shape. This is consistent with GFP-MinD recognizing the developing septum as a new cell pole. The ability of GFP-MinD to move from one side of the septum to the other instead of always back to an old pole implies that the new cell poles become competent targets for MinD assembly and compete effectively with the old cell poles. This also indicates that once MinE induces hydrolysis of the ATP

bound to MinD, MinD does not always have to move several microns away from its previous assembly point to assemble a new zone.

I also documented the transition of GFP-MinD oscillation from an undivided to a divided cell. The data indicate that the irregular oscillation pattern, which includes extensive septal pausing, ultimately switches to a stable double oscillation around the time of septum closure. This can occur in several ways, as illustrated in the model (Figure 3.7). Importantly, the affinity of GFP-MinD for the developing septum is crucial for any of these pathways to doubling and therefore for the symmetric partitioning of MinD into daughter cells. My data are consistent with mathematical simulations of this process (Sengupta and Rutenberg, 2007), in which the highest probability of correct partitioning of Min proteins into daughter cells correlates with frequent localization to the developing division septum. It will also be interesting to understand how the distribution of MinE is coordinated with MinD.

FIG 3.7

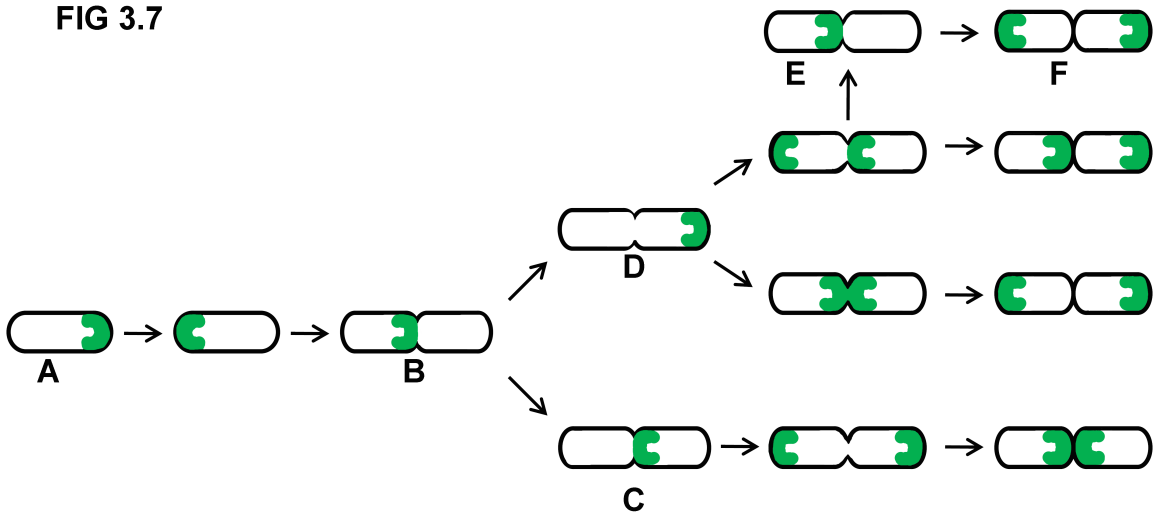

Figure 3.7: Model of MinD oscillation patterns before and after cell division. The regular pole-to-pole oscillation of a newborn cell (A) switches to an irregular pattern of a single MinD zone, with pausing not only at cell poles but also at either side of the developing septum (B). In cells approaching cytokinesis, a single MinD zone at the septum (C) or cell pole (D) will split into two zones and initiate a stable, doubled oscillation in both daughter cell compartments. Sometimes the doubled oscillation pattern reverts to the irregular pattern with only a single MinD zone per mother cell (E), although a stable doubling pattern will ultimately emerge (F). Each panel represents different pathways toward stable doubling observed over the course of many time-lapse experiments. The affinity of MinD for the developing septum is crucial for each pathway, which leads to symmetric partitioning of MinD into daughter cells.

As MinC interacts with FtsZ and MinD, one explanation for septal pausing is that interaction between MinC and the Z ring might cause MinD to stall transiently at the Z ring during its rapid transit from pole to pole. Indeed, MinC was also previously shown to pause at the septum (Hu and Lutkenhaus, 1999), and the idea that MinC helps the Z ring to disassemble is attractive. However, I found that GFP-MinD often pauses midcell in cells lacking MinC. This suggests that MinC-FtsZ interactions are not required for the equal distribution of MinD to daughter cells, arguing against a model in which MinC is the sole trigger of septal closure (Sengupta and Rutenberg, 2007), although MinC has a role in activating divisome function in general, as many Z rings are not used right away in the absence of Min (Yu and Margolin, 1999).

My data suggest that MinD itself may recognize a membrane determinant for developing a new pole that competes with its old-pole–to–old-pole regime. I propose that this determinant may be membrane curvature induced by the invaginating Z ring. This explains the high frequency of midcell pauses in cells with deep constrictions and is consistent with the behavior of proteins, such as DivIVA, that localize to areas of high membrane curvature (Lenarcic et al., 2009). However, cells with no visible constrictions also exhibited midcell pausing. One possibility is that once the Z ring is assembled and activated, it can induce small shape changes in the cytoplasmic membrane, possibly in association with penicillin-insensitive peptidoglycan synthesis (Rothfield, 2003), and MinD can sense these changes. Another possibility is that MinD may target anionic phospholipids such as cardiolipin, which are enriched at cell poles and division

septa. Consistent with this, I showed that MinD still could oscillate robustly in asymmetric minicells, which are enriched for these lipids. A third possibility is that MinD may bind directly to a divisome protein. Further studies will be needed to distinguish among these models, although it will be difficult to separate the effects of phospholipid composition from membrane curvature, as one is correlated with the other. In any case, I postulate that MinD pauses at the developing division septum for two purposes—to stimulate Z ring constriction and to ensure its equal distribution to daughter cells.

Chapter 4: Suppression of *ftsA27*, a thermosensitive *ftsA* mutant of *Escherichia coli*, suggests interplay between ATP binding and protein-protein interactions

INTRODUCTION

In *E. coli*, both FtsA and ZipA are essential for cell division and work together to anchor the Z ring to the cytoplasmic membrane (Hernández-Rocamora et al., 2012; Pichoff and Lutkenhaus, 2002). Both proteins bind to the carboxy-terminal tail of FtsZ (Din et al., 1998; Hale et al., 2000; Liu et al., 1999; Ma and Margolin, 1999; Moreira et al., 2006; Mosyak et al., 2000; Shen and Lutkenhaus, 2009; Szwedziak et al., 2012), and both are required for Z ring maturation, including recruitment of downstream division proteins (Busiek and Margolin, 2014; Busiek et al., 2012; Corbin et al., 2004; Hale and de Boer, 2002; Pichoff and Lutkenhaus, 2002; Rico et al., 2004). In addition to anchoring the Z ring to the cytoplasmic membrane and recruiting downstream proteins, ZipA has been shown to be important for stabilizing the Z ring and is required for the FtsZ-dependent formation of preseptal peptidoglycan (Kuchibhatla et al., 2011; Pazos et al., 2013; Potluri et al., 2012; RayChaudhuri, 1999). ZipA also promotes bundling of FtsZ protofilaments *in vitro* (Hale et al., 2000; RayChaudhuri, 1999). However, *zipA* is only conserved among the gamma-proteobacteria (Margolin, 2000), and no evidence currently exists for direct recruitment of downstream division proteins by ZipA. In addition, a number of point mutations in *ftsA* allow a complete bypass of *zipA* requirement in *E. coli* (Geissler et al., 2003; Margolin, 2000; Pichoff et al., 2012). This has led to the hypothesis that FtsA is the dominant Z ring anchor required for septation.

FtsA is almost as widely conserved in bacteria as FtsZ (Margolin, 2000). FtsA belongs to the actin, HSP70, sugar kinase superfamily of ATPases, and maintains a structural homology to actin with the exception of one of its four subdomains (Bork et al., 1992; van den Ent and Löwe, 2000). Each subdomain plays a role in FtsA self-interaction, with the FtsA-FtsA subunit interface defined in the atomic structure of an oligomer (Szwedziak et al., 2012). Subdomains 1A, 2A and 2B make up the conserved ATP binding pocket (van den Ent and Löwe, 2000). Subdomain 2B also contains the residues required for interaction with FtsZ (Pichoff and Lutkenhaus, 2007). The unique subdomain 1C interacts directly with downstream division proteins (Busiek et al., 2012; Corbin et al., 2004; Rico et al., 2004). With all of these functions, FtsA is not only a membrane anchor for the Z ring, but is probably a key regulator of bacterial cell division.

Recent evidence supports the idea that FtsA regulates the Z ring. In 2009, I showed that the FtsA hypermorph, FtsA-R286W, also known as FtsA*, can curve and shorten FtsZ polymers in vitro in the presence of ATP (Beuria et al., 2009; Osawa and Erickson, 2013). This led us to hypothesize that FtsA must bind and/or hydrolyze ATP to affect the Z ring. There have been reports of FtsA from *Bacillus subtilis* and *Pseudomonas aeruginosa* having ATPase activity (Feucht et al., 2001; Paradis-Bleau et al., 2005), but the role of ATPase activity in FtsA function or what stimulates it remains unknown. Little progress has been made in deciphering how ATP influences FtsA activity because of the need to refold FtsA from insoluble inclusion bodies (Martos et al., 2012; Paradis-Bleau et al., 2005). However, Loose and Mitchison recently had success in isolating

soluble, active *E. coli* FtsA and reported that ATP is required for FtsA to interact with FtsZ in a supported lipid bilayer system (Loose and Mitchison, 2014).

To investigate the role of ATP binding by FtsA *in vivo*, I took advantage of an *ftsA* temperature sensitive (ts) allele. Other known FtsA lesions at the ATP binding site, such as FtsA-G336D, confer complete loss of function *in vivo,* making them recalcitrant to analysis. The advantage of temperature sensitive mutants is that they allow mostly normal cell division at 30˚C and thus their function can be switched off by shifting to the non-permissive temperature (42˚C), facilitating *in vivo* studies. Our ability to purify FtsA in soluble form allows complementary biochemical analyses, such as nucleotide binding and hydrolysis measurements. In this study, I investigate a previously uncharacterized ts mutant, *ftsA27* (S195P) and a panel of thermoresistant, intragenic suppressors. In addition, I further characterize the biochemical properties of wild-type FtsA and FtsA*.

RESULTS

Thermosensitive alleles of *E. coli* ftsA map to residues in or adjacent to the ATP binding site

As a first step in understanding the mechanism behind the thermosensitivity of *E. coli ftsA* alleles, I mapped the mutations in *ftsA12*, *ftsA27* and *ftsA1882*, which have been used to conditionally inhibit FtsA function. I found that the proteins encoded by *ftsA12*, *ftsA27* and *ftsA1882* had the amino acid changes A188V, S195P, and T378M, respectively. A188 corresponds to S190 of the crystallized *Thermotoga maritima* FtsA, which is located at the beginning of helix H4 and identified as an active site residue (van den Ent and Löwe, 2000). S195 corresponds to *T. maritima* G197, at the end of H4 and not in the active site, but in the Mg^{++} binding site. T378 corresponds to *T. maritima* D378, on strand S11 near the α phosphate of ATP. Each is in the ATP binding pocket of FtsA as defined by the *T. maritima* FtsA crystal structure. Interestingly, all other published *ftsA* (ts) mutant alleles are dispersed along the primary sequence but are also within or adjacent to the ATP binding pocket of the tertiary structure of FtsA (Table 4.1 and Figure 4.1) (Robinson et al., 1988, 1991; Sanchez et al., 1994). This suggests that there are many lesions that can render FtsA thermosensitive, but they probably all share defects in ATP binding and/or hydrolysis.

Table 4.1: All sequenced temperature-sensitive *ftsA* mutants map to the active site.

***ftsA*(ts) Mutant**	**Identity & Location of Lesion**
ftsA8-25	L83F in S4 near the γ phosphate (Robinson et al., 1988)
ftsA22	C90W in S5 near the γ phosphate (Robinson et al., 1988)
ftsA12	A188V in H4 in the Mg binding pocket (this work)
ftsA40	S192L in H4 in the Mg binding pocket (Robinson et al., 1988)
ftsA27	S195P in H4 in the Mg binding pocket (this work)
ftsA38/21	G205S between H5 & S9 – Mg^{++} binding, phosphate binding/hydrolysis (Robinson et al., 1988)
ftsA6	D217N in S11, predicted to be involved in ATP hydrolysis (Robinson et al., 1988)
ftsA3	T240I in H6 in the adenosine binding pocket (Sanchez et al., 1994)
ftsA2	A338T between S14 & H9 in the adenosine binding pocket (Sanchez et al., 1994)
ftsA13	I341N between S14 & H9 in the adenosine binding pocket (Robinson et al., 1991)
ftsA1882	T378M in S11 near the α-phosphate of ATP (this work)

FIG. 4.1

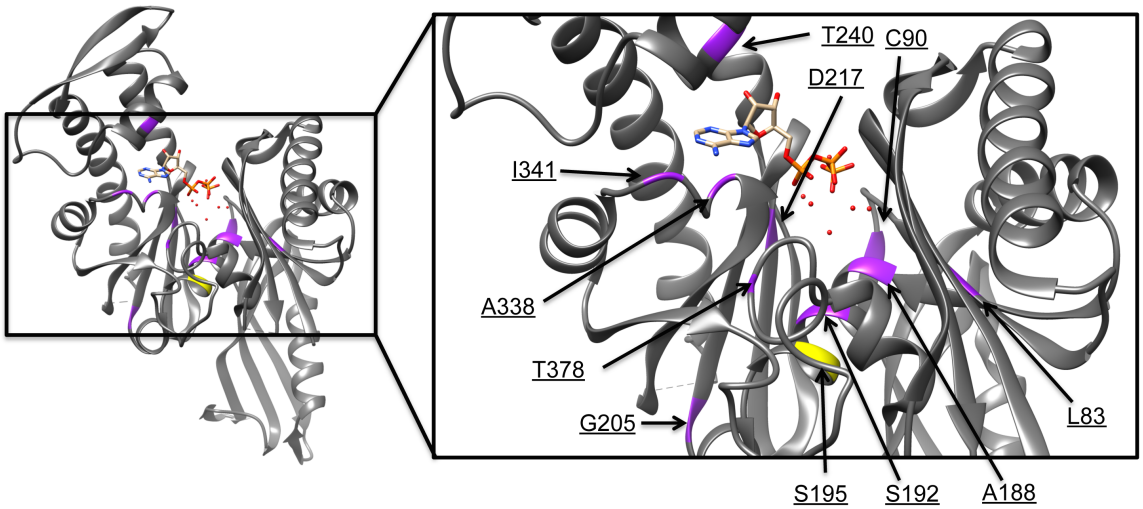

Figure 4.1: Thermosensitive mutations of *ftsA* map to the ATP-binding site. A structure of FtsA from *T. maritima* with a magnified region highlighting locations of lesions that render *E. coli* FtsA thermosensitive highlighted in yellow (S195P, encoded by *ftsA27* and the focus of this study) or purple (all other known lesions). ATP is shown in the binding pocket and the red dots indicate water molecules.

Intragenic suppressors of *ftsA27* suggest that FtsA27 is deficient in protein-protein interactions in addition to ATP binding/hydrolysis

It was shown previously that FtsA27 localization at division sites is lost within 30 minutes of shifting the cells to 42˚C, but the protein remained relatively stable and Z rings remained intact (Addinall et al., 1996). This suggested that FtsA27 loses its interaction with the Z ring upon temperature shift. I confirmed these observations (Figure 4.2A), and further showed that the delocalization occurred as soon as 5 minutes after the temperature shift (Figure 4.2B). This strongly suggests that FtsA-FtsZ interactions were rapidly destabilized by the shift.

To understand more about how FtsA-FtsZ interactions are affected by thermoinactivation of FtsA27, I selected thermoresistant spontaneous suppressors of *ftsA27* by plating serial dilutions of each strain at 42˚C (see Chapter 2, Materials and Methods). Aside from the expected revertants, I obtained multiple intragenic suppressors. These were identified as single point mutations that were able to suppress the temperature sensitivity of S195P *in cis* (Figure 4.3A). When isolated from the S195P lesion and expressed from an IPTG-inducible *trc* promoter on plasmid pWM2784, these mutants were able to support viability in a strain containing an *ftsA* null allele (Figure 4.4), indicating that each allele can function as the sole copy of *ftsA* in the cell.

FIG. 4.2

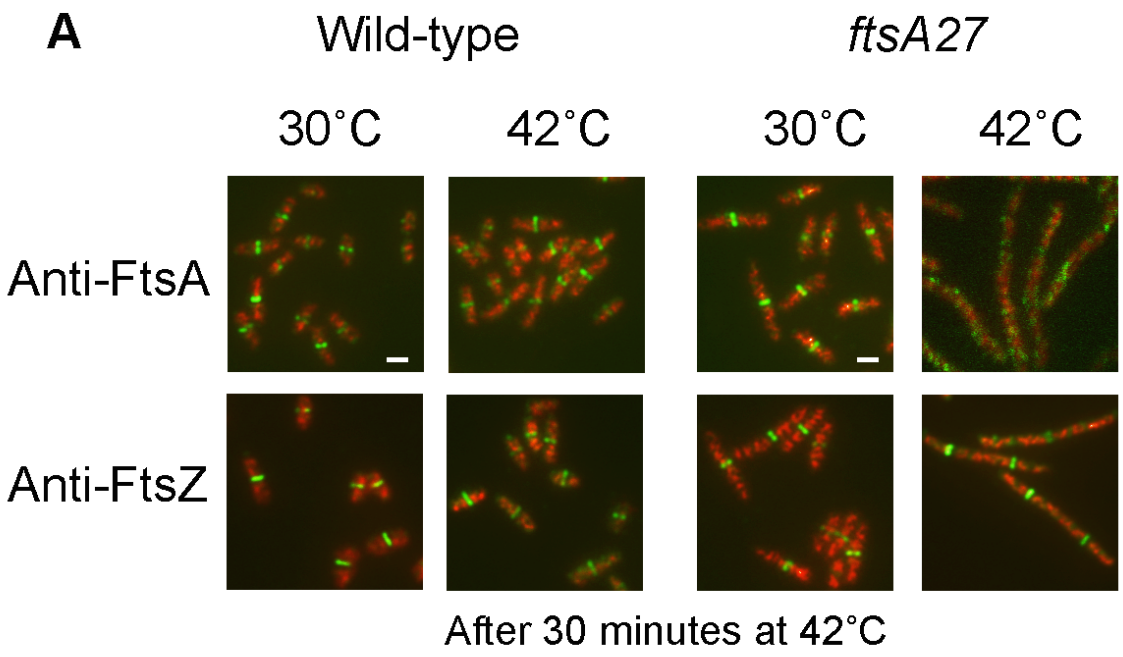

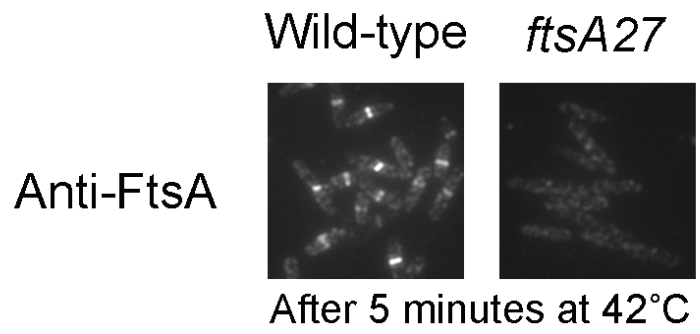

Figure 4.2: FtsA27 delocalizes from the Z ring at high temperatures. Shown are anti-FtsA and anti-FtsZ IFM images (false-colored green in panel A with DAPI stain in red) of wild-type and *ftsA27* cells grown at the indicated temperatures. Cells were shifted from 30˚C to 42˚C for 30 minutes (A) or 5 minutes (B) before fixation. Scale bar is 2 μm. Images in panels A and B are the same scale. Diep Nguyen performed the IFM in panel A.

I expected that the intragenic suppressors might map to the ATP binding pocket, compensating for the original lesion. Indeed, one suppressor mutation, G213A, is consistent with this idea. G213 corresponds to Y215 in *T. maritima* and is predicted to make contacts with the alpha, beta and gamma phosphates of ATP (van den Ent and Löwe, 2000). However, additional suppressors mapped outside the ATP binding pocket. G50E, in subdomain 1A, and Y139D, in subdomain 1C, were located at or near the proposed FtsA-FtsA interface (Figure 4.3B), with G50E at the top of one subunit and Y139D at the bottom of a corresponding subunit. Another mutation, H159L, was located within subdomain 1C but not near any known binding interface (Figure 4.3B). The other three suppressor mutations were in three consecutive residues within subdomain 2B: T249M, P250T and P251L. These residues are near the FtsA-FtsA interface, but also near the ATP binding site (Figure 4.3B).

The ability of a lesion in the ATP binding site to be strongly suppressed by lesions in diverse domains of the protein led us to hypothesize that a defect in ATP binding or hydrolysis leads to problems interacting with other cell division proteins and/or problems in FtsA oligomerization. The locations of the intragenic suppressors suggest that these defects can be overcome by restoring normal activity to the ATP-binding site or by adjusting protein-protein interactions to compensate for the putative ATP binding and hydrolysis defects.

FIG. 4.3

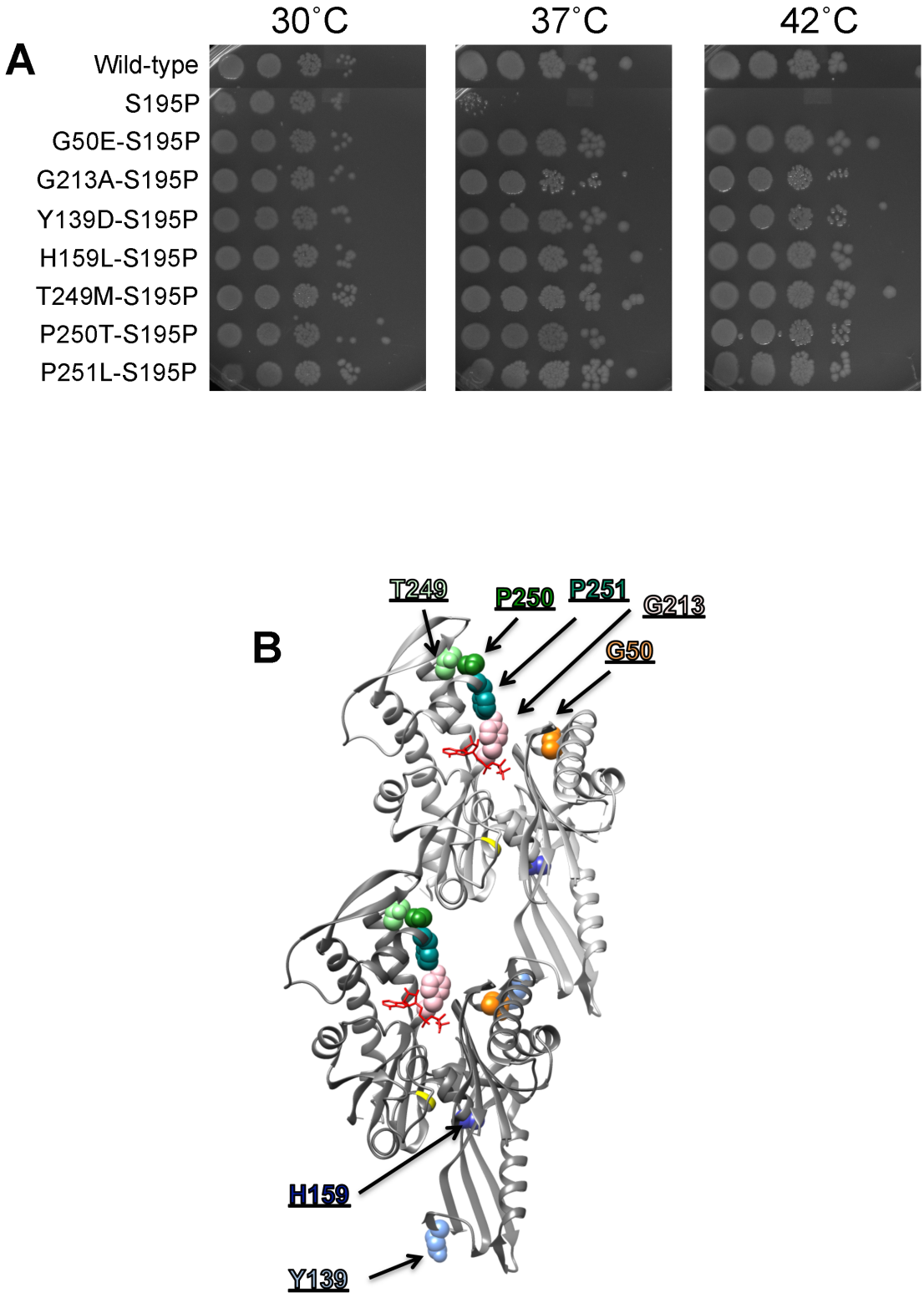
A
30˚C
37˚C
42˚C
Wild-type
S195P
G50E-S195P
G213A-S195P
Y139D-S195P
H159L-S195P
T249M-S195P
P250T-S195P
P251L-S195P
B
T249
P250
P251
G213
G50
H159
Y139

Figure 4.3: Intragenic suppressors of *ftsA27* restore thermoresistance and map to different regions of FtsA. A) Serial dilution growth assay of wild-type *E. coli* and cells expressing chromosomal *ftsA27* or an intragenic suppressor of *ftsA27* spotted on plates incubated at the indicated temperatures. B) Locations of the intragenic suppressor mutations on the dimer structure of *T. maritima* FtsA.

FIG. 4.4

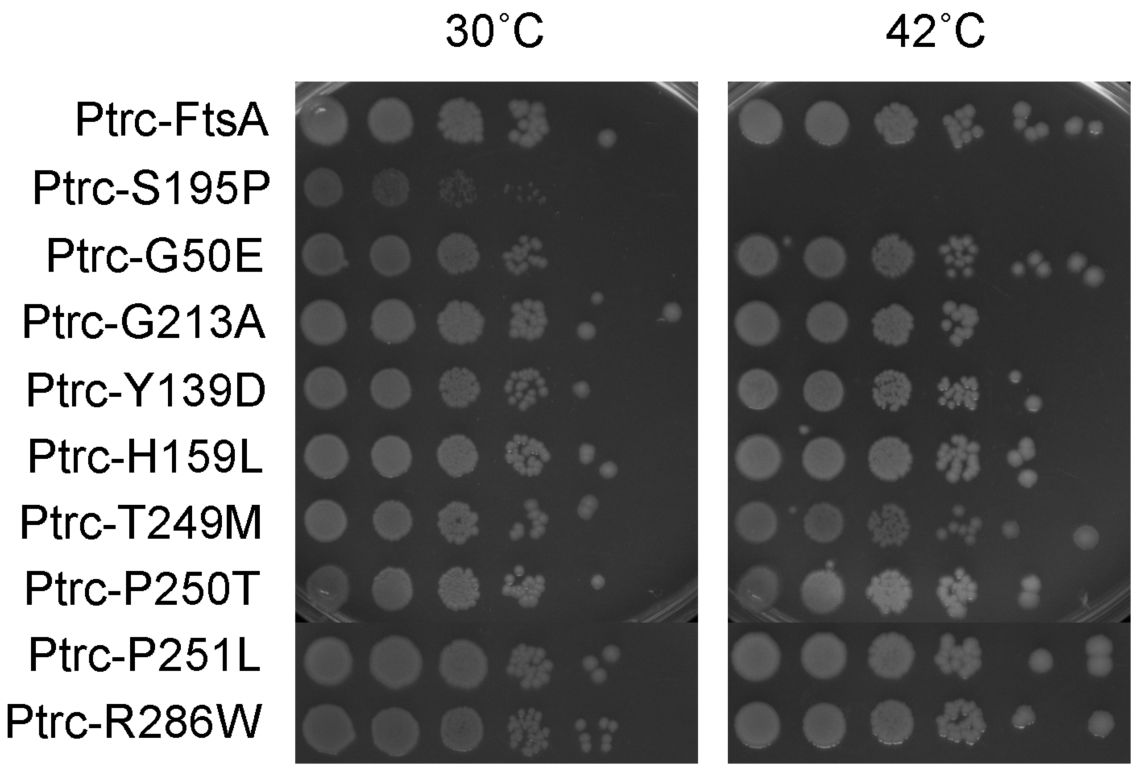

Figure 4.4: Viability of cells expressing *ftsA27* suppressor alleles without the S195P lesion. Shown is a serial dilution growth assay at the indicated temperatures. The *ftsA* mutants were FLAG-tagged and expressed as the only copy of *ftsA* from the IPTG-inducible *trc* promoter (uninduced) on plasmid pWM2784 in an MG1655 background into which an *ftsA* null allele has been transduced (see Chapter 2, Materials and Methods, for details).

Increased sensitivity of FtsA27 to ZipA overproduction at the permissive temperature suggests a weaker interaction with FtsZ

The rapid delocalization of FtsA27 from the Z ring after the temperature shift to 42˚C (Figure 4.2A) suggests that the mutant protein may be defective in interacting with FtsZ, despite having no lesions in the FtsZ-interacting domain. Because the lesion is near the ATP binding site, this idea is consistent with previous findings, which suggest that FtsA must bind to ATP to interact with FtsZ (Beuria et al., 2009; Fujita et al., 2014; Loose and Mitchison, 2014; Osawa and Erickson, 2013). To explore whether a lesion in the ATP binding pocket affects FtsA-FtsZ interactions *in vivo*, I exploited the idea that ZipA and FtsA should compete for binding to the same conserved segment of the carboxy-terminus of FtsZ.

Like overproduction of FtsA, overproduction of ZipA is toxic to *E. coli*, causing strong inhibition of cell division (Hale and de Boer, 1997). The mechanism of this inhibition is not well understood, but one likely factor is that excess ZipA prevents FtsA from interacting with FtsZ. This seems reasonable, as ZipA seems to bind to the FtsZ C-terminal tail more strongly than does FtsA *in vivo* (Shen and Lutkenhaus, 2009), and the original search for FtsZ interacting proteins identified ZipA but not FtsA (Hale and de Boer, 1997).

To determine if ZipA indeed competes with FtsA for binding to the Z ring, we overproduced ZipA in wild-type cells and measured FtsA localization by immunofluorescence microscopy (IFM). We used a sodium salicylate-inducible promoter to drive *zipA* expression on a plasmid (pWM3073) in a merodiploid

strain, expecting that FtsA would delocalize at higher ZipA concentrations. At uninduced or low levels (1 μM) of salicylate, FtsA remained localized to Z rings. However, at high (10 μM) salicylate levels, FtsA localization at midcell decreased dramatically, suggesting that FtsA was competed away from the Z ring although FtsZ localization was unaffected (Figure 4.5A). These data demonstrate that FtsA cannot bind to the Z ring in the presence of high levels of ZipA, and suggest either direct or indirect competition between ZipA and FtsA for binding to the Z ring.

I then reasoned that any FtsA that had stronger interactions with FtsZ should be more resistant to ZipA overproduction, whereas FtsA mutants with weaker binding to FtsZ should be even more sensitive. All assays were done at 30˚C, where FtsA27 localizes normally to Z rings. With no induction of extra *zipA*, *ftsA27* cells grew normally in a serial dilution assay and exhibited normal FtsA rings, indicating that these levels of ZipA were not inhibitory (Figure 4.5A-B). However, in contrast to wild-type cells, even a low level of *zipA* induction (1 μM sodium salicylate) was toxic to *ftsA27* cells, which displayed >10-fold lower plating efficiency and lost FtsA localization at the Z ring (Figure 4.5A-B). High levels of inducer (10 μM) were lethal to both wild type and *ftsA27* strains (Figure 4.5B). Figure 4.6 shows that ZipA was overproduced to approximately the same levels in each strain background. These results are consistent with the idea that FtsA27 delocalizes from the Z ring at high temperature because of an already weakened interaction with FtsZ, possibly caused by defects in binding or hydrolyzing ATP.

FIG. 4.5

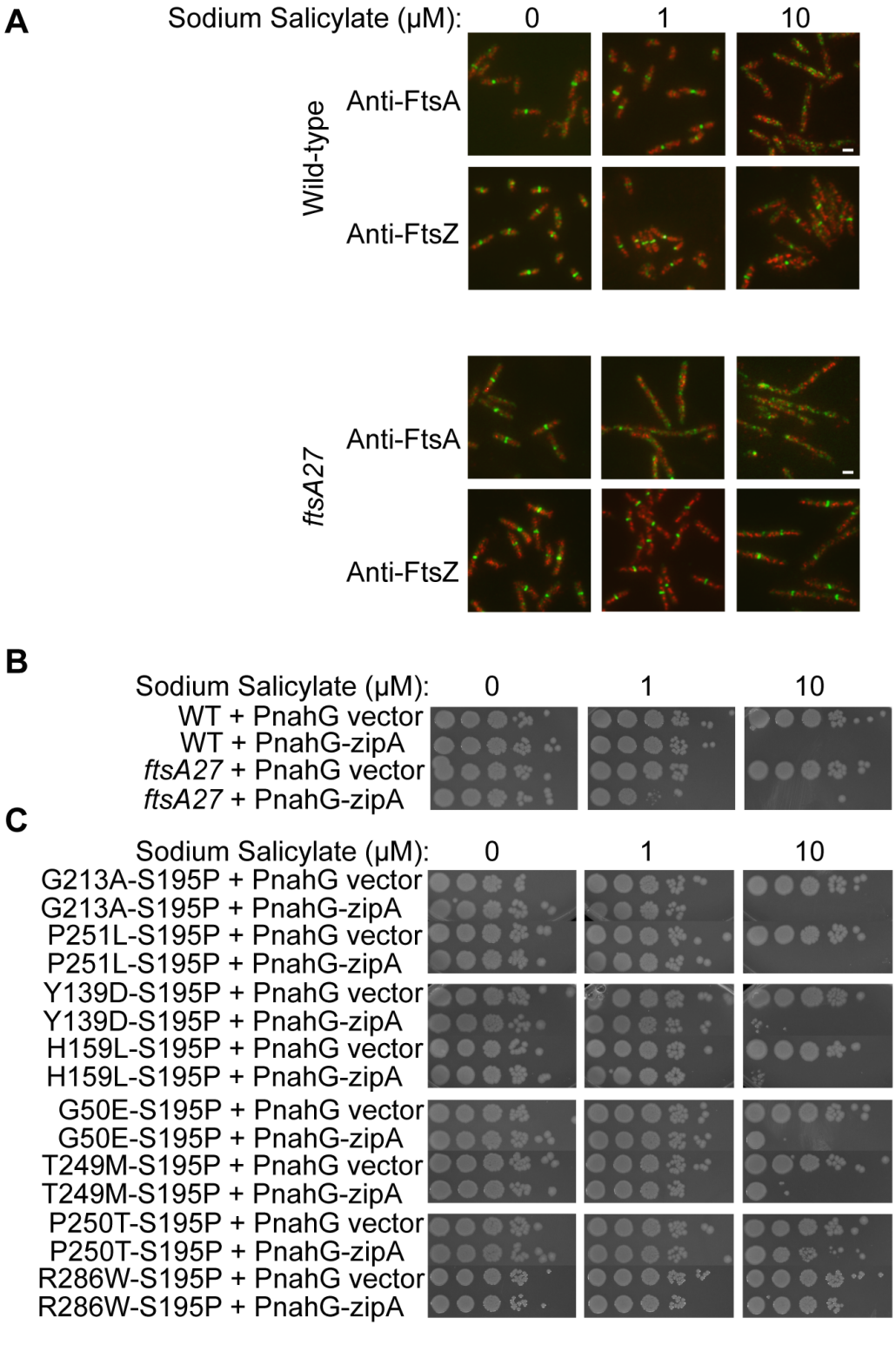
A
Sodium Salicylate (μM):
0
1
10
Wild-type
Anti-FtsA
Anti-FtsZ
ftsA27
Anti-FtsA
Anti-FtsZ
B
Sodium Salicylate (μM):
0
1
10
WT + PnahG vector
WT + PnahG-zipA
ftsA27 + PnahG vector
ftsA27 + PnahG-zipA
C
Sodium Salicylate (μM):
0
1
10
G213A-S195P + PnahG vector
G213A-S195P + PnahG-zipA
P251L-S195P + PnahG vector
P251L-S195P + PnahG-zipA
Y139D-S195P + PnahG vector
Y139D-S195P + PnahG-zipA
H159L-S195P + PnahG vector
H159L-S195P + PnahG-zipA
G50E-S195P + PnahG vector
G50E-S195P + PnahG-zipA
T249M-S195P + PnahG vector
T249M-S195P + PnahG-zipA
P250T-S195P + PnahG vector
P250T-S195P + PnahG-zipA
R286W-S195P + PnahG vector
R286W-S195P + PnahG-zipA

Figure 4.5: Resistance of FtsA27 and FtsA27 suppressors to overproduced ZipA. A) IFM images showing localization of FtsA or FtsZ in wild-type and *ftsA27* cells containing *zipA* expressed from a sodium salicylate-inducible plasmid. Scale bars are 2 μm. B) Serial dilution growth assay of wild-type and *ftsA27* cells containing *zipA* expressed from a sodium salicylate-inducible plasmid, under the indicated inducer concentrations. C) Growth assay performed as described in B, with *ftsA27* suppressor cells. I oversaw the work of Diep Nguyen, who assisted with the growth assays and did the IFM.

FIG 4.6

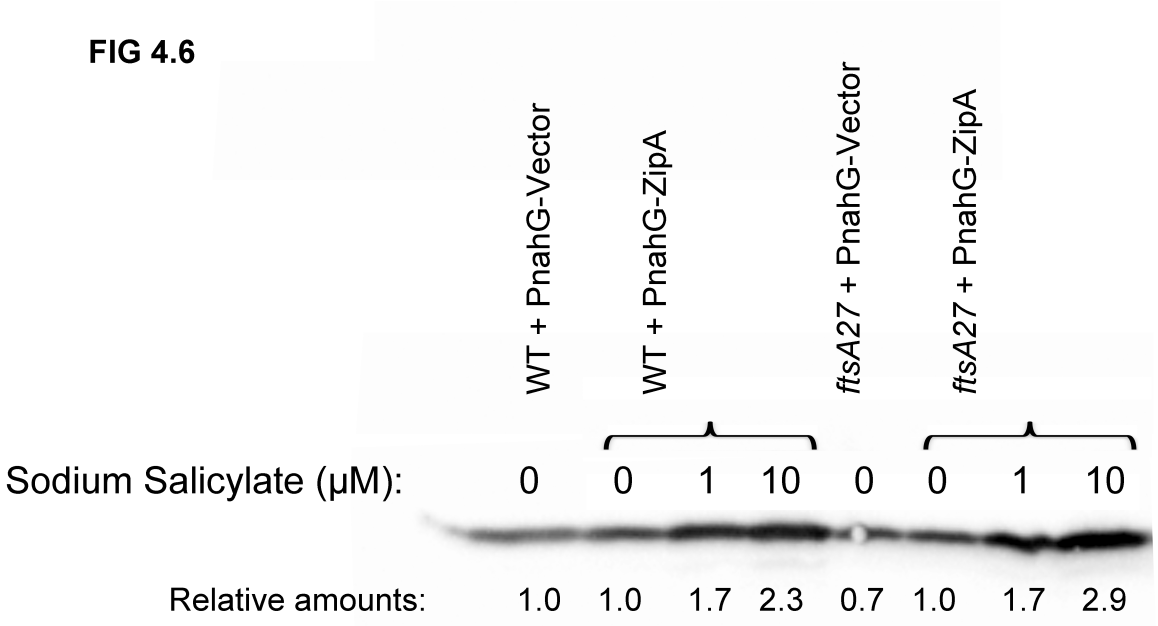

Figure 4.6: ZipA overexpression. Anti-ZipA Western blot of cells from Figure 4.5A and B.

Two independent *in vivo* assays reveal that several FtsA27 suppressors may have stronger affinity for FtsZ than wild-type FtsA *in vivo*

If the primary mechanism for the FtsA27 defect is a problem in interacting with FtsZ, then we predicted that the suppressors should correct this, possibly even at the permissive temperature. In support of this, the *ftsA27* suppressor strains restored resistance to low levels of *zipA* overexpression (1 μM salicylate, Figure 4.5C). Strikingly, several of these double mutants conferred resistance to higher levels of *zipA* overexpression (10 μM sodium salicylate) that were toxic to cells with wild-type *ftsA* (Figure 4.5C). These included, in decreasing order of resistance, P250T, T249M, G50E, H159L, Y139D, and lastly P251L and G213A. These results suggested that some FtsA27 suppressor proteins, despite having the S195P lesion on the same molecule, bind to FtsZ more strongly than does wild-type FtsA, conferring resistance to ZipA overproduction.

As the hypermorph FtsA* (R286W) shows several gain-of-function properties, including the ability to bypass ZipA as well as the ability to bind more strongly to FtsZ in yeast-two-hybrid assays (Geissler et al., 2003, 2007; Pichoff et al., 2012), I hypothesized that FtsA* also would confer increased resistance to ZipA overproduction. Using spot dilution assays, we observed that FtsA* indeed conferred resistance to the highest levels of ZipA overproduction that we tested (Figure 4.5C). These results corroborate the idea that resistance to ZipA is due to increased affinity of FtsA for FtsZ.

To lend further support to the idea that the suppressor lesions promote stronger FtsA-FtsZ interactions, I developed an independent genetic assay for

measuring these interactions. FtsA contains a highly conserved arginine residue at position 300 that is required for binding to FtsZ (Szwedziak et al., 2012). Changing this residue to a glutamate, which has the opposite charge, completely abolishes FtsA binding to FtsZ by several criteria, as well as FtsA function in cell division (Pichoff and Lutkenhaus, 2007). Interestingly, overproduction of R300E is significantly more toxic than wild-type FtsA at equivalent levels of protein. The postulated reason for this increased toxicity is that the R300E mutant protein effectively titrates later divisome proteins away from the Z ring whereas wild-type FtsA recruits them to the ring (Pichoff and Lutkenhaus, 2007).

I surmised that mutations in FtsA that increased its resistance to competition by ZipA might exhibit increased affinity for FtsZ, and therefore could potentially restore some FtsZ binding activity to the R300E mutant. Such increased binding to FtsZ by R300E should result in reduced toxicity and potentially restoration of function. To test this idea, we combined the individual mutations that suppressed *ftsA27* with R300E *in cis* on a plasmid with the IPTG-inducible *trc* promoter (pWM2784) and measured toxicity upon induction with IPTG. Western blot analysis confirmed that each construct tested was produced at equivalent levels (data not shown). We used WM1115 (*ftsA12* (ts)) as the strain background so that toxicity could be tested at 30˚C and complementation tested at 42˚C.

Without induction, all R300E derivatives grew normally at 30˚C and failed to complement at 42˚C (Figure 4.7). However, upon induction with 0.1 mM IPTG, the mutations that had suppressed ZipA toxicity, even weakly, also strongly

suppressed R300E toxicity at 30˚C (Figure 4.7). On the other hand, the weakest suppressors of ZipA toxicity, G213A and P251L, were unable to suppress R300E toxicity. Surprisingly, five of the six non-toxic R300E double mutants successfully complemented *ftsA12* (ts) at 42˚C, indicating that these mutants restored function to FtsA proteins containing the R300E lesion. In contrast, FtsA* (R286W) could only partially complement R300E at even higher levels of induction (1 mM IPTG, data not shown), although it suppressed toxicity at 30˚C (Figure 4.7). Overproduction of the R300E double mutant constructs was needed for complementation, possibly because the R300E lesion may still inhibit binding to FtsZ, which can only be overcome by higher protein concentrations.

I conclude that some of the suppressors of *ftsA27* can provide extra resistance to ZipA overproduction compared to wild-type *ftsA* and can complement an R300E mutant *in cis*. These results support the idea that residue changes outside the ATP binding pocket but not at the FtsA:FtsZ interface can allosterically enhance FtsA's interaction with FtsZ. Moreover, because the FtsA27 lesion is in the ATP binding site, these results further support the idea that FtsA needs ATP to interact efficiently with FtsZ *in vivo*.

FIG. 4.7

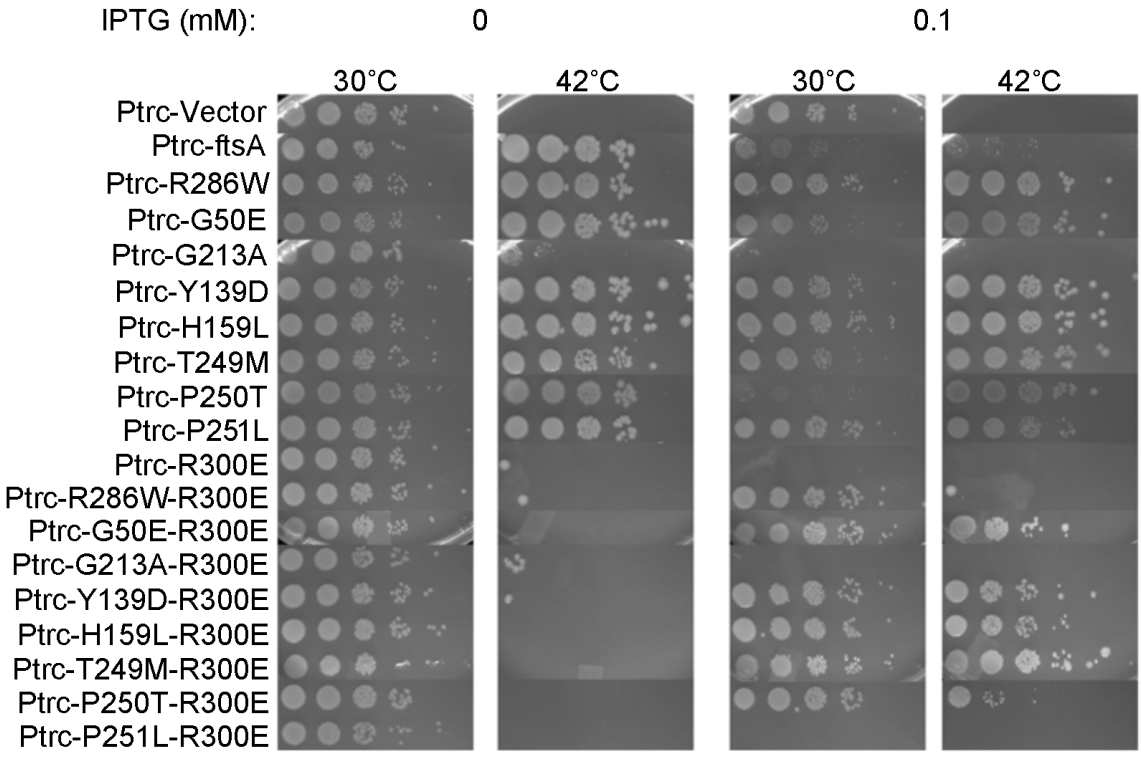

Figure 4.7: Some mutations that suppress *ftsA27* (S195P) also suppress R300E toxicity and loss of function. *ftsA* alleles indicated were FLAG-tagged and expressed from the IPTG-inducible *trc* promoter on plasmid pWM2784 in WM1115 (*ftsA12* (ts)) and grown in serial dilution spots at the indicated temperature with indicated amounts of IPTG. Diep Nguyen assisted in the construction of the double mutants and replicated some of the growth assays shown here.

Several suppressors of *ftsA27* bypass the requirement for *zipA*

I noticed that some suppressors of *ftsA27* were nearly identical (and one, T249M, was identical) to some of the mutants described by the Lutkenhaus group (Pichoff et al., 2012), which were characterized by their decreased FtsA-FtsA interaction and ability to bypass the requirement for the normally essential ZipA protein in cell division. I therefore hypothesized that my mutants could also bypass the requirement for ZipA. To test this, I attempted to transduce a Δ*zipA*::*kan* allele into the *ftsA27* suppressor strains, as well as strains harboring plasmids containing the individual *ftsA27* suppressor mutations without the S195P mutation *in cis*. Surprisingly, I was unable to obtain any transductants except from strains expressing *ftsA** (R286W), which was originally identified because of its ability to strongly bypass the *zipA* requirement (Geissler et al., 2003) and remains one of the strongest *zipA* bypass alleles of *ftsA* (Geissler et al., 2007; Pichoff et al., 2012).

I expected that T249M would also bypass ZipA as shown previously, but because it did not, I reasoned that this could be due to strain differences. The previous study used a W3110 strain background (Geissler et al., 2007; Pichoff et al., 2012), whereas I used MG1655 for my analyses. To determine if strain background affected the ability to bypass *zipA,* I tested the ability of the individual *ftsA27* suppressor alleles to suppress a *zipA1* (ts) allele in a W3110 background (Busiek et al., 2012; Corbin et al., 2004; Pichoff and Lutkenhaus, 2002; Rico et al., 2004). As with my other constructs described above, these single mutants (without the mutation for S195P) were expressed from the IPTG inducible *trc*

promoter on plasmid pWM2784. I found that G213A and P251L, which conferred ZipA resistance similar to that of wild-type FtsA and could not complement an R300E mutation, also could not suppress the *zipA1*(ts) strain. However, other suppressors of *ftsA27* that conferred higher levels of ZipA resistance were able to suppress *zipA1* (ts) (Figure 4.8A).

To test if these alleles could bypass the complete loss of ZipA in a W3110 background, I transduced the Δ*zipA::kan* allele into the *zipA1* (ts) strains exogenously expressing the *ftsA27* suppressors (Figure 4.8B). Intriguingly, the W3110 background allowed transduction of the Δ*zipA::kan* allele into some of the strains that expressed mutant *ftsA* alleles other than *ftsA*.* As expected, the strain expressing *ftsA** (R286W) was able to robustly bypass the requirement for ZipA, whereas strains expressing the G213A or P251L alleles did not yield transductants, indicating they could not bypass ZipA loss. Strains expressing H159L, Y139D or P250T resulted in the smallest transductant colonies. In contrast, strains expressing T249M or G50E yielded slightly larger transductant colonies, indicating that they could bypass ZipA more robustly, however, the colonies were not as large as those from the strain expressing R286W.

FIG 4.8

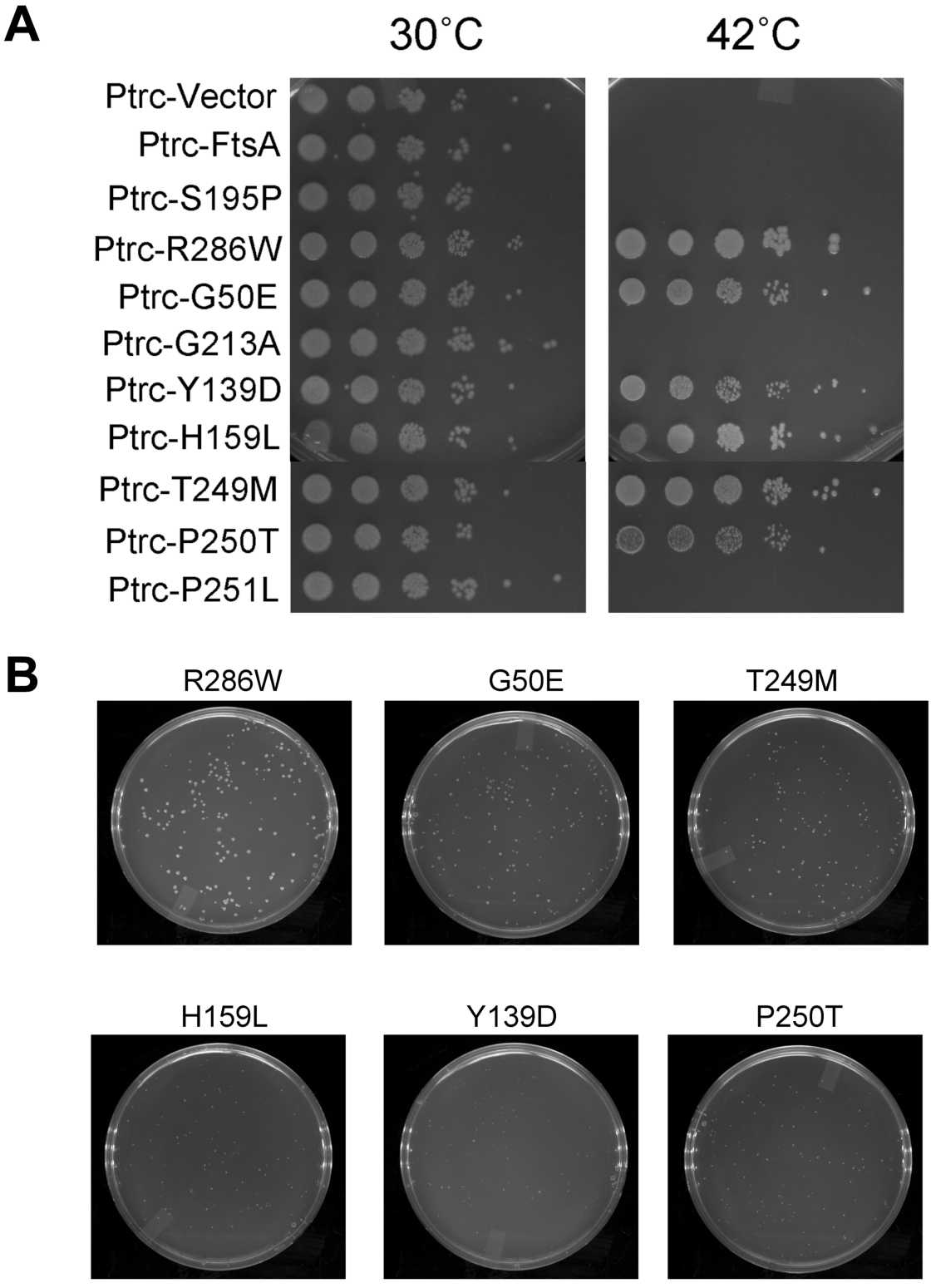
A
30°C
42°C
Ptrc-Vector
Ptrc-FtsA
Ptrc-S195P
Ptrc-R286W
Ptrc-G50E
Ptrc-G213A
Ptrc-Y139D
Ptrc-H159L
Ptrc-T249M
Ptrc-P250T
Ptrc-P251L
B
R286W
G50E
T249M
H159L
Y139D
P250T

Figure 4.8: Several mutations that suppress *ftsA27* also allow bypass of *zipA*. A) Serial dilution growth assay of indicated FLAG-tagged *ftsA* alleles expressed from the IPTG inducible *trc* promoter on plasmid pWM2784 (uninduced) in a W3110 *zipA1* (ts) background at indicated temperatures. B) Results of transducing a Δ*zipA::kan* allele into the strains shown in panel A, selecting for kanamycin resistance. Strains not shown in panel B (expressing G213A and P251L) failed to form colonies after transduction.

Together these findings suggest that in addition to decreasing FtsA-FtsA interaction, enhancing FtsA-FtsZ interaction may be another way to bypass ZipA. It is also possible that the mutants identified in this study have decreased FtsA-FtsA interactions, such as T249M. Most intriguing was that I identified amino acid changes that may affect protein-protein interactions that suppress a lesion in the ATP binding site. Again, this reinforces the notion that *in vivo,* FtsA must bind ATP to interact with FtsZ and function properly in cell division, and suggests that FtsA-FtsA interactions may also be involved in this interplay.

Purified FtsA27 is defective in binding ATP, but its suppressors restore ATP binding

To ascertain whether the decreased or increased binding to FtsZ correlated with a change in the ability of these FtsA proteins to bind ATP, I purified His_6-tagged versions of wild type and mutant FtsA (all purified proteins referred to in this dissertation are His_6-tagged). I then measured their ability to bind ATP using a filter-binding assay with a fluorescent ATP analog. As predicted, based on the location of its lesion, FtsA27 (S195P) showed a reduction in its ability to bind ATP compared to wild-type FtsA (Figure 4.9).

FIG 4.9

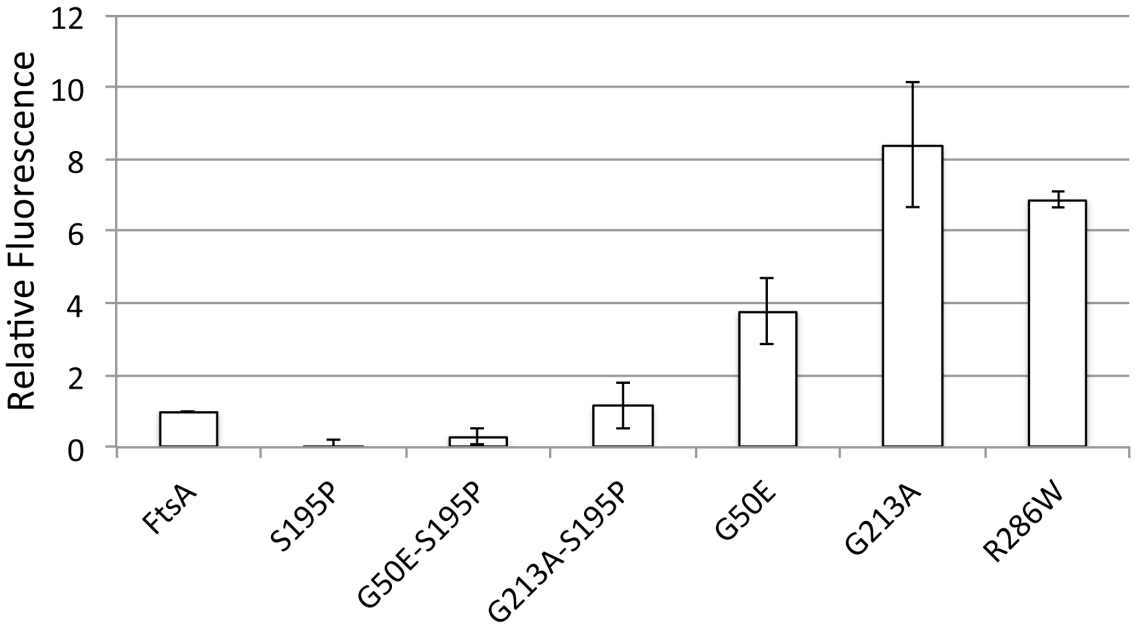

Figure 4.9: ATP-binding properties of FtsA mutants compared to wild-type FtsA. The graph shows quantitation of BodipyFL-ATP fluorescence after a filter-binding assay with the indicated His_6-tagged purified proteins. This experiment was repeated 3 times with similar results. For each experiment, 3 technical replicates of each sample were used. Fluorescent signal was averaged for each of the 3 replicates, and any background fluorescence was subtracted. The values displayed are relative to wild-type FtsA, which was normalized to 1.

I then tested two suppressors of *ftsA27*, FtsA-G50E-S195P and FtsA-G213A-S195P. These two mutants were chosen because they displayed different genetic phenotypes in the assays described above, and they are located in different domains of the protein. G50 is located at the FtsA-FtsA interface, provides extra resistance to ZipA overexpression, complements R300E *in cis*, and has the ability to bypass the requirement for ZipA. G213, on the other hand, is located in the ATP binding site and does not show any gain-of-function compared to wild-type FtsA. I suspected that the G213A lesion would restore normal ATP binding to the FtsA27 protein by directly altering the conformation of the ATP binding site. However, I hypothesized that the G50E lesion could either allosterically restore ATP binding to FtsA27 or that it could restore FtsA27 function solely via a distinct mechanism, such as reducing FtsA-FtsA interactions, which is suggested by its location on FtsA and its genetic similarity to T249M. As shown in Figure 4.9, both the G213A and G50E mutations *in cis* with S195P restored ATP binding *in vitro*, although G213A enhanced ATP binding slightly more than G50E.

I then asked whether these lesions, when isolated from S195P in an otherwise wild-type protein, might exhibit hypermorphic properties. Figure 4.9 shows that the G50E and G213A proteins had a drastically increased ability to bind to ATP, retaining 3-6 times more ATP on the filter than wild-type FtsA. I then asked whether FtsA* (R286W), like G50E and G213A, might bind ATP better than wild-type FtsA, because FtsA activity on FtsZ *in vitro* was not observed with wild-type FtsA but only with the FtsA* protein (Beuria et al., 2009;

Osawa and Erickson, 2013). As predicted, purified FtsA* also showed a significant (~5-fold) increase in its ability to bind to ATP compared to wild-type FtsA. These data indicate that a decrease in ATP binding by FtsA is correlated to a decrease in FtsA-FtsZ binding (at least for FtsA27), and an increase in FtsA ATP binding is correlated to an increased FtsA-FtsZ binding (as seems to be the case for G50E and R286W).

Purified *E. coli* FtsA can hydrolyze ATP

Given its ability to bind ATP, I then investigated whether my preparation of FtsA could hydrolyze ATP. After extensive optimization of protein purification (Figure 4.10) and assay conditions (described in Experimental Procedures) I were able to detect significant ATPase activity as measured by a sensitive phosphate release assay (Figures 4.11 and 4.12). Interestingly, I found that of the protein concentrations I tested, 0.25 μM His_6-FtsA produced the highest ATPase activity, ~3 mol ATP/mol FtsA/min. When the protein concentration was increased to 0.5 or 1 μM, the specific ATPase activity decreased (Figure 4.11A), such that 1 μM His_6-FtsA had about half the specific hydrolysis activity (~1.5 mol ATP hydrolyzed per mol FtsA per minute) of 0.25 μM FtsA. I also found that FtsA ATP hydrolysis required metal cations, with Mg^{++} preferred over Ca^{++} (Figure 4.12A). In addition, increasing Mg^{++} concentrations inhibited ATPase activity (Figure 4.12B) and ATPase activity increased with temperature, as expected (Figure 4.12B & C).

FIG 4.10

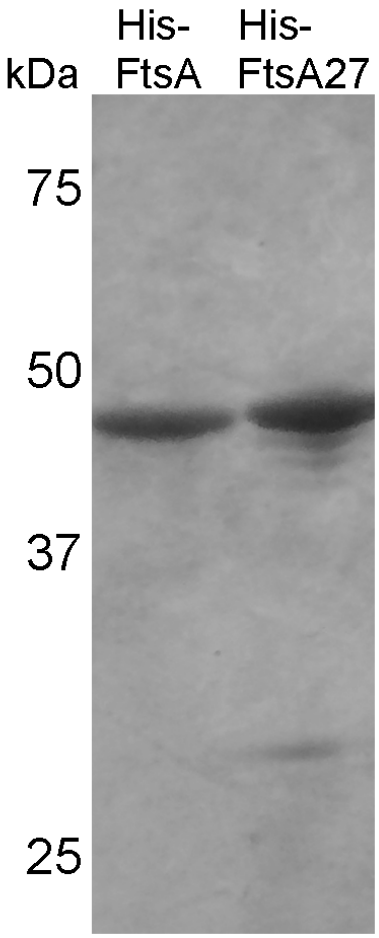

Figure 4.10: Purified His_6-FtsA and His_6-FtsA27. Shown is a Coomassie-stained gel of His_6-FtsA (A) and His_6-FtsA27 (A27) after purification and SDS-PAGE, migrating between the 37 kDa and 50 kDa protein markers (M). Proteins of similar purity were used for all biochemical assays described in this study.

FIG 4.11

A

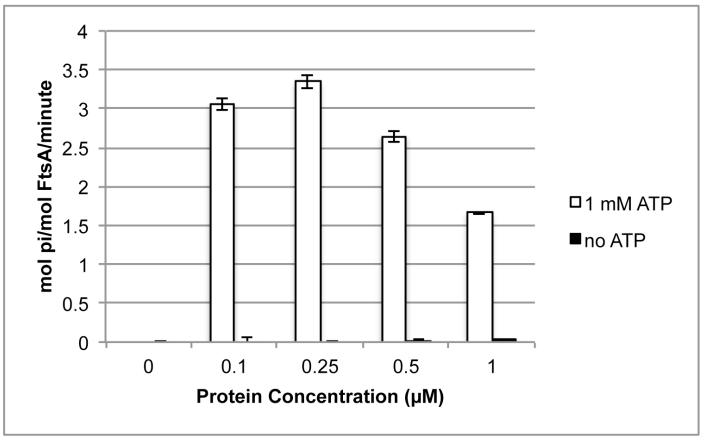
mol pi/mol FtsA/minute
4
3.5
3
2.5
2
1.5
1
0.5
0
0
0.1
0.25
0.5
1
Protein Concentration (μM)
1 mM ATP
no ATP

B

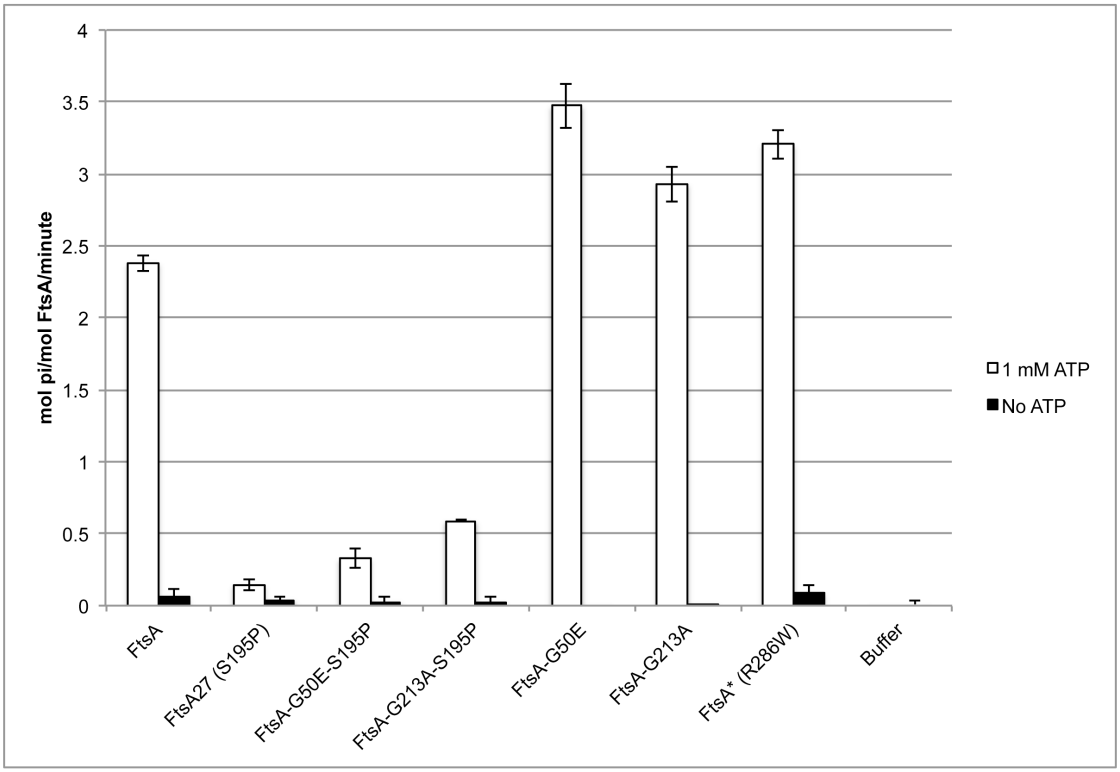
mol pi/mol FtsA/minute
4
3.5
3
2.5
2
1.5
1
0.5
0
FtsA
FtsA27 (S195P)
FtsA-G50E-S195P
FtsA-G213A-S195P
FtsA-G50E
FtsA-G213A
FtsA* (R286W)
Buffer
1 mM ATP
No ATP

Figure 4.11: FtsA and FtsA mutants display ATPase activity. A) Rates of wild-type FtsA ATPase activity with indicated concentrations of FtsA protein and ATP. B) Rates of ATPase activity with 0.25 μM of indicated FtsA protein.

FIG 4.12

A

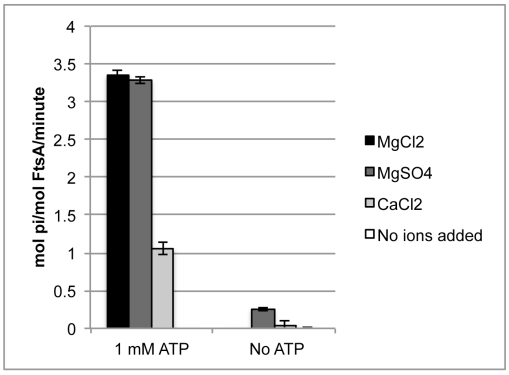
mol pi/mol FtsA/minute
4
3.5
3
2.5
2
1.5
1
0.5
0
1 mM ATP
No ATP
MgCl2
MgSO4
CaCl2
No ions added

B

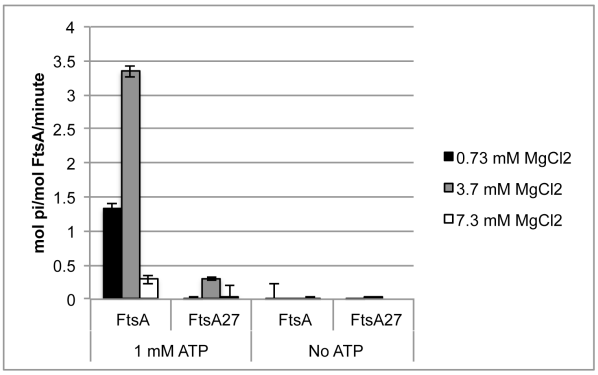
mol pi/mol FtsA/minute
4
3.5
3
2.5
2
1.5
1
0.5
0
FtsA
FtsA27
FtsA
FtsA27
1 mM ATP
No ATP
0.73 mM MgCl2
3.7 mM MgCl2
7.3 mM MgCl2

C

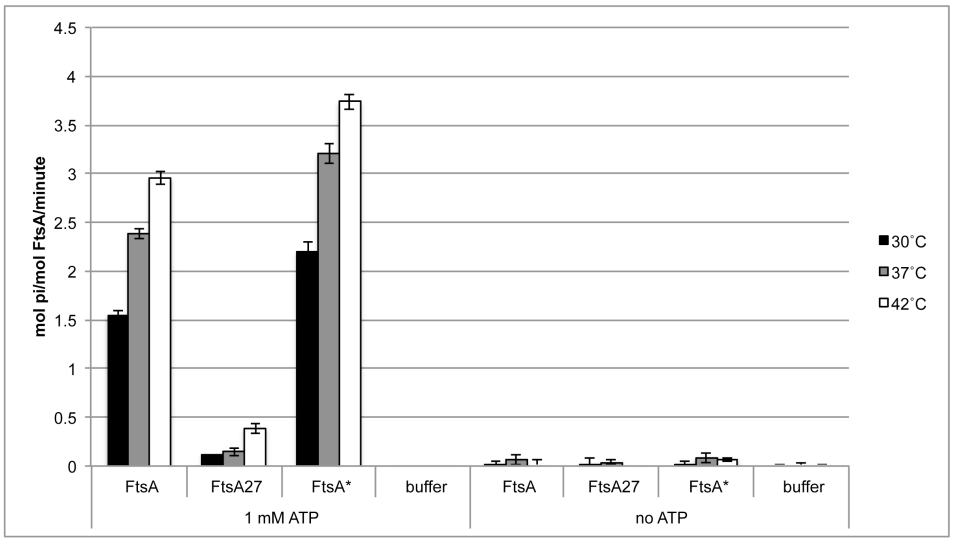
mol pi/mol FtsA/minute
4.5
4
3.5
3
2.5
2
1.5
1
0.5
0
FtsA
FtsA27
FtsA*
buffer
FtsA
FtsA27
FtsA*
buffer
1 mM ATP
no ATP
30˚C
37˚C
42˚C

Figure 4.12: Rates of FtsA ATPase activity depend on type and amount of metal ions as well as temperature. A) Rates of ATPase activity by wild-type FtsA in the presence of indicated metal ions. B) Rates of ATPase activity by wild-type FtsA and FtsA27 with the indicated concentration of $MgCl_2$. C) Rates of ATPase activity of indicated FtsA protein at indicated temperatures. All reactions contained 0.25 μM protein.

Because ATP binding is a prerequisite for ATP hydrolysis, I reasoned that ATPase activity of my mutant proteins might correlate with the degree of ATP binding. As expected, the rate of hydrolysis from FtsA27 protein was extremely low, between 0.1 and 0.5 mol ATP/mol FtsA/min (Figure 4.11B, 4.12B-C). Although low, this was slightly higher than the spontaneous rate of ATP hydrolysis under the conditions I used. This indicates that FtsA27 may be able to bind low levels of ATP that could not be detected in the ATP binding assay, and that it can hydrolyze this low amount of ATP. Interestingly, the FtsA27 suppressor proteins FtsA-G213A-S195P and FtsA-G50E-S195P showed an increase in ATPase activity compared to FtsA-S195P alone, but the levels were still significantly lower than wild-type levels (Figure 4.11B). Because proteins with the individual residue changes R286W, G50E and G213A (separated from S195P) displayed 3-6 times more ATP binding than the wild-type protein, I thought I would detect a similar increase in the rates of hydrolysis. Although I did observe an increase, it was only about 1.5 times greater than the rate of ATP hydrolysis from the wild-type protein (Figure 4.11B).

My data show that ATP binding by the various mutants roughly parallels ATP hydrolysis. Despite binding to ATP as efficiently as wild-type FtsA, G213A-S195P and G50E-S195P display very low levels of ATP hydrolysis, supporting the notion that ATP binding may be a more important regulator of FtsA activity on the Z ring than ATP hydrolysis (Beuria et al., 2009; Loose and Mitchison, 2014; Osawa and Erickson, 2013; Szwedziak et al., 2012). However, it is also possible that other factors *in vivo* can stimulate FtsA ATPase activity above the levels I

can detect *in vitro*, or that the conditions of my assay can be further optimized. I attempted to identify the former by adding additional purified divisome proteins or protein domains to the ATPase activity assay, but so far I have not identified any factor or combination of factors that stimulate further ATP hydrolysis by FtsA (data not shown).

DISCUSSION

In this work, I characterized the *ftsA27* thermosensitive mutant, which has been previously used to inactivate FtsA in genetic experiments. Like all other known thermosensitive alleles of *ftsA, ftsA27* has a point mutation in or near the ATP binding site, and I confirmed that the FtsA27 protein is defective at binding and hydrolyzing ATP *in vitro*. *In vivo* conditions for ATP binding may be more favorable, allowing FtsA27 to be at least partially functional at 30˚C. My results suggest that FtsA27 is also defective at binding to FtsZ at the permissive temperature, but the defect is likely exacerbated at higher temperatures, leading to delocalization of FtsA27 from the Z ring. Together, my genetic and biochemical data are consistent with the idea that ATP enhances the ability of FtsA to bind FtsZ (Beuria et al., 2009; Loose and Mitchison, 2014).

The genetic characteristics of the *ftsA27* suppressor mutants are summarized in Figure 4.13. They fall roughly into two different classes: (1) mutants that likely affect ATP binding directly and (2) mutants that likely affect protein-protein interaction directly. The G213A and P251L lesions, which correspond to Y215 and F253 in *T. maritima*, are the closest to the ATP binding site, and fall into the first category. F253 is near to, although not part of, the active site. Y215, on the other hand, is in the active site and is predicted to make contacts with the alpha, beta, and gamma phosphates of ATP (van den Ent and Löwe, 2000). According to my genetic and cytological assays, the G213A and P251L mutant proteins of *E. coli* restore FtsA27-FtsZ binding to wild-type levels,

but do not further enhance these interactions. These results add *in vivo* support for the idea that ATP binding by FtsA is required for FtsA-FtsZ interaction. However, my results with G213A suggest that increased ATP binding above wild-type levels does not correlate with significantly increased FtsZ binding above wild-type levels.

The G50E and T249M lesions at the FtsA-FtsA interface (Szwedziak et al., 2012) fall into the second category and probably affect oligomerization directly. Both of these mutants display increased affinity for FtsZ by my genetic assays, and bypass the requirement for *zipA* more efficiently than any of the other *ftsA27* suppressor mutants. This phenotype is consistent with decreased FtsA oligomerization (Pichoff et al., 2012), but the ability of these FtsA mutants to self-interact still needs to be tested directly. The striking increase in ATP binding and hydrolysis by proteins with lesions at the dimer interface suggests that decreased oligomerization may lead to enhanced ATP binding.

FIG 4.13

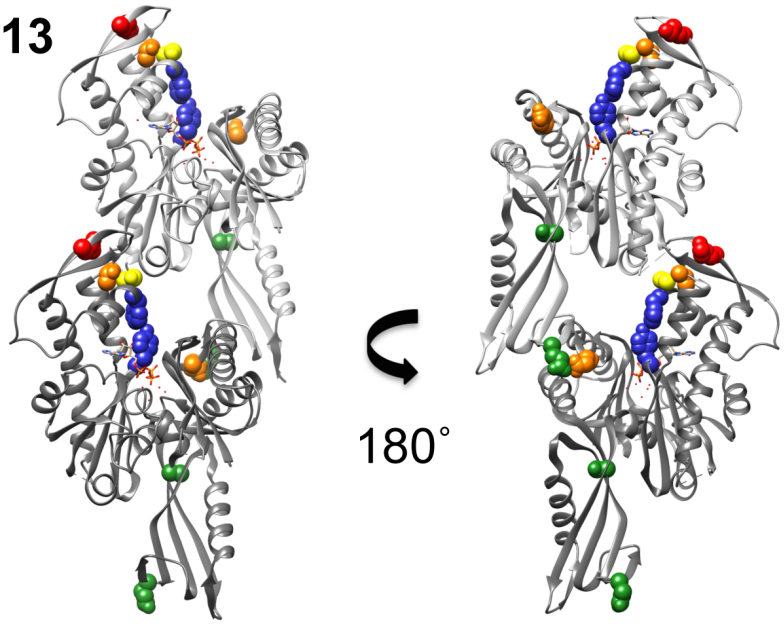

FtsA Lesion	Restores wild-type resistance to ZipA overproduction	Provides extra resistance to ZipA overproduction	Suppresses R300E defect	*zipA* bypass
R286W	+++	+++	+	+++
G50E	+++	+	+++	++
T249M	+++	+	+++	++
P250T	+++	++	++	+
Y139D	+++	-	++	+
H159L	+++	-	++	+
P251L	+++	-	-	-
G213A	+++	-	-	-

Figure 4.13: Summary of genetic characteristics of lesions that suppress *ftsA27*. Shown is a table summarizing the genetic characteristics of lesions that suppress FtsA27, as well as the characteristics of R286W. Alleles that phenotypically group together are indicated by color. The location of each lesion is shown in the structures above the table in the corresponding colors.

Despite exhibiting some phenotypes associated with increased interaction with FtsZ *in vivo* according to my assays, the H159L, P250T and Y139D proteins all have intermediate phenotypes, with H159L and Y139D being more similar to the mutants in category 1, and P250T being more similar to the mutants in category 2. Overall, my results suggest that gain-of-function mutations in the ATP binding site have a considerable effect on ATP binding and hydrolysis, but my genetic experiments suggest these three mutations only mildly affect FtsA-FtsZ interactions. Conversely, mutations closer to the FtsA-FtsA interface had significant impacts on both ATP binding and FtsA-FtsZ interaction. Work by others suggests that mutations in some of the residues I analyzed or adjacent residues also significantly affect FtsA-FtsA interactions (Hsin et al., 2013; Pichoff et al., 2012), as would be predicted by their location. This suggests to us that FtsA self-interaction strongly influences, and probably competes with, its ability to bind ATP and interact with FtsZ. The combination of biochemical and genetic data from this study led us to propose a new model for early Z ring formation in *E. coli* that incorporates experimental data from FtsA ATP binding, oligomerization and interactions with FtsZ (Figure 4.14A).

FIG 4.14

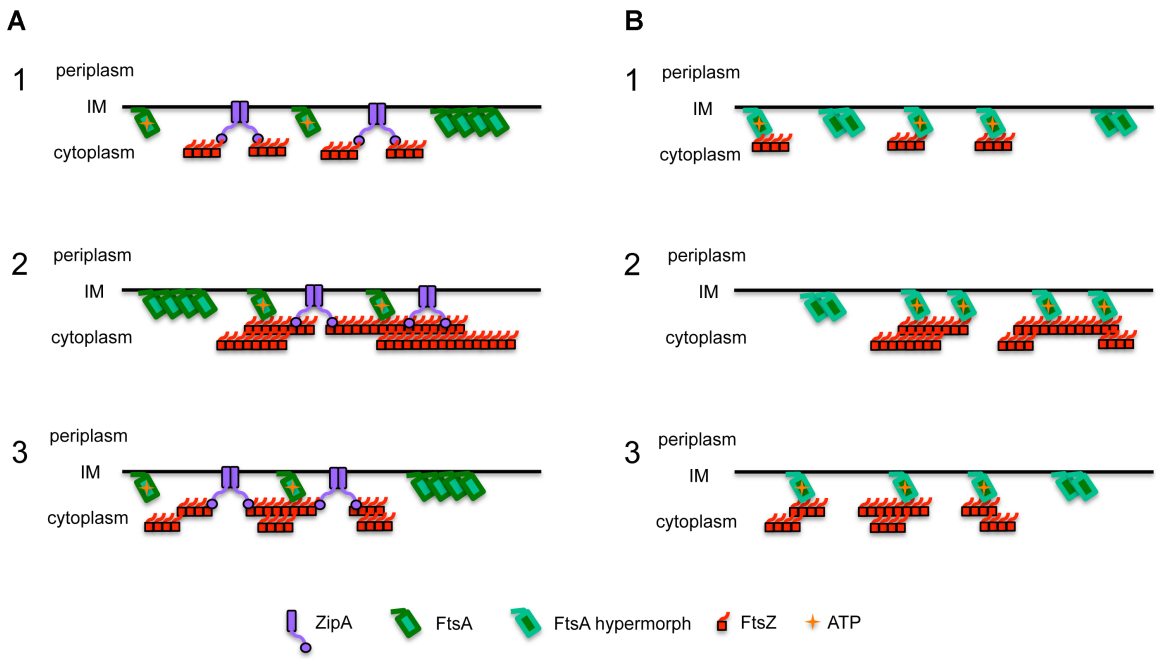

Figure 4.14: Model of Z ring formation and disassembly with and without ZipA. (A) (1) ZipA encourages bundling and polymerization of FtsZ at midcell, (2) enhancing the binding of monomeric, ATP-bound FtsA to FtsZ polymers. (3) Nucleotide binding and hydrolysis by FtsA and FtsZ promotes dynamic turnover of subunits and controlled disassembly of the divisome. (B) In the absence of ZipA, the hypermorphic FtsA mutant needed for survival is more monomeric and can bind FtsZ (and ATP) more efficiently, without the need for ZipA to promote bundling and polymerization.

The fact that FtsA27 can divide cells quite normally at permissive temperatures despite its defect in ATP binding and probable weaker interaction with FtsZ supports the idea that other divisome factors such as ZipA have overlapping functions. ZipA, apart from its membrane tethering properties, likely functions mainly to keep FtsZ bundled and polymerized in order to promote FtsA-FtsZ binding during early stages of Z ring formation. I suggest that mutants of FtsA that can bypass ZipA do so by increasing the ability of FtsA to bind to the Z ring, with decreasing oligomerization as one pathway towards this end (Figure 4.14B). For the most well-characterized of the ZipA bypass suppressors, R286W, this comes at the cost of circumventing a cell size checkpoint, as R286W cells divide at too small a size (Geissler et al., 2007; Pichoff et al., 2012). This is consistent with a role for ZipA in managing the earliest stages of proto-ring assembly, possibly suppressing FtsZ treadmilling until the ring is more mature (Loose and Mitchison, 2014).

As *zipA* is only conserved in the gamma-proteobacteria, my model suggests that in other classes of bacteria, (i) FtsA-FtsZ interactions may be stronger and do not require a ZipA-like protein to promote their interaction; (ii) FtsZ may polymerize and/or bundle more efficiently *in vivo,* allowing FtsA to interact more efficiently; or (iii) other bundling proteins perform the function of ZipA and promote FtsZ polymerization and FtsA-FtsZ interactions.

Finally, I have shown that *E. coli* FtsA does indeed hydrolyze ATP, with the ATPase activity of various mutant proteins correlating with ATP binding activity. This raises another question: What is the role of FtsA ATP hydrolysis?

By using a non-hydrolyzable ATP analog, Loose & Mitchison (2014) showed that ATP hydrolysis by FtsA was not essential for dynamic FtsA-FtsZ interactions *in vitro*. However, there are several other possibilities to consider. One is that ATP hydrolysis by FtsA provides energy for the constriction of the divisome. Another could be that ATP hydrolysis leads to conformational changes in FtsA that allow it to recruit downstream divisome proteins in its ADP-bound form. Interestingly, FtsA* displays increased ATP binding and hydrolysis *in vitro* as well as increased subunit turnover at the Z ring (Geissler et al., 2007). Future work will attempt to determine if the increase in turnover is due to an increase in ATP binding or ATP hydrolysis. Mutants with hydrolysis defects, but not ATP binding defects, may be able to uncouple the role of ATP binding and ATP hydrolysis. This work will continue to drive our understanding of bacterial cytokinesis.

Chapter 5: Other defects caused by FtsA active-site mutants

INTRODUCTION

Several lines of evidence indicate that FtsA-FtsZ interactions are regulated, at least in part, by the ability of FtsA to bind ATP (Herricks et al., unpublished; Loose and Mitchison, 2014; Osawa and Erickson, 2013). Chapter 4 of this dissertation describes the characterization of *ftsA27* and its intragenic suppressors, which has led to a model suggesting that when FtsA is bound to ATP it can more tightly associate with the Z ring. This supports recent *in vitro* work, which showed that ATP enhanced the interaction of FtsA and FtsZ on membranes (Loose and Mitchison, 2014; Osawa and Erickson, 2013). Furthermore, the location of the intragenic suppressors of FtsA27 implies that FtsA self-association is affected by its ability to bind ATP.

This chapter presents a study of other FtsA variants with lesions in the ATP binding site in an effort to further elucidate the role of ATP in FtsA function. One of the mutants I characterize is *ftsA12*(ts). As with the *ftsA27*(ts) allele, I was able to take advantage of the capability to inhibit *ftsA12*(ts) function by increasing the growth temperature of cells from 30˚C to 42˚C. Because FtsA12 is also known to delocalize from the divisome at the non-permissive temperature (Addinall et al., 1996), we hypothesized that it has defects similar to FtsA27. However, my results indicate that these two proteins have different defects.

In addition I created site-directed point mutations that mapped to the ATP-binding site of FtsA in an attempt to create mutants that may be partially functional, but not temperature sensitive. To do this, I targeted residues E14 and

K19, predicting that these residues are important for ATP hydrolysis, rather than ATP binding. My results indicate that FtsA proteins containing lesions at E14 or K19 display defects that are distinct from each other and from FtsA12 and FtsA27. Further study of these and other FtsA mutants should allow us to refine current models of FtsA function and the role of ATP in FtsA activity.

RESULTS

Intragenic suppressors of *ftsA12* suggest that FtsA12 is deficient in multiple protein-protein interactions in addition to ATP binding/hydrolysis

To learn more about the defects of *ftsA* temperature-sensitive alleles that encode proteins with lesions at or near the ATP binding site, I investigated *ftsA12*(ts). A single point mutation in *ftsA12* changes residue A188 to a valine (Table 4.1). Similar to residue S195 (the residue changed in the FtsA27 protein), A188 is predicted to be located at the Mg^{++} ion-binding pocket based on the *T. maritima* FtsA crystal structure (Table 4.1 and Figure 4.1) (van den Ent and Löwe, 2000). To determine if the defect of *ftsA12* is similar to that of *ftsA27*, we first tested whether it could localize at the non-permissive temperature. As with FtsA27, previous work has shown that FtsA12 delocalizes from Z rings after cells were grown at 42˚C for 30 minutes, while FtsZ remains localized to potential sites of division (Addinall et al., 1996). We confirmed these results (Figure 5.1A) and showed that FtsA12, like FtsA27, delocalizes within 5 minutes after the temperature shift (Figure 5.1B).

FIG 5.1

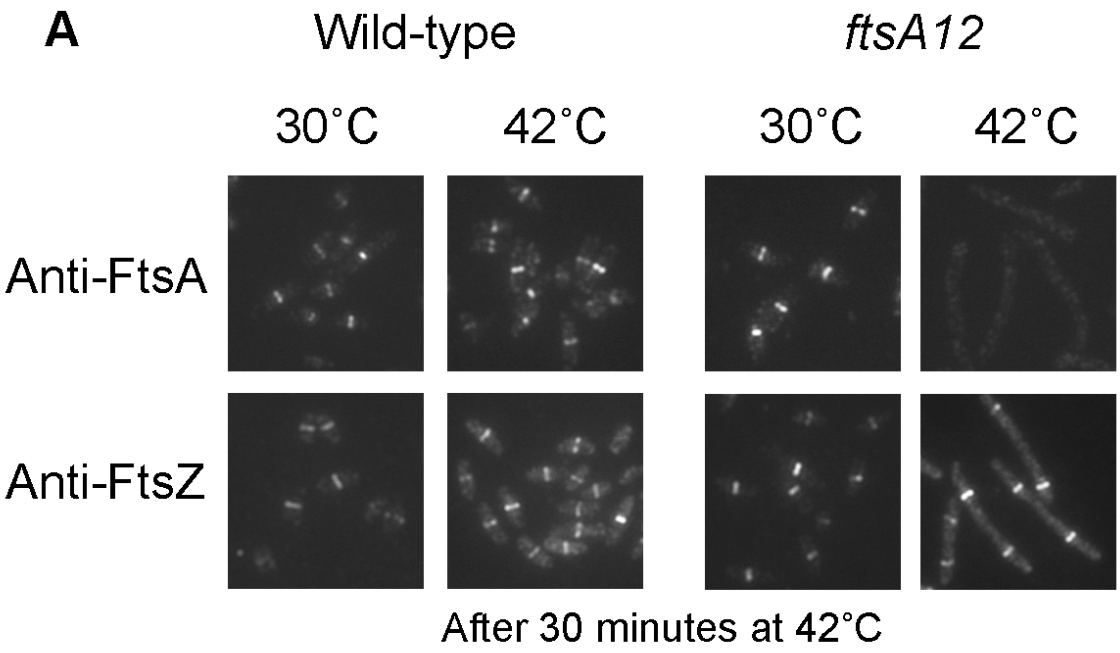

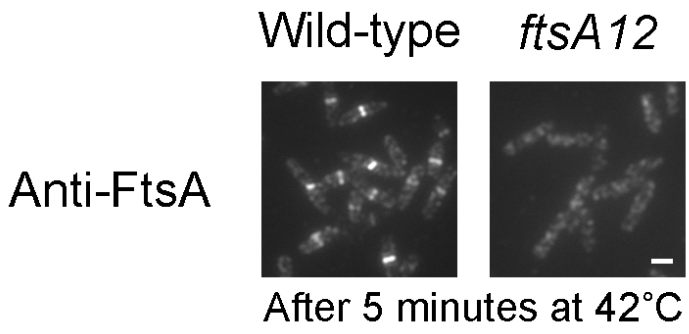

Figure 5.1: FtsA12 delocalizes from the Z ring at high temperatures. Shown are anti-FtsA and anti-FtsZ IFM images of wild-type and *ftsA12* cells grown at the indicated temperatures. Cells were shifted from 30˚C to 42˚C for 30 minutes (A) or 5 minutes (B) before fixation. Scale bar is 2 μm. Images in panels A and B are the same scale. Diep Nguyen performed the IFM in panel A.

I then selected for intragenic suppressors of *ftsA12* (Figure 5.2) as I did for *ftsA27*. Because S195 and A188 map to the same region of FtsA and both proteins delocalize after 5 minutes at the non-permissive temperature, I thought I might identify intragenic suppressor mutations of *ftsA12* that were similar to those isolated as intragenic suppressors of *ftsA27* (described in Chapter 4). I did not isolate the same suppressors, although I do not expect that the screen was saturating. As expected, I did find mutations that resulted in lesions at the ATP-binding site, A18S and A18V. A18 of *E. coli* FtsA corresponds to R18 of *T. maritima* FtsA, and residues 16-19 of *T. maritima* FtsA make up one of two loops that bind the ATP phosphate moiety (van den Ent and Löwe, 2000).

In addition, I found mutations resulting in lesions in subdomain 2B. One of the lesions in subdomain 2B is P299A, which is located on helix H8 adjacent to the highly conserved R300 residue. R300 has been shown to be a critical residue involved in FtsA-FtsZ interactions (Pichoff and Lutkenhaus, 2007; Szwedziak et al., 2012). P299 of *E. coli* FtsA corresponds to A300 of *T. maritima* FtsA, located next to the conserved arginine residue at position 301. The location of P299 suggests that it may directly affect FtsA-FtsZ interactions. The other lesion in the 2B subdomain is G266V. G266 corresponds with the *T. maritima* residue Y268, which maps to an unstructured region that links strand S12 with helix H7 (van den Ent and Löwe, 2000). Residues in helix H7 are important for positioning the adenosine in a hydrophobic pocket (van den Ent and Löwe, 2000). Strand S12 is located near the FtsA-FtsA and the FtsA-FtsZ

interface (Szwedziak et al., 2012). This suggests that altering G266 could alter FtsA's affinity for ATP, FtsZ or itself.

Two *ftsA12* intragenic suppressors mapped to subdomain 1C and correspond to residue changes E102G and V113L. This subdomain is involved in FtsA self-interactions and recruitment of downstream division proteins (Busiek et al., 2012; Corbin et al., 2004; Rico et al., 2004; Szwedziak et al., 2012). E102 corresponds to *T. maritima* FtsA residue E101, which is located at the bottom of the 1C subdomain on an unstructured region that links helix H2 with strand S5 and is very close to the FtsA-FtsA interface (Szwedziak et al., 2012). This indicates that E102 could be involved in either FtsA-FtsA interaction or recruitment of downstream division proteins. V113 corresponds to *T. maritima* FtsA residue E112, which is located on helix H2 (van den Ent and Löwe, 2000). This helix faces out and away from the FtsA-FtsA interface (Szwedziak et al., 2012) and so it may be more likely that V113 is involved in recruiting downstream proteins. However, I cannot rule out that a slight conformational shift in helix H2 of *E. coli* FtsA compared to *T. maritima* FtsA affects FtsA-FtsA interactions.

I have shown that lesions that map to diverse regions of FtsA, including the ATP-binding site and subdomains 2B and 1C, can suppress the defects of A188V. These results indicate that the suppressors of *ftsA12* may restore protein-protein interactions in addition to ATP binding/hydrolysis.

FIG. 5.2

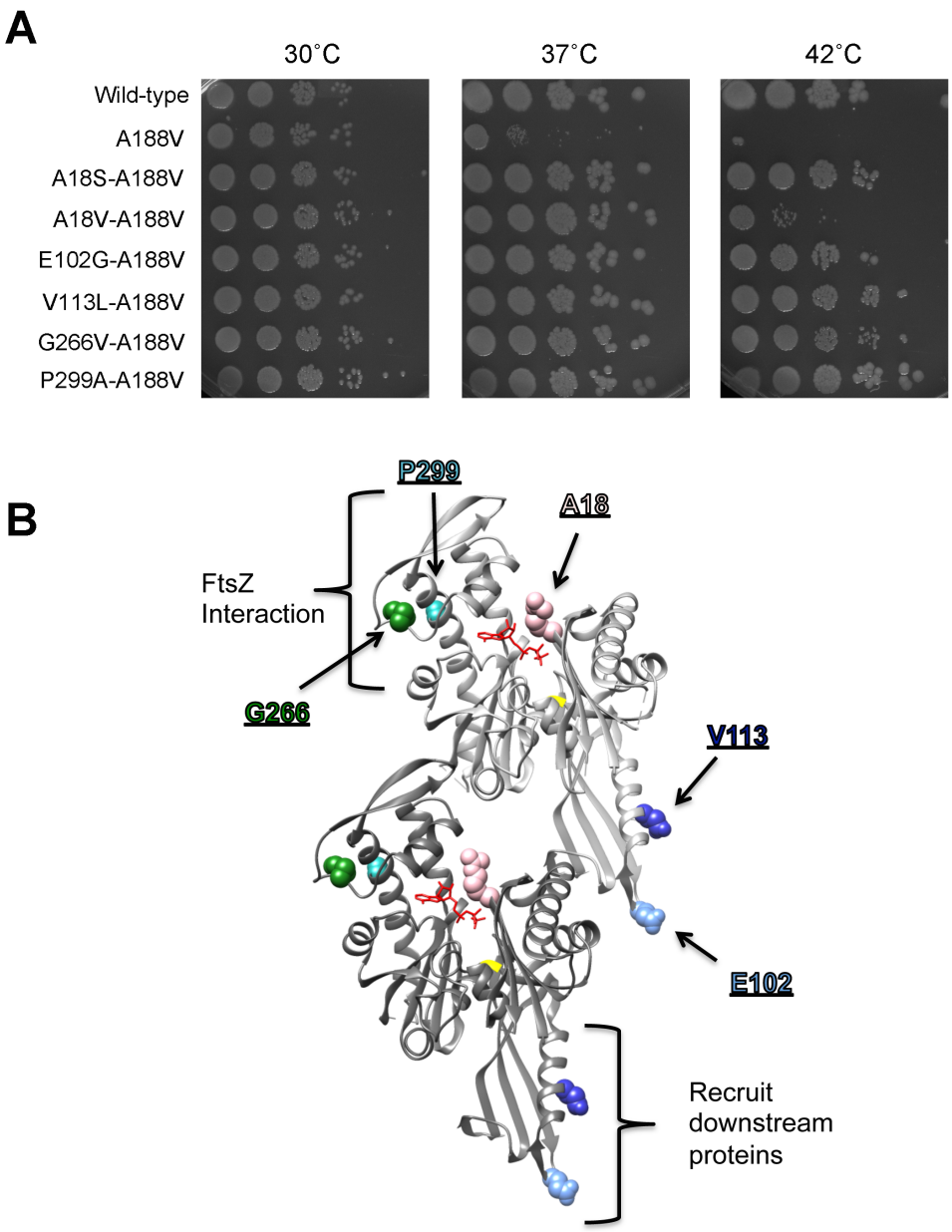

Figure 5.2: Intragenic suppressors of *ftsA12* restore thermoresistance and map to different regions of FtsA. A) Serial dilution growth assay of wild-type *E. coli* and cells expressing chromosomal *ftsA12* or an intragenic suppressor of *ftsA12* spotted on plates incubated at the indicated temperatures. B) Locations of the intragenic suppressor mutations on the dimer structure of *T. maritima* FtsA.

Complementation analysis suggests that *ftsA12* and *ftsA27* have distinct defects

The lesions on FtsA12 and FtsA27 are located near each other at the Mg^{++} binding site on FtsA, and the defects of both can be suppressed by an additional lesion located in the ATP-binding site or an area involved in protein-protein interaction. This data led us to hypothesize that *ftsA12* and *ftsA27* have similar defects. Since my screens for suppressor mutations were likely not saturating, I decided to combine mutations that could suppress *ftsA12 in cis* with *ftsA27*. Double and single mutants were created by site-directed mutagenesis and expressed from an IPTG-inducible *trc* promoter on plasmid pWM2784 in an *ftsA* depletion strain (WM1281). A frameshift insertion interrupts the chromosomal copy of *ftsA* in this strain. Wild-type *ftsA* exists on a plasmid that also contains a *repA*(ts) allele. This construct allows depletion of wild-type *ftsA* upon temperature shift from 30˚C to 42˚C. Conveniently, shifting to 42˚C also allowed us to determine if the temperature-sensitive defects of *ftsA12* or *ftsA27* could be suppressed by the additional mutations under these conditions.

Using this system I tested the ability of three *ftsA12* suppressor mutations (one from each subdomain: A18V, V113L, and P299A), to suppress *ftsA27* (Table 5.1). When grown at 30˚C without IPTG, all strains survived as expected. IPTG was added to compare the toxicity of the mutants to the toxicity of wild-type *ftsA*. I saw that nearly all of the alleles I tested were toxic at 30˚C, except for A18V and the A18V-A188V double mutant. At 42˚C, V113L and V113L-A188V were also less toxic. The ability of A18V to reduce toxicity seems to be dominant

when combined with A188V (*ftsA12*), but not S195P (*ftsA27*). Surprisingly, only A18V was able to suppress the defects of *ftsA27* at 42˚C. Inducing the construct with IPTG seemed to improve complementation, and surprisingly did not cause toxicity. These results suggest that FtsA12 and FtsA27 share defects binding ATP, but that they also have other distinct defects.

FtsA12 is less stable *in vivo* than wild-type FtsA or FtsA27

The reason that overexpression of *ftsA* is toxic is not known; neither is the reason that some point mutations are able to make *ftsA* less toxic. One possible explanation for lack of toxicity when expressing *ftsA* alleles ectopically is lower levels of expression. To determine if this was the case for the any of the non-toxic alleles displayed in Table 5.1 I performed Western blot analysis to determine if protein levels were the same (Figure 5.3). For simplicity, the plasmids were transformed into a wild-type *E. coli* background (WM1074) and expression from the *trc* promoter was induced with IPTG. Both FtsA27 and FtsA12 seemed to be produced at slightly lower levels than wild-type FtsA when cells were grown at 30˚C. At 42˚C, levels of FtsA27 were higher than they were at 30˚C, but levels for FtsA12 fell further. Strains expressing *ftsA* alleles containing a suppressor mutation were produced at levels comparable to wild-type FtsA.

Table 5.1: Not all mutations that suppress *ftsA12* can suppress *ftsA27*

***ftsA* allele expressed**	**30˚C Control**	**30˚C + IPTG**	**42˚C**	**42˚C + IPTG**
Empty vector	++++	++++	--	--
Wild-type *ftsA*	++++	--	++++	--
A18V	++++	++++	++++	++++
V113L	++++	+	++++	+++
P299A	++++	--	++++	-
A188V (*ftsA12* ts)	++++	--	--	--
A18V-A188V	++++	++++	++	++++
V113L-A188V	++++	--	++	+++
A188V-P299A	++++	--	+++	--
S195P (*ftsA27* ts)	++++	--	--	--
A18V-S195P	++++	--	+	++++
V113L-S195P	++++	--	--	--
S195P-P299A	++++	--	--	--

Data is shown for serial dilution growth assays. Specified alleles were expressed in WM1281 from an IPTG inducible promoter with no IPTG added (non-toxic, complementing levels of wild-type *ftsA* expressed) or 1 mM IPTG (toxic, non-complementing levels of wild-type *ftsA* expressed). 4 (+) indicates cells could grow at a 10^{-4} dilution; 3 (+), 10^{-3} dilution; 2 (+), 10^{-2} dilution; and 1 (+),10^{-1} dilution. (--) indicates that cells were not viable under the specified conditions.

FIG. 5.3

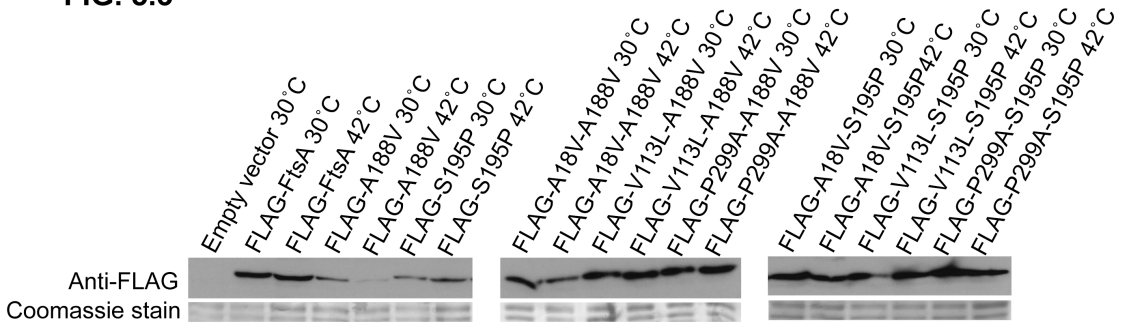

Figure 5.3: FtsA12 levels are lower than wild-type FtsA when produced from an exogenously expressed allele. Anti-FLAG Western blot analysis of indicated proteins produced from exponentially growing WM1074 cells at 30˚C and after temperature shift to 42˚C for 1 hour. Alleles are expressed from the *trc* promoter of pWM2784 (which also contains a *flag*-tag) and induced with 1 mM IPTG. Coomassie stain is shown as a loading control.

I hypothesized that FtsA12 is also unstable *in vivo* when expressed from its native chromosomal locus with its native promoter. To test this, I probed for FtsA on Western blots from wild-type, *ftsA12,* and *ftsA27* cells (WM1074, WM1115, and WM4107, respectively). I looked at protein levels while cells were growing at 30˚C and at several time points after shifting growth to 42˚C. At steady-state, levels of FtsA12 dropped only slightly after 30 minutes at 42˚C (Figure 5.4A). To determine if unstable protein was being degraded and replaced by newly synthesized protein, I performed a similar assay using chloramphenicol to stop protein synthesis. Protein levels were measured at time zero (T0) after adding chloramphenicol to cells growing exponentially at 30˚C. Part of the culture was then shifted to 42˚C and samples collected at 15, 30, and 60 minutes. The rest of the culture continued to grow at 30˚C and samples were collected after 3 hours. Results of this assay showed that both FtsA (ts) proteins were less stable than wild-type FtsA at 42˚C, but FtsA12 was also less stable at the permissive temperature (Figure 5.4B).

These results suggest that FtsA12 is very unstable *in vivo*, even at the permissive temperature. To determine if the suppressors of *ftsA12* were restoring protein stability I repeated the stability assay with the *ftsA12* suppressor strains (Figure 5.5). The stabiltiy of FtsA12 was at least partially restored by each of the suppressor mutations.

FIG. 5.4

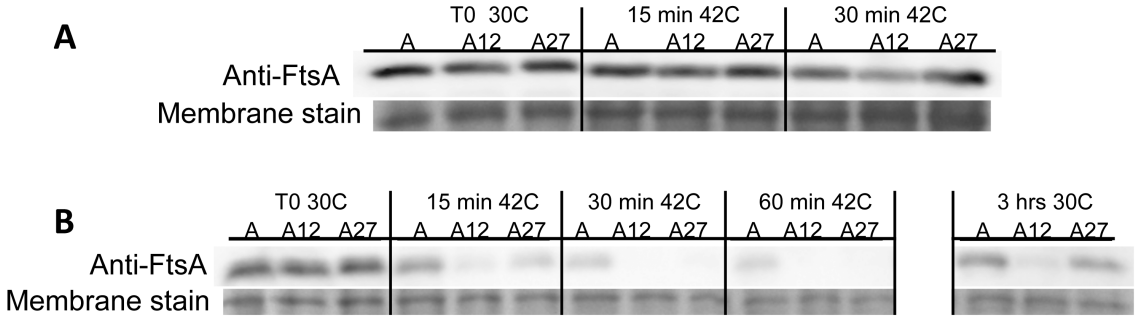

Figure 5.4: FtsA ts mutants are unstable at 42˚C compared to wild-type FtsA, but steady state levels remain similar. WM1074, WM1115, and WM4107 cells (labeled A, A12, and A27, respectively) were grown in the absence (A) or presence (B) of chloramphenicol. Protein samples were collected at indicated time points before and after temperature was shifted to 42˚C. Membranes were probed with anti-FtsA antibody. Prior to Western blot analysis, membranes were stained to show levels of total protein per sample.

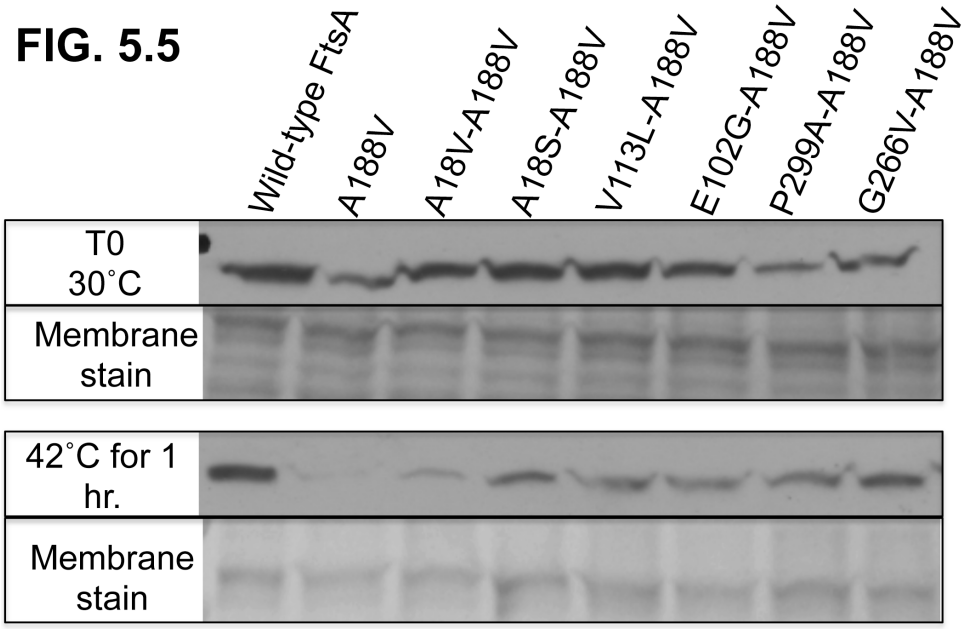

Figure 5.5: Intragenic suppressors of *ftsA12* partially restore protein stability. Strains expressing the indicated alleles from the native chromosomal locus were grown to logarithmic growth phase at 30˚C before chloramphenicol was added to inhibit protein synthesis. T0 samples were taken immediately after addition of 20 μg ml^{-1} chloramphenicol. Membranes were probed with anti-FtsA antibody. Prior to Western blot analysis, membranes were stained to show levels of total protein per sample.

Genetic and biochemical analyses of site-directed mutations (E14A and K19M) that map to the ATP-binding site of FtsA

In an effort to understand the role of ATP hydrolysis by FtsA, we attempted to isolate stable FtsA variants with lesions at the ATP-binding site that were not temperature-sensitive and had a defect in ATP hydrolysis, but not ATP binding. To do this I studied the ATP-binding site of *T. maritima* FtsA, compared it to residues from *E. coli* FtsA that are predicted to be in the ATP-binding site, and decided to target residues E14A and K19M (Figure 5.6).

E14 and K19 of *E. coli* FtsA align with D14 and A19, respectively, of *T. maritima* FtsA. I think that K19 from *E. coli* may be more analogous to K21 of *T. maritima* FtsA (Figure 5.6), despite the primary sequence alignment. These residues are located near the phosphate moiety, as well as the Mg^{++} binding pocket. We cloned the E14A and K19M mutants into plasmid pWM2784, which contains an IPTG-inducible *trc* promoter. These constructs were transformed into WM1115 (*ftsA12* ts) to test for functionality *in vivo* (Figure 5.7). E14A was extremely toxic even without IPTG induction and was not functional at 42˚C. This suggests that E14A has a dominant negative effect on the cells. K19M was also more toxic than wild-type FtsA, but not as toxic as E14A. In addition K19M was functional at 42˚C with low levels of IPTG induction. This indicates that K19M is functional and non-toxic, so I decided to further investigate its *in vivo* and *in vitro* properties.

FIG. 5.6

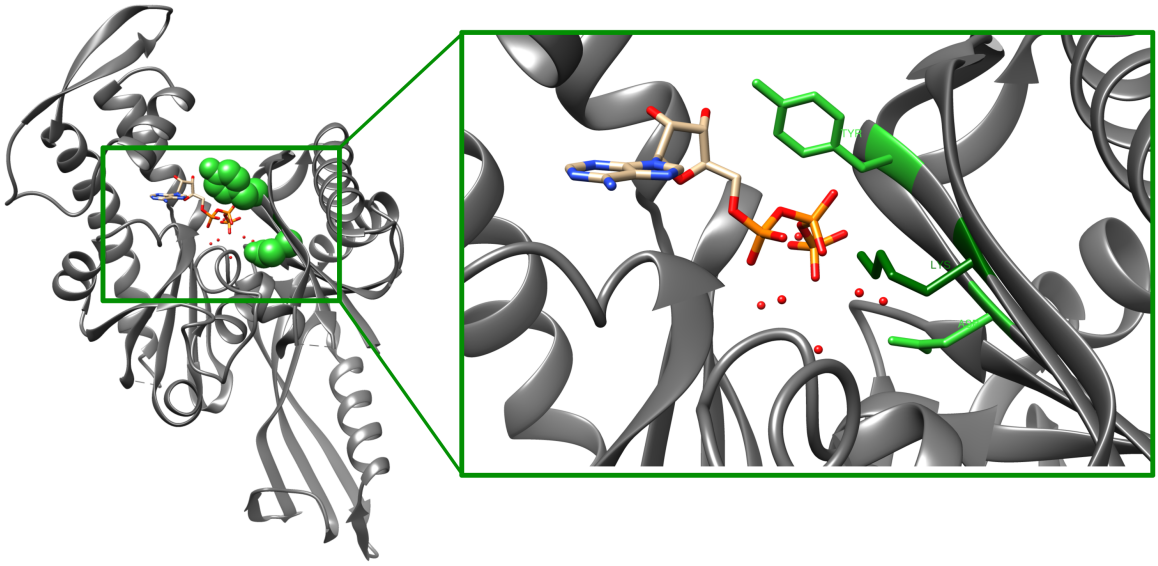

Figure 5.6: Predicted locations of E14 and K19 in the FtsA ATP-binding site. A structure of FtsA from *T. maritima* with a magnified region highlighting locations of K19M (top) or E14A (bottom) lesions is shown in lime green. The magnified region shows not only where E14 (D14 in *T. maritima*) and K19 (Y19 in *T. maritima*), but also highlights *T. maritima* K21 (could be equivalent to K19 in *E. coli*) in dark green. ATP is shown in the active site and the red dots indicate water molecules.

FIG. 5.7

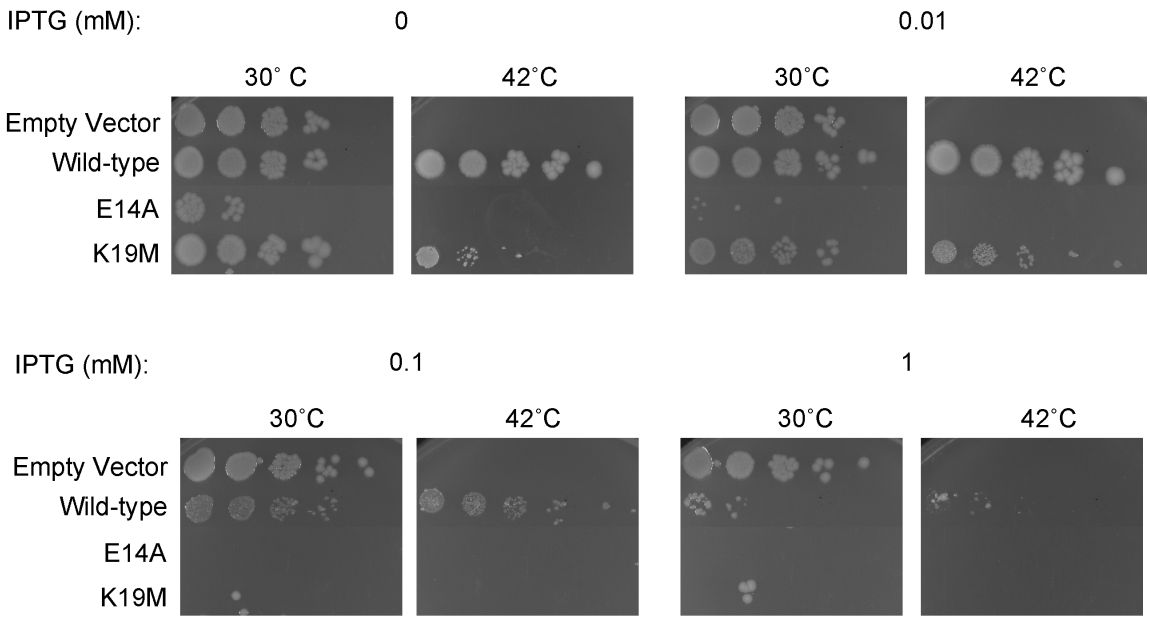

Figure 5.7: Growth of *E. coli* expressing *ftsA(E14A)* and *ftsA(K19M).* Serial dilution growth assay of indicated *ftsA* alleles that are FLAG-tagged and expressed from the IPTG inducible *trc* promoter on pWM2784 in a WM1115 *ftsA12* (ts) background. Temperatures and induction levels are indicated. Chris Evans, M.S., assisted with these growth assays.

Since K19M could complement an *ftsA12*(ts) mutant, I decided to see if it could survive as the only genetic copy of *ftsA* in the cell. To do this we introduced a frameshift mutation into the chromosomal copy of *ftsA* and expressed K19M exogenously from the *trc* promoter of pWM2784. Although these cells survived, they did not divide normally and formed very long filaments (Figure 5.8A). We compared the growth of these K19M cells to an isogenic strain that expressed wild-type *ftsA* from the *trc* promoter. Cells expressing wild-type *ftsA* appeared morphologically normal. Neither of the alleles needed to be induced with IPTG in order to promote viability, which is not surprising considering that more FtsA is produced from the uninduced *trc* promoter than from the native *ftsA* promoter (Figure 5.8B). I hypothesized that K19M has trouble localizing to the Z ring, perhaps due to decreased interaction with FtsZ. However, IFM analysis revealed that K19M localized normally to potential division sites within the filamentous cells (Figure 5.8C).

FIG. 5.8

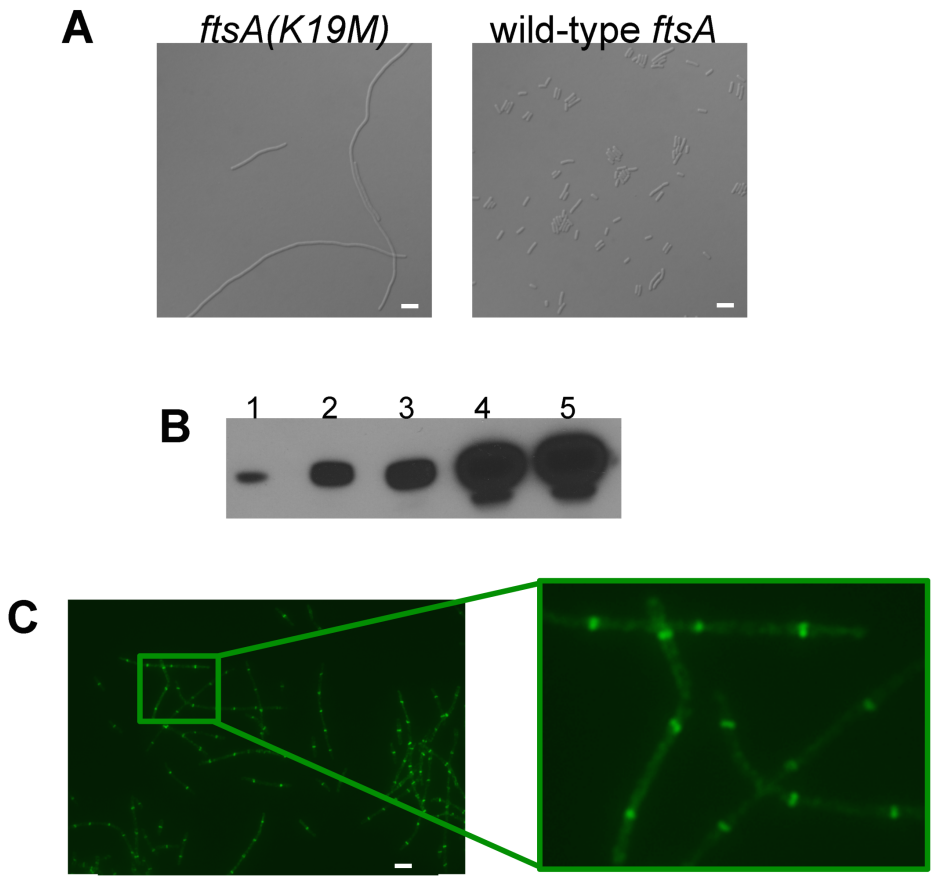

Figure 5.8: Morphology of cells expressing *ftsA(K19M)* and FtsA(K19M) localization *in vivo*. (A) DIC images of exponentially growing cells expressing either *ftsA(K19M)* or wild-type *ftsA* from the *trc* promoter of pWM2784 as the only copy of *ftsA*. (B) Anti-FtsA Western blot of WM1074 (lane 1), and cells from panel A expressing wild-type *ftsA* (lanes 2-5) with no (lane 2), 0.01 mM (lane 3), 0.1 mM (lane 4), or 1 mM (lane 5) IPTG. (C) Anti-FtsA IFM of exponentially growing cells from panel A expressing *ftsA(K19M)*. Chris Evans, M.S., performed the microscopic analyses presented in this figure. Scale bars are 2 μm.

Since K19M did not seem to have a defect in localizing to the septum but clearly caused a cell division defect, I decided to test the ability of purified His_6-tagged K19M to bind and hydrolyze ATP. ATP binding was determined using a filter-binding assay with a fluorescent ATP analog and ATP hydrolysis was tested using the EnzChek phosphate detection assay. K19M showed a decrease in ATP binding (Figure 5.9A). As expected, based on the low level of ATP binding, hydrolysis of ATP was also low (Figure 5.9B). This low rate was above the rate of spontaneous hydrolysis of ATP and increased with temperature, indicating that K19M is capable of hydrolyzing the small amount of ATP it binds. These results suggest that a defect in ATP binding is preventing K19M from being fully functional, while still localizing to the Z ring. Because K19M can localize to the Z ring, its defect in ATP binding must be preventing its function via another mechanism.

FIG. 5.9

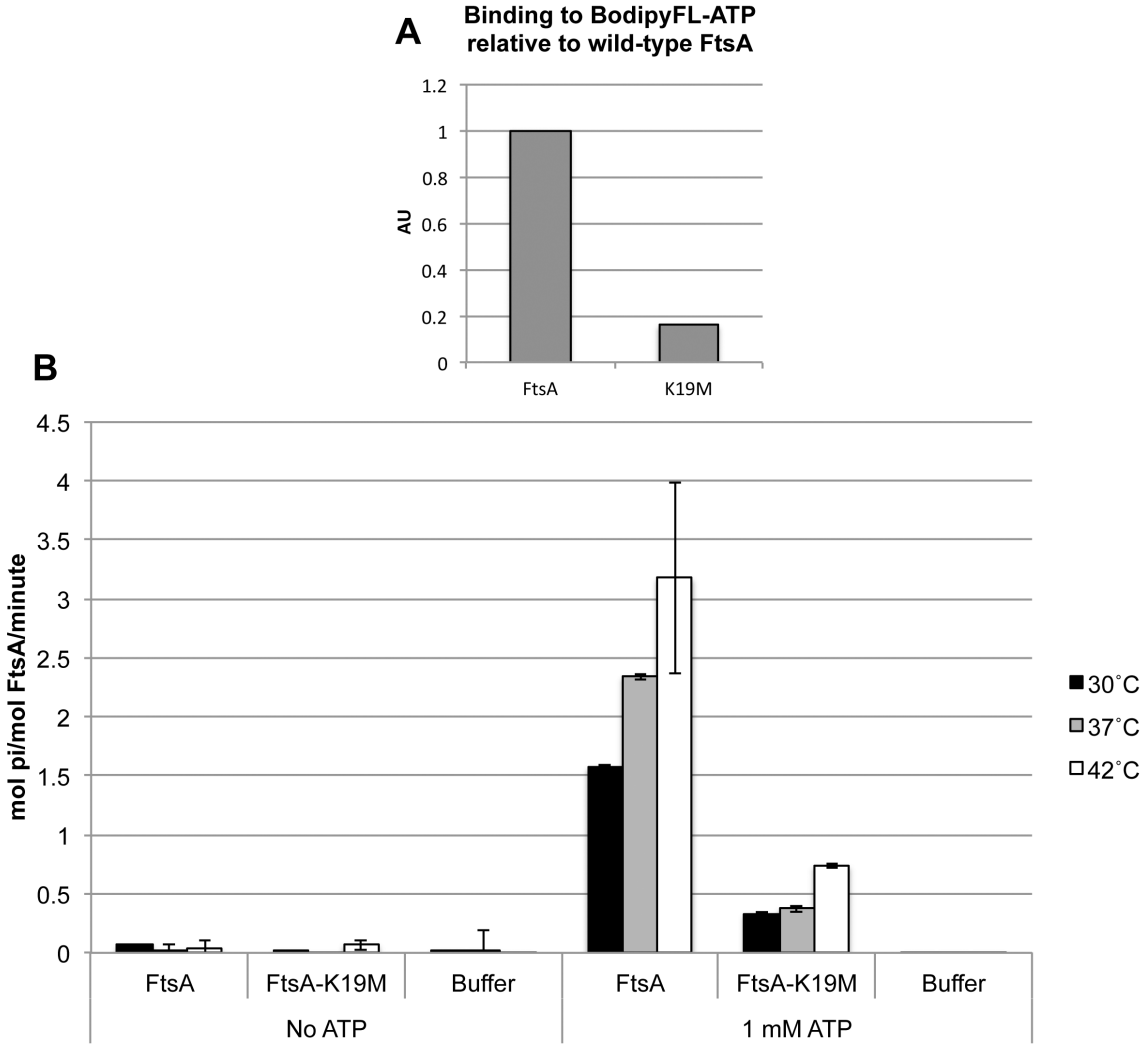

Figure 5.9: ATP binding and hydrolysis properties of FtsA-K19M. (A) ATP binding of K19M compared to wild-type FtsA; (B) ATPase rates of indicated FtsA protein at indicated temperatures. All reactions contained 0.25 μM protein. Chris Evans, M.S., assisted with the ATP hydrolysis assays.

DISCUSSION

This work suggests that different functional defects of FtsA can occur from lesions resulting in decreased ATP binding. For example, in chapter 4 I showed that FtsA27, which delocalizes from the Z ring at high temperature *in vivo* and is defective in binding ATP *in vitro,* could be suppressed by an additional lesion that either enhanced its ability to bind ATP or enhanced its ability to bind to the Z ring. The intragenic suppressors of *ftsA12* suggest that the FtsA12 protein may also have defects in binding the Z ring and/or self-associating, but Western blot analyses show that FtsA12 is unstable *in vivo* compared to wild-type FtsA. The additional lesions caused by the suppressor mutations somehow stabilize FtsA12. FtsA27 also seemed to be less stable than wild-type FtsA at high temperatures, but it was more stable than FtsA12. This indicates that defects in ATP binding result in decreased stability of FtsA.

What is most interesting about the instability of FtsA12 is the ability of lesions far away from the ATP binding site to restore its stability. This may occur for several reasons. One possibility is that these distant lesions create a more stable structure. However, I favor the idea that these lesions affect protein-protein interactions. Increasing protein-protein interactions may be enough to stabilize the protein, or could alter the conformation of FtsA to allow more efficient ATP binding, which could enhance its stability. Several protein-protein interaction assays could be used to test this idea. Conformational changes may

be more difficult to determine without structural information, but protease digestion assays may give some clues.

Preliminary genetic experiments testing for sensitivity to *zipA* overexpression suggest that FtsA12 can compete with ZipA for Z ring binding as efficiently as wild-type FtsA, and that *ftsA12* suppressors do not enhance the ability of FtsA12 to bind the Z ring (data not shown). Although these preliminary results need to be confirmed, they support my conclusion that FtsA12 and FtsA27 have distinct defects. Further evidence for this is presented in Table 5.1, which indicates that only *ftsA12* suppressor mutations that mapped to the ATP-binding site of FtsA can also suppress the defects of *ftsA27*, whereas mutations that mapped to other regions of the protein cannot. In both cases, however, the location of the suppressor mutations indicate that ATP-binding defects can be suppressed by directly restoring ATP-binding or by enhancing another property of FtsA, such as protein-protein interaction, that may normally be regulated by ATP binding. Of course, this conclusion is based on the conjecture that FtsA12 is indeed defective in ATP binding, which has not yet been assessed directly.

FtsA-K19M differs from FtsA27 and FtsA12 in that it can localize to the Z ring *in vivo* at any temperature, although it is not completely functional, and it is still defective at binding ATP *in vitro.* This indicates that ATP binding is important not only for FtsA localization to the Z ring, but also for FtsA function at the Z ring. This raises the question of why some ATP-binding mutants of FtsA are defective in localizing to the Z ring, whereas others are not. One possible answer could be the degree to which each of these proteins is able to bind to ATP. I propose that

FtsA12 has the largest ATP-binding defect, followed by FtsA27, and then K19M. If this were true, it could explain why FtsA12 is very unstable and FtsA27 is only partially unstable. Another prediction is that FtsA12 would be the weakest at localizing to the Z ring and K19M would be the strongest. To determine if this is the case, a more sensitive ATP-binding assay and more quantitative FtsZ-binding analysis are needed.

The fact that K19M is able to localize to the Z ring, but cells still show a significant defect in cell division, indicates that there is another FtsA function affected by inefficient ATP binding. There are several possible explanations. One is that FtsA needs to bind to ATP in order to recruit downstream division proteins to the Z ring. This could be tested by expressing fusions of downstream division proteins to GFP to see if they can localize in a strain that expresses *ftsA(K19M)* instead of wild-type *ftsA*. Another possibility is that FtsA turnover at the Z ring is being affected, and that efficient turnover of FtsA is required for efficient cell division.

Interestingly, a key lysine residue in the ATP binding site of ParA (K122) created different ATP-associated defects when changed to a glutamate, glutamine, or arginine (Vecchiarelli et al., 2013). One lesion caused an ATP binding defect, another caused an ATP hydrolysis defect, and the other caused a nucleotide exchange defect. It is possible that we could see the same effects when changing K19 of *E. coli* FtsA. In addition, site-directed mutagenesis targeting residues T215 and D217 of *E. coli* FtsA may create defects in ATP hydrolysis (Figure 5.10). Our group has already begun to characterize T215

lesions (Shiomi and Margolin, unpublished). Like the lesions at K122 of ParA, preliminary results suggest that changing T215 to A, D or E has different effects on protein function *in vivo*. Biochemical analysis of these mutants is still needed. *E. coli* FtsA residues T215 and D217 align with F217 and G219 of *T. maritima* FtsA, which are structurally equivalent to V159 and H161 of actin (van den Ent and Löwe, 2000). In actin, these residues position a water molecule that acts as the attacking nucleophile in the hydrolysis reaction (Flaherty et al., 1991). The point mutation in the *ftsA6*(ts) allele is D217N (Table 4.1, Figure 4.1). This mutant, in addition to other site-directed mutants at these residues should shed light on which residues are involved in ATP hydrolysis. Once identified, such mutants will aid in our understanding of the importance of ATP binding and hydrolysis for the activity of FtsA.

FIG. 5.10

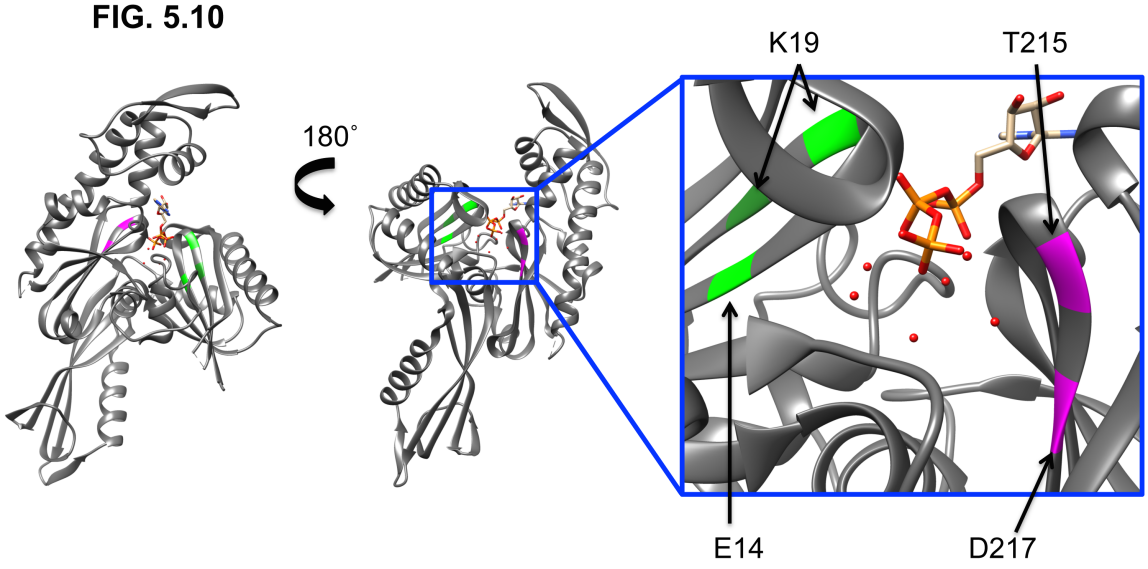

Figure 5.10: *E. coli* FtsA residues predicted to be involved in ATP hydrolysis. A structure of FtsA from *T. maritima* is shown from different angles. The magnified region highlights locations of residues predicted to cause ATP hydrolysis defects in *E. coli* FtsA. *T. maritima* Y19 and K21 (dark green) are shown as potential structural equivalents for *E. coli* K19. ATP is shown in the active site and the red dots indicate water molecules.

Chapter 6: Discussion

CONCLUSIONS & PERSPECTIVES

Segregation of the Min proteins into daughter cells

The work presented in chapter 3 of this dissertation showed that the oscillating MinD protein of *E. coli* pauses not only at the cell poles, but also at each side of the developing septum with increasing frequency as cells elongate. Eventually this irregular oscillation pattern doubles and forms two regularly oscillating groups of GFP-MinD, and presumably the oscillation patterns of MinC and MinE are coordinated. I proposed that the splitting of a single oscillating population of Min proteins into two occurs before cells complete septation as a way to ensure that both daughter cells receive equivalent levels of Min proteins.

Another possibility is that the double oscillation pattern does not stabilize until the septum between forming daughter cells has completely closed. The exact moment of septum closure was difficult for us to determine, because I defined divided cells by the appearance of deep constrictions that appeared fully separated in DIC images. To carry this work further, it will be important to define exactly when cells divide while observing Min oscillation patterns. I attempted to define the moment of septation using the lipophilic fluorescent dye FM 4-64, which preferentially binds to the inner cell membrane of *E. coli* (Fishov and Woldringh, 1999). Unfortunately, GFP-MinD ceased to oscillate in FM 4-6-stained cells. It is possible that this dye disturbed membrane potential, which is necessary for Min oscillation (Strahl and Hamoen, 2010). Another potential way to visualize septum closure in *E. coli* is to observe the separation of the

periplasmic space. This could be done using an mCherry derivative targeted to periplasm. To attain more precise images, these experiments could be performed with super-resolution microscopy.

While I favor the idea that MinD pausing at midcell acts as a precursor to the doubled oscillation pattern, creating an efficient mechanism for segregating the Min proteins into daughter cells, we must consider other possibilities as well. For example, although I found that MinD pausing at each side of the septum was not dependent on MinC-FtsZ interaction, it is possible that this pattern of oscillation occurs to enhance MinC-FtsZ interactions at the Z ring. We previously showed that the Min system in *E. coli* is important for promoting constriction of the divisome (Yu and Margolin, 1999). In *B. subtilis,* it has been shown that MinC is targeted to the septum to prevent the formation of new Z rings adjacent to an already active divisome (Bramkamp et al., 2008; Gregory et al., 2008). It is possible that midcell pausing of MinD promotes one or both of these activities. In addition, *in vitro* work has shown that MinD binding can actually alter membrane properties (Mazor et al., 2008). This suggests an intriguing possibility that MinD could be helping to form the newly developing cell poles.

The best way to determine which function, if any, can be attributed to midcell pausing of MinD would be to separate midcell pausing from normal pole-to-pole oscillation, as cell division is significantly inhibited in Δ*min* cells. This will only be possible when we know the mechanism by which midcell pausing occurs. If midcell pausing occurs via a mechanism that also promotes pole-to-pole oscillation, such as membrane composition or curvature, then it may be difficult

to block midcell pausing without also affecting pole-to-pole oscillations. Possible mechanisms controlling midcell pausing of MinD are discussed below.

Defining the molecular mechanism for MinD pausing at midcell

Perhaps the most likely mechanism by which MinD pauses at the septum is by recognizing the changing membrane architecture and phospholipid composition in this area of the cell. It is possible to directly visualize these domains in live bacteria using the cardiolipin (CL)-specific fluorescent dye nonyl acridine orange (NAO) (Mileykovskaya and Dowhan, 2000). However, it is also possible that NAO, like FM 4-64, will interfere with Min oscillation. Another approach to determining whether CL affects MinD oscillation is to alter the cellular levels of CL. Growing *E. coli* cells in high osmolarity medium increases the intracellular levels of CL, while making *cls* mutants decreases CL levels (Romantsov et al., 2010). NAO can be used to detect CL localization in the mutants, and MinD oscillation can be monitored separately using the GFP-MinD construct, if necessary. Interpretation of the results of such experiments should be made very carefully, as CL composition almost certainly influences MinD localization (Mileykovskaya et al., 2003) but may not be solely responsible for its midcell pausing.

Another possibility is that MinD pauses at midcell because it interacts with a divisome protein. Because the pausing starts before a visible constriction can be detected by DIC microscopy, proteins that localize to the divisome early would be the most likely targets. Two-hybrid and immunoprecipitation techniques could

be used to screen for potential interacting partners. Positive results would need to be independently confirmed either through immunoprecipitation or ELISA techniques using purified proteins or mutagenesis that results in a loss of GFP-MinD midcell pausing.

Interestingly, MinD was recently found to interact with DNA, similar to other ParA homologs (Di Ventura et al., 2014). The Sourjik group proposed a model in which MinD contributes to chromosome segregation, which is consistent with previous work showing that *min* mutants display defects in chromosome segregation (Mulder et al., 1990). Similarly, DivIVA, which is not a ParA homolog but is a part of the Min system in Gram-positive species, has been shown to play a role in chromosome segregation in *B. subtilis* and *Mycobacterium smegmatis* (Ginda et al., 2013; Thomaides et al., 2001). A specific nucleotide binding sequence for MinD was not identified, but several mutants that are deficient in interacting with DNA have been found (Di Ventura et al., 2014). It is possible that MinD recognizes DNA near the chromosome terminus and origin of replication. During cell division, the replicated chromosome origins move to the cell poles and the replicated terminus regions are located close to the septum. The mutants of MinD that are deficient in DNA binding could be used in the context of GFP-MinD to investigate whether MinD midcell pausing is caused by MinD-DNA interaction near the septum.

The role of ATP in FtsA activity

The work presented in chapters 4 and 5 of this dissertation enhance our understanding of the role of ATP in FtsA function. Although the molecular mechanisms are still unclear, we are now able to propose models that can be tested. I propose a model in which monomeric FtsA binds ATP and enhances FtsA-FtsZ interaction, and as the Z ring matures, FtsZ and FtsA oligomerize. The GTPase activity of FtsZ induces curvature and shortening of FtsZ protofilaments (Li et al., 2013) and FtsA-mediated FtsZ dynamics induces shortening of FtsZ protofilaments. Recent work confirms previous data from our group that these FtsZ dynamics occur only in the presence of FtsA (Beuria et al., 2009; Loose and Mitchison, 2014). Only ATP binding, and not hydrolysis, was necessary to induce such dynamics from FtsZ *in vitro* (Loose and Mitchison, 2014). I propose that FtsA ATP hydrolysis induces depolymerization of FtsA, allowing it to leave the Z ring and rebind ATP. Thus, creating a feedback loop that promotes constriction of the divisome (Figure 6.1).

FIG. 6.1

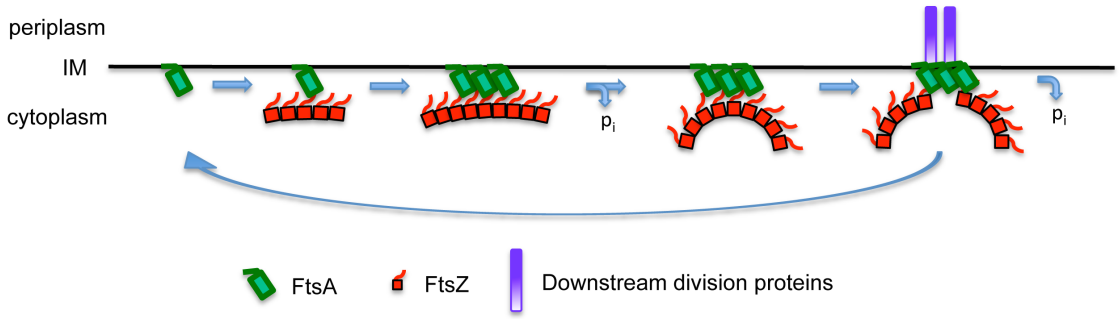

Figure 6.1: A model of FtsA activity at the Z ring. Monomeric FtsA binds ATP, enhancing its affinity for FtsZ by an unknown mechanism. FtsA and FtsZ polymerize as the Z ring matures. GTP hydrolysis by FtsZ induces curving of FtsZ protofilaments (Li et al., 2013). FtsA-mediated FtsZ dynamics induces shortening of FtsZ protofilaments (Loose and Mitchison, 2014). FtsA recruits downstream proteins to the constricting Z ring to coordinate the constriction of the inner membrane with the cell wall and outer membrane. FtsA ATPase activity induces monomerization of FtsA, which leaves the Z ring, rebinds ATP, and cycles back into the Z ring. This creates a feedback loop that enhances Z ring constriction until the new cell poles are complete. Some of these steps may occur simultaneously.

The relationship between ATP binding, FtsA-FtsZ interaction, and FtsA oligomerization

Previous work shows that ATP is required for FtsA to interact with FtsZ *in vitro* (Beuria et al., 2009; Loose and Mitchison, 2014; Osawa and Erickson, 2013). My work with the *ftsA27* allele supports this conclusion and suggests that FtsA ATP-binding regulates FtsA interaction with the Z ring by directly influencing FtsA interaction with FtsZ *in vivo*. The genetic effect that O saw on FtsA-FtsZ interactions can be confirmed using biochemical protein-protein interaction assays such as pull-downs or surface plasmon resonance (SPR). Although previous work indicates that lipids are not necessary for FtsA-FtsZ interactions *in vitro* (Beuria et al., 2009; Szwedziak et al., 2012), it is possible that this interaction could be enhanced in the presence of lipids. Lipid sedimentation assays in the presence of FtsZ, FtsA or an FtsA mutant, and nucleotides could be used to directly address this idea.

Notably, the effect of non-functional or defective FtsA mutants on FtsZ dynamics has not yet been examined. Based on current evidence, FtsA that cannot bind ATP would likely not associate with FtsZ. However, my results with FtsA27 and FtsA-K19M indicate that FtsA proteins with decreased affinity for ATP, but not complete abolishment of ATP binding, can still interact with FtsZ. I predict FtsA and FtsZ dynamics are altered in strains expressing these mutants. This can be tested both *in vivo* by FRAP and *in vitro* on supported lipid bilayers as shown previously (Geissler et al., 2007; Loose and Mitchison, 2014).

My data also indicate that ATP binding may also influence FtsA oligomerization, but this needs to be confirmed biochemically. Existing data relies on yeast two-hybrid analysis and/or the ability of an FtsA with a membrane-targeting sequence deletion that is fused to GFP to form fluorescent cytoplasmic rods in *E. coli* (Pichoff et al., 2012). Using *in vitro* methods to get quantitative data for FtsA-FtsA interaction is challenging due to the difficulty of working with purified FtsA (Martos et al., 2012). So far, Blue-native PAGE analysis with these FtsA preparations has resulted in un-interpretable smears of protein. This could be due to lipids that might be in the protein preparations and affecting the migration of the protein through the gel. Currently we are only able to purify low concentrations (5-10 μM) of active FtsA protein. It may be possible to further optimize my current protein purification scheme to allow purification of higher concentrations of active protein. This would permit the use of techniques that require more protein, such as dynamic light scattering.

Gradient sedimentation assays are now being optimized with our current FtsA preparations. Analytical ultra-centrifugation (AU) is another technique that could be used to detect the oligomerization state of FtsA. However, DTT (which is used at 1 mM in FtsA buffer to prevent aggregation) and ATP would cause significant background signal at an absorbance of 280 nm. This issue can be remedied by fluorescently labeling FtsA. Purifying fluorescently tagged FtsA should not be the first option, since we know that large tags perturb FtsA function *in vivo.* I have recently purified an active version of FtsA containing a pentaglycine tag that allows fluorescent labeling *in vitro* using a method known

as sortagging (Loose and Mitchison, 2014; Popp et al., 2007). If this version of FtsA is still active after labeling, it may be possible to use AU to detect differences in the oligomerization of different FtsA mutants and whether nucleotide affects FtsA oligomerization.

Another interesting question is whether ATP-binding mutants of FtsA alter the structure of the Z ring when they are produced *in vivo* under conditions in which Z rings still form. This can be addressed using super-resolution microscopy. Recent reports using this technique to study the Z ring of *E. coli, B. subtilis, S. aureus,* and *C. crescentus* show obvious gaps in the Z ring, and suggest the Z ring is composed of discontinuous overlapping filaments (Biteen et al., 2012; Fu et al., 2010; Holden et al., 2014; Jennings et al., 2011; Rowlett and Margolin, submitted; Strauss et al., 2012). Based on the model in figure 6.1, I predict that there would be noticeably more or less gaps in the Z ring of cells expressing FtsA mutants with lesions in the ATP binding site.

Determining the physiological role for ATP hydrolysis by FtsA

For the first time I have shown that *E. coli* FtsA can hydrolyze ATP. However, the physiological role of ATP hydrolysis by FtsA remains unknown. The same is true for *B. subtilis* and *P. aeruginosa* FtsA, for which ATPase activity has been known for some time (Feucht et al., 2001; Paradis-Bleau et al., 2005). *In vitro* work has shown that FtsA and FtsZ can interact in the presence of non-hydrolyzable ATP (Loose and Mitchison, 2014), indicating that ATP binding, but

not hydrolysis, is necessary for FtsA-FtsZ interaction. I hypothesize that FtsA ATP hydrolysis influences FtsA dynamics and Z ring constriction.

Consistent with this hypothesis, I found that the gain-of-function mutant FtsA* displays increased ATPase activity and we previously showed that this mutant exhibits increased turnover at the Z ring compared to wild-type FtsA (Geissler et al., 2007). Because I have identified other mutant FtsAs with increased ATPase activity, it will be important to measure the turnover rate of these mutants and compare them to wild-type FtsA and FtsA* turnover rates. Fluorescence recovery after photobleaching (FRAP), which was used to calculate the turnover rates of FtsA-GFP and FtsA*-GFP, can also be used to determine the rate of turnover for other FtsA mutants *in vivo*. To further test the hypothesis that FtsA ATP hydrolysis influences FtsA dynamics and Z ring constriction, it will be important to identify ATPase mutants of FtsA as described at the end of chapter 5 of this dissertation. If the hypothesis is correct, FtsA mutants specifically deficient in ATP hydrolysis should display decreased turnover at the Z ring and cell division that relies on these mutants should be delayed compared to wild-type cells.

The dynamics of FtsZ in the presence of the FtsA mutants should also be investigated. FtsA* was not shown to affect FtsZ turnover in FRAP studies (Geissler et al., 2007), suggesting that increased ATPase activity has no effect on FtsZ turnover. This is consistent with more recent *in vitro* data that suggest FtsA-FtsZ association in the presence of ATP or a non-hydrolysable ATP can influence FtsZ dynamics, whereas FtsZ alone or in the presence of ZipA shows

little to no dynamics (Loose and Mitchison, 2014). The same study showed that FtsZ dynamics were not altered in the presence of FtsA mutants, including FtsA*. Differences between FtsA* and the gain-of-function mutants identified in this work may be expected since they were isolated differently (*ftsA** as a suppressor of *zipA* deletion (Geissler et al., 2003) and the gain-of-function mutants identified in this work were isolated as suppressors of *ftsA27*). Therefore, it is possible that these mutants are working by slightly different mechanisms. Another possibility is that the *in vitro* system bypasses normal cell cycle controls, making it seem that the different FtsA derivatives have no effect when they actually have different responses to regulation *in vivo*.

FtsA as a target for novel antibiotics

Antibiotic resistance is a current threat to decades of medical advancement. One way to combat this problem is to create new antibiotics with novel targets, such as the bacterial cytokinetic machinery. In fact, many studies have already identified inhibitors of FtsZ that maybe useful as potential therapeutics for bacterial infections, and that do not seem to affect the eukaryotic tubulin of mammalian cells (den Blaauwen et al., 2014; Ojima et al., 2014; Sass and Brötz-Oesterhelt, 2013).

Because drug resistance can easily develop, more effective drugs should target more than a single step in a pathway. To date, research into inhibitors of FtsA or other cell division proteins has been extremely limited (Paradis-Bleau et al., 2005), most likely because we know so much less about how these protiens

function, in addition to the fact that they can be difficult to work with both *in vivo* and *in vitro*. We now have the capability to screen small molecules for inhibition of ATP binding/hydrolysis. High-throughput monitoring of bacterial growth in the presence of such compounds can be used to confirm potential drug candidates. The more we increase our knowledge of bacterial cytokinesis, the more FtsA and other bacterial cell division proteins will become better targets for rational drug design.

FINAL REMARKS

FtsA is an important part of the bacterial cytokinetic machinery and likely serves as a key regulator of the Z ring. In *E. coli*, FtsA tethers the Z ring to the membrane, promotes the integrity of the Z ring, and may also play a role in constriction of the divisome. Its wide conservation among bacteria suggests it serves a similar function in other organisms as well. To determine if this is the case, it will be important to continue investigations into the divisome architecture of a variety of organisms.

Now that an *in vitro* system has been developed to study the dynamic nature of the *E. coli* FtsZ-FtsA relationship (Loose and Mitchison, 2014), the system can be applied to learn more about the interaction between *E. coli* FtsZ and FtsA, as well as the FtsZ and FtsA proteins of other bacteria. Does FtsZ from *B. subtilis* or *C. crescentus* display a similar dynamic behavior in the presence of its cognate FtsA, or are other compents required?

In addition to studying the relationship between FtsA and FtsZ, it will be important to study the role of other Z ring-associated proteins. A recently identified protein, SepF, which is conserved in Gram-positive bacteria (Hamoen et al., 2006), may bring to light the general role of FtsA in bacterial cell division. SepF was recently found to serve as an important membrane anchor for the Z ring in *B. subtilis*, even in the absence of FtsA (Duman et al., 2013). In cyanobacteria, no *ftsA* homolog has been identified, but *sepF* is essential

(Marbouty et al., 2009). Together this data indicate that SepF and FtsA may have similar functions in bacterial cytokinesis.

The first part of this work focused on another widely conserved regulator of the Z ring, the Min system. Both Min and FtsA are important for controlling Z ring formation. The work described herein adds to our understanding of the oscillating bacterial Min system and the importance of ATP in FtsA activity. The continuation of this work will enhance our knowledge of the basic molecular mechanism of cell division.

REFERENCES

Adams, D.W., and Errington, J. (2009). Bacterial cell division: assembly, maintenance and disassembly of the Z ring. Nat. Rev. Microbiol. *7*, 642–653.

Addinall, S.G., Bi, E., and Lutkenhaus, J. (1996). FtsZ ring formation in fts mutants. J. Bacteriol. *178*, 3877–3884.

Addinall, S.G., Cao, C., and Lutkenhaus, J. (1997a). Temperature shift experiments with an *ftsZ84* (Ts) strain reveal rapid dynamics of FtsZ localization and indicate that the Z ring is required throughout septation and cannot reoccupy division sites once constriction has initiated. J. Bacteriol. *179*, 4277–4284.

Addinall, S.G., Cao, C., and Lutkenhaus, J. (1997b). FtsN, a late recruit to the septum in *Escherichia coli*. Mol. Microbiol. *25*, 303–309.

Addinall, S.G., Small, E., Whitaker, D., Sturrock, S., Donachie, W.D., and Khattar, M.M. (2005). New temperature-sensitive alleles of *ftsZ* in *Escherichia coli*. J. Bacteriol. *187*, 358–365.

Allard, J.F., and Cytrynbaum, E.N. (2009). Force generation by a dynamic Z-ring in *Escherichia coli* cell division. Proc. Natl. Acad. Sci. *106*, 145–150.

Amos, L.A., van den Ent, F., and Löwe, J. (2004). Structural/functional homology between the bacterial and eukaryotic cytoskeletons. Curr. Opin. Cell Biol. *16*, 24–31.

Anderson, D.E., Gueiros-Filho, F.J., and Erickson, H.P. (2004). Assembly dynamics of FtsZ rings in *Bacillus subtilis* and *Escherichia coli* and effects of FtsZ-regulating proteins. J. Bacteriol. *186*, 5775–5781.

Arumugam, S., Chwastek, G., Fischer-Friedrich, E., Ehrig, C., Mönch, I., and Schwille, P. (2012). Surface topology engineering of membranes for the mechanical investigation of the tubulin homologue FtsZ. Angew. Chem. Int. Ed. *51*, 11858–11862.

Aussel, L., Barre, F.-X., Aroyo, M., Stasiak, A., Stasiak, A.Z., and Sherratt, D. (2002). FtsK is a DNA motor protein that activates chromosome dimer resolution by switching the catalytic state of the XerC and XerD recombinases. Cell *108*, 195–205.

van Baarle, S., and Bramkamp, M. (2010). The MinCDJ system in *Bacillus subtilis* prevents minicell formation by promoting divisome disassembly. PLoS ONE *5*, e9850.

Balasubramanian, M.K., Bi, E., and Glotzer, M. (2004). Comparative analysis of cytokinesis in budding yeast, fission yeast and animal cells. Curr. Biol. *14*, R806–R818.

Barák, I. (2013). Open questions about the function and evolution of bacterial Min systems. Front. Microbiol. *4*.

Begg, K., Nikolaichik, Y., Crossland, N., and Donachie, W.D. (1998). Roles of FtsA and FtsZ in activation of division sites. J. Bacteriol. *180*, 881–884.

Bernard, C.S., Sadasivam, M., Shiomi, D., and Margolin, W. (2007). An altered FtsA can compensate for the loss of essential cell division protein FtsN in *Escherichia coli*. Mol. Microbiol. *64*, 1289–1305.

Bernhardt, T.G., and de Boer, P.A.J. (2003). The *Escherichia coli* amidase AmiC is a periplasmic septal ring component exported via the twin-arginine transport pathway. Mol. Microbiol. *48*, 1171–1182.

Bernhardt, T., and de Boer, P. (2005). SlmA, a nucleoid-associated, FtsZ binding protein required for blocking septal ring assembly over chromosomes in *E. coli*. Mol. Cell *18*, 555–564.

Beuria, T.K., Mullapudi, S., Mileykovskaya, E., Sadasivam, M., Dowhan, W., and Margolin, W. (2009). Adenine nucleotide-dependent regulation of assembly of bacterial tubulin-like FtsZ by a hypermorph of bacterial Actin-like FtsA. J. Biol. Chem. *284*, 14079–14086.

Bhatia, P., Hachet, O., Hersch, M., Rincon, S.A., Berthelot-Grosjean, M., Dalessi, S., Basterra, L., Bergmann, S., Paoletti, A., and Martin, S.G. (2014). Distinct levels in Pom1 gradients limit Cdr2 activity and localization to time and position division. Cell Cycle *13*, 0–14.

Bi, E.F., and Lutkenhaus, J. (1991). FtsZ ring structure associated with division in *Escherichia coli*. Nature *354*, 161–164.

Bisicchia, P., Arumugam, S., Schwille, P., and Sherratt, D. (2013). MinC, MinD, and MinE drive counter-oscillation of early-cell-division proteins prior to *Escherichia coli* septum formation. mBio *4*, e00856–13–e00856–13.

Biteen, J.S., Goley, E.D., Shapiro, L., and Moerner, W.E. (2012). Three-dimensional super-resolution imaging of the mid-plane protein FtsZ in live *Caulobacter crescentus* cells using astigmatism. ChemPhysChem *13*, 1007–1012.

den Blaauwen, T., Andreu, J.M., and Monasterio, O. (2014). Bacterial cell division proteins as antibiotic targets. Bioorganic Chem.

de Boer, P.A. (2010). Advances in understanding *E. coli* cell fission. Curr. Opin. Microbiol. *13*, 730–737.

de Boer, P.A., Crossley, R.E., and Rothfield, L.I. (1989). A division inhibitor and a topological specificity factor coded for by the minicell locus determine proper placement of the division septum in *E. coli*. Cell *56*, 641–649.

de Boer, P.A., Crossley, R.E., and Rothfield, L.I. (1992). Roles of MinC and MinD in the site-specific septation block mediated by the MinCDE system of *Escherichia coli*. J. Bacteriol. *174*, 63–70.

Bork, P., Sander, C., and Valencia, A. (1992). An ATPase domain common to prokaryotic cell cycle proteins, sugar kinases, actin, and hsp70 heat shock proteins. Proc. Natl. Acad. Sci. *89*, 7290–7294.

Boyd, D., Weiss, D.S., Chen, J.C., and Beckwith, J. (2000). Towards single-copy gene expression systems making gene cloning physiologically relevant: lambda InCh, a simple *Escherichia coli* plasmid-chromosome shuttle system. J. Bacteriol. *182*, 842–847.

Bramkamp, M., Emmins, R., Weston, L., Donovan, C., Daniel, R.A., and Errington, J. (2008). A novel component of the division-site selection system of *Bacillus subtilis* and a new mode of action for the division inhibitor MinCD. Mol. Microbiol. *70*, 1556–1569.

Buddelmeijer, N., and Beckwith, J. (2004). A complex of the *Escherichia coli* cell division proteins FtsL, FtsB and FtsQ forms independently of its localization to the septal region. Mol. Microbiol. *52*, 1315–1327.

Busiek, K.K., Eraso, J.M., Wang, Y., and Margolin, W. (2012). The early divisome protein FtsA interacts directly through Its 1c subdomain with the cytoplasmic domain of the late divisome protein FtsN. J. Bacteriol. *194*, 1989–2000.

Busiek, K.K., and Margolin, W. (2014). A role for FtsA in SPOR-independent localization of the essential Escherichia coli cell division protein FtsN. Mol. Microbiol. n/a–n/a.

Camberg, J.L., Hoskins, J.R., and Wickner, S. (2009). ClpXP protease degrades the cytoskeletal protein, FtsZ, and modulates FtsZ polymer dynamics. Proc. Natl. Acad. Sci. *106*, 10614–10619.

Camberg, J.L., Hoskins, J.R., and Wickner, S. (2011). The interplay of ClpXP with the cell division machinery in *Escherichia coli*. J. Bacteriol. *193*, 1911–1918.

Camberg, J.L., Viola, M.G., Rea, L., Hoskins, J.R., and Wickner, S. (2014). Location of dual sites in *E. coli* FtsZ important for degradation by ClpXP; one at the C-terminus and one in the disordered linker. PLoS ONE *9*, e94964.

Cha, J.-H., and Stewart, G.C. (1997). The divIVA minicell locus of *Bacillus subtilis*. J. Bacteriol. *179*, 1671–1683.

Cho, H., and Bernhardt, T.G. (2013). Identification of the SlmA active site responsible for blocking bacterial cytokinetic ring assembly over the chromosome. PLoS Genet. *9*, e1003304.

Cho, H., McManus, H.R., Dove, S.L., and Bernhardt, T.G. (2011). Nucleoid occlusion factor SlmA is a DNA-activated FtsZ polymerization antagonist. Proc. Natl. Acad. Sci. *108*, 3773–3778.

Corbin, B.D., Geissler, B., Sadasivam, M., and Margolin, W. (2004). Z-ring-independent interaction between a subdomain of FtsA and late septation proteins as revealed by a polar recruitment assay. J. Bacteriol. *186*, 7736–7744.

Corbin, B.D., Yu, X.-C., and Margolin, W. (2002). Exploring intracellular space: function of the Min system in round-shaped *Escherichia coli*. EMBO J. *21*, 1998–2008.

Dajkovic, A., Lan, G., Sun, S.X., Wirtz, D., and Lutkenhaus, J. (2008). MinC spatially controls bacterial cytokinesis by antagonizing the scaffolding function of FtsZ. Curr. Biol. *18*, 235–244.

Di Ventura, B., Knecht, B., Andreas, H., Godinez, W.J., Fritsche, M., Rohr, K., Nickel, W., Heermann, D.W., and Sourjik, V. (2014). Chromosome segregation by the *Escherichia coli* Min system. Mol. Syst. Biol. *9*, 686–686.

Diagne, C.T., Salhi, M., Crozat, E., Salome, L., Cornet, F., Rousseau, P., and Tardin, C. (2014). TPM analyses reveal that FtsK contributes both to the assembly and the activation of the XerCD-dif recombination synapse. Nucleic Acids Res. *42*, 1721–1732.

Din, N., Quardokus, E.M., Sackett, M.J., and Brun, Y.V. (1998). Dominant C-terminal deletions of FtsZ that affect its ability to localize in *Caulobacter* and its interaction with FtsA. Mol. Microbiol. *27*, 1051–1063.

Ditkowski, B., Holmes, N., Rydzak, J., Donczew, M., Bezulska, M., Ginda, K., Kedzierski, P., Zakrzewska-Czerwinska, J., Kelemen, G.H., and Jakimowicz, D. (2013). Dynamic interplay of ParA with the polarity protein, Scy, coordinates the growth with chromosome segregation in *Streptomyces coelicolor*. Open Biol. *3*, 130006–130006.

Donovan, C., Schwaiger, A., Kramer, R., and Bramkamp, M. (2010). Subcellular localization and characterization of the ParAB system from *Corynebacterium glutamicum*. J. Bacteriol. *192*, 3441–3451.

Donovan, C., Schauss, A., Krämer, R., and Bramkamp, M. (2013). Chromosome segregation impacts on cell growth and division site selection in *Corynebacterium glutamicum*. PLoS ONE *8*, e55078.

Draper, G.C., McLennan, N., Begg, K., Masters, M., and Donachie, W.D. (1998). Only the N-terminal domain of FtsK functions in cell division. J. Bacteriol. *180*, 4621–4627.

Du, Y., and Arvidson, C.G. (2003). Identification of ZipA, a signal recognition particle-dependent protein from *Neisseria gonorrhoeae*. J. Bacteriol. *185*, 2122–2130.

Dubarry, N., Possoz, C., and Barre, F.-X. (2010). Multiple regions along the *Escherichia coli* FtsK protein are implicated in cell division. Mol. Microbiol. *78*, 1088–1100.

Duman, R., Ishikawa, S., Celik, I., Strahl, H., Ogasawara, N., Troc, P., Lowe, J., and Hamoen, L.W. (2013). Structural and genetic analyses reveal the protein SepF as a new membrane anchor for the Z ring. Proc. Natl. Acad. Sci. *110*, E4601–E4610.

Dziedzic, R., Kiran, M., Plocinski, P., Ziolkiewicz, M., Brzostek, A., Moomey, M., Vadrevu, I.S., Dziadek, J., Madiraju, M., and Rajagopalan, M. (2010). *Mycobacterium tuberculosis* ClpX Interacts with FtsZ and Interferes with FtsZ Assembly. PLoS ONE *5*, e11058.

Edwards, D.H., and Errington, J. (1997). The *Bacillus subtilis* DivIVA protein targets to the division septum and controls the site specificity of cell division. Mol. Microbiol. *24*, 905–915.

van den Ent, F., and Löwe, J. (2000). Crystal structure of the cell division protein FtsA from *Thermotoga maritima*. EMBO J. *19*, 5300–5307.

Erickson, H.P. (2009). Modeling the physics of FtsZ assembly and force generation. Proc. Natl. Acad. Sci. *106*, 9238–9243.

Erickson, H.P., Anderson, D.E., and Osawa, M. (2010). FtsZ in bacterial cytokinesis: cytoskeleton and force generator all in one. Microbiol. Mol. Biol. Rev. *74*, 504–528.

Feng, J., Michalik, S., Varming, A.N., Andersen, J.H., Albrecht, D., Jelsbak, L., Krieger, S., Ohlsen, K., Hecker, M., Gerth, U., et al. (2013). Trapping and proteomic identification of cellular substrates of the ClpP protease in *Staphylococcus aureus*. J. Proteome Res. *12*, 547–558.

Feucht, A., Lucet, I., Yudkin, M.D., and Errington, J. (2001). Cytological and biochemical characterization of the FtsA cell division protein of *Bacillus subtilis*. Mol. Microbiol. *40*, 115–125.

Fishov, I., and Woldringh, C.L. (1999). Visualization of membrane domains in *Escherichia coli*. Mol. Microbiol. *32*, 1166–1172.

Flaherty, K.M., McKay, D.B., Kabsch, W., and Holmes, K.C. (1991). Similarity of the three-dimensional structures of actin and the ATPase fragment of a 70-kDa heat shock cognate protein. Proc. Natl. Acad. Sci. *88*, 5041–5045.

Fraipont, C., Alexeeva, S., Wolf, B., van der Ploeg, R., Schloesser, M., den Blaauwen, T., and Nguyen-Disteche, M. (2011). The integral membrane FtsW protein and peptidoglycan synthase PBP3 form a subcomplex in *Escherichia coli*. Microbiology *157*, 251–259.

Fu, G., Huang, T., Buss, J., Coltharp, C., Hensel, Z., and Xiao, J. (2010). In vivo structure of the *E. coli* FtsZ-ring revealed by photoactivated localization microscopy (PALM). PLoS ONE *5*, e12680.

Fujita, J., Maeda, Y., Nagao, C., Tsuchiya, Y., Miyazaki, Y., Hirose, M., Mizohata, E., Matsumoto, Y., Inoue, T., Mizuguchi, K., et al. (2014). Crystal structure of FtsA from *Staphylococcus aureus*. FEBS Lett.

Geissler, B., Elraheb, D., and Margolin, W. (2003). A gain-of-function mutation in *ftsA* bypasses the requirement for the essential cell division gene *zipA* in *Escherichia coli*. Proc. Natl. Acad. Sci. U. S. A. *100*, 4197–4202.

Geissler, B., and Margolin, W. (2005). Evidence for functional overlap among multiple bacterial cell division proteins: compensating for the loss of FtsK. Mol. Microbiol. *58*, 596–612.

Geissler, B., Shiomi, D., and Margolin, W. (2007). The *ftsA** gain-of-function allele of *Escherichia coli* and its effects on the stability and dynamics of the *Z* ring. Microbiology *153*, 814–825.

Gerding, M.A., Ogata, Y., Pecora, N.D., Niki, H., and de Boer, P.A.J. (2007). The trans-envelope Tol-Pal complex is part of the cell division machinery and required for proper outer-membrane invagination during cell constriction in *E. coli*. Mol. Microbiol. *63*, 1008–1025.

Ginda, K., Bezulska, M., Ziółkiewicz, M., Dziadek, J., Zakrzewska-Czerwińska, J., and Jakimowicz, D. (2013). ParA of *Mycobacterium smegmatis* co-ordinates chromosome segregation with the cell cycle and interacts with the polar growth determinant DivIVA. Mol. Microbiol. *87*, 998–1012.

Goehring, N.W., and Beckwith, J. (2005). Diverse paths to midcell: assembly of the bacterial cell division machinery. Curr. Biol. *15*, R514–R526.

Goehring, N.W., Gonzalez, M.D., and Beckwith, J. (2006). Premature targeting of cell division proteins to midcell reveals hierarchies of protein interactions involved in divisome assembly. Mol. Microbiol. *61*, 33–45.

Goehring, N.W., Gueiros-Filho, F., and Beckwith, J. (2005). Premature targeting of a cell division protein to midcell allows dissection of divisome assembly in *Escherichia coli*. Genes Dev. *19*, 127–137.

Goehring, N.W., Petrovska, I., Boyd, D., and Beckwith, J. (2007). Mutants, suppressors, and wrinkled colonies: mutant alleles of the cell division gene *ftsQ*

point to functional domains in FtsQ and a role for domain 1C of FtsA in divisome assembly. J. Bacteriol. *189*, 633–645.

Gregory, J.A., Becker, E.C., and Pogliano, K. (2008). *Bacillus subtilis* MinC destabilizes FtsZ-rings at new cell poles and contributes to the timing of cell division. Genes Dev. *22*, 3475–3488.

Grenga, L., Luzi, G., Paolozzi, L., and Ghelardini, P. (2008). The *Escherichia coli* FtsK functional domains involved in its interaction with its divisome protein partners. FEMS Microbiol. Lett. *287*, 163–167.

Guzman-Vendrell, M., Baldissard, S., Almonacid, M., Mayeux, A., Paoletti, A., and Moseley, J.B. (2013). Blt1 and Mid1 provide overlapping membrane anchors to position the division plane in fission yeast. Mol. Cell. Biol. *33*, 418–428.

Hale, C.A., and de Boer, P.A. (1997). Direct binding of FtsZ to ZipA, an essential component of the septal ring structure that mediates cell division in *E. coli*. Cell *88*, 175–185.

Hale, C.A., and de Boer, P.A. (1999). Recruitment of ZipA to the septal ring of *Escherichia coli* is dependent on FtsZ and independent of FtsA. J. Bacteriol. *181*, 167–176.

Hale, C.A., and de Boer, P.A.J. (2002). ZipA Is required for recruitment of FtsK, FtsQ, FtsL, and FtsN to the septal ring in *Escherichia coli*. J. Bacteriol. *184*, 2552–2556.

Hale, C.A., Meinhardt, H., and de Boer, P.A. (2001). Dynamic localization cycle of the cell division regulator MinE in *Escherichia coli*. EMBO J. *20*, 1563–1572.

Hale, C.A., Rhee, A.C., and de Boer, P.A. (2000). ZipA-induced bundling of FtsZ polymers mediated by an interaction between C-terminal domains. J. Bacteriol. *182*, 5153–5166.

Hamoen, L.W., Meile, J.-C., de Jong, W., Noirot, P., and Errington, J. (2006). SepF, a novel FtsZ-interacting protein required for a late step in cell division. Mol. Microbiol. *59*, 989–999.

Haney, S.A., Glasfeld, E., Hale, C., Keeney, D., He, Z., and de Boer, P. (2001). Genetic analysis of the *Escherichia coli* FtsZ-ZipA interaction in the yeast two-hybrid system. Characterization of FtsZ residues essential for the interactions with ZipA and with FtsA. J. Biol. Chem. *276*, 11980–11987.

Hernandez-Rocamora, V.M., Garcia-Montanes, C., Reija, B., Monterroso, B., Margolin, W., Alfonso, C., Zorrilla, S., and Rivas, G. (2013). MinC protein shortens FtsZ protofilaments by preferentially interacting with GDP-bound subunits. J. Biol. Chem. *288*, 24625–24635.

Hernández-Rocamora, V.M., García-Montañés, C., Rivas, G., and Llorca, O. (2012). Reconstitution of the *Escherichia coli* cell division ZipA–FtsZ complexes in nanodiscs as revealed by electron microscopy. J. Struct. Biol. *180*, 531–538.

Holden, S.J., Pengo, T., Meibom, K.L., Fernandez Fernandez, C., Collier, J., and Manley, S. (2014). High throughput 3D super-resolution microscopy reveals

Caulobacter crescentus in vivo Z-ring organization. Proc. Natl. Acad. Sci. *111*, 4566–4571.

Hsieh, C.-W., Lin, T.-Y., Lai, H.-M., Lin, C.-C., Hsieh, T.-S., and Shih, Y.-L. (2010). Direct MinE-membrane interaction contributes to the proper localization of MinDE in *E. coli*. Mol. Microbiol. *75*, 499–512.

Hsin, J., Fu, R., and Huang, K.C. (2013). Dimer dynamics and filament organization of the bacterial cell division protein FtsA. J. Mol. Biol. *425*, 4415–4426.

Hsin, J., Gopinathan, A., and Huang, K.C. (2012). Nucleotide-dependent conformations of FtsZ dimers and force generation observed through molecular dynamics simulations. Proc. Natl. Acad. Sci. *109*, 9432–9437.

Hu, Z., Gogol, E.P., and Lutkenhaus, J. (2002). Dynamic assembly of MinD on phospholipid vesicles regulated by ATP and MinE. Proc. Natl. Acad. Sci. *99*, 6761–6766.

Hu, Z., and Lutkenhaus, J. (1999). Topological regulation of cell division in *Escherichia coli* involves rapid pole-to-pole oscillation of the division inhibitor MinC under the control of MinD and MinE. Mol. Microbiol. *34*, 82–90.

Hu, Z., and Lutkenhaus, J. (2000). Analysis of MinC reveals two independent domains involved in interaction with MinD and FtsZ. J. Bacteriol. *182*, 3965–3971.

Hu, Z., and Lutkenhaus, J. (2001). Topological regulation of cell division in *E. coli*: spatiotemporal oscillation of MinD requires stimulation of its ATPase by MinE and phospholipids. Mol. Cell *7*, 1337–1343.

Hu, Z., and Lutkenhaus, J. (2003). A conserved sequence at the C-terminus of MinD is required for binding to the membrane and targeting MinC to the septum. Mol. Microbiol. *47*, 345–355.

Huang, K.C., Meir, Y., and Wingreen, N.S. (2003). Dynamic structures in *Escherichia coli*: spontaneous formation of MinE rings and MinD polar zones. Proc. Natl. Acad. Sci. *100*, 12724–12728.

Jennings, P.C., Cox, G.C., Monahan, L.G., and Harry, E.J. (2011). Super-resolution imaging of the bacterial cytokinetic protein FtsZ. Micron *42*, 336–341.

Johnson, J.E., Lackner, L.L., Hale, C.A., and de Boer, P.A.J. (2004). ZipA is required for targeting of DMinC/DicB, but not DMinC/MinD, complexes to septal ring assemblies in *Escherichia coli*. J. Bacteriol. *186*, 2418–2429.

Jordan, S.N., and Canman, J.C. (2012). Rho GTPases in animal cell cytokinesis: an occupation by the one percent. Cytoskeleton *69*, 919–930.

Juarez, J.R., and Margolin, W. (2010). Changes in the Min oscillation pattern before and after cell birth. J. Bacteriol. *192*, 4134–4142.

Karimova, G., Dautin, N., and Ladant, D. (2005). Interaction network among *Escherichia coli* membrane proteins involved in cell division as revealed by bacterial two-hybrid analysis. J. Bacteriol. *187*, 2233–2243.

Keijser, B.J.., Noens, E.E.., Kraal, B., Koerten, H.K., and Wezel, G.P. (2003). The *Streptomyces coelicolor ssgB* gene is required for early stages of sporulation. FEMS Microbiol. Lett. *225*, 59–67.

Kiekebusch, D., Michie, K.A., Essen, L.-O., Löwe, J., and Thanbichler, M. (2012). Localized dimerization and nucleoid binding drive gradient formation by the bacterial cell division inhibitor MipZ. Mol. Cell *46*, 245–259.

Koppelman, C.-M., Den Blaauwen, T., Duursma, M.C., Heeren, R.M.A., and Nanninga, N. (2001). *Escherichia coli* minicell membranes are enriched in cardiolipin. J. Bacteriol. *183*, 6144–6147.

Kuchibhatla, A., Bhattacharya, A., and Panda, D. (2011). ZipA binds to FtsZ with high affinity and enhances the stability of FtsZ protofilaments. PLoS ONE *6*, e28262.

Lackner, L.L., Raskin, D.M., and de Boer, P.A.J. (2003). ATP-dependent interactions between *Escherichia coli* Min proteins and the phospholipid membrane *in vitro*. J. Bacteriol. *185*, 735–749.

Lan, G., Daniels, B.R., Dobrowsky, T.M., Wirtz, D., and Sun, S.X. (2009). Condensation of FtsZ filaments can drive bacterial cell division. Proc. Natl. Acad. Sci. *106*, 121–126.

Lenarcic, R., Halbedel, S., Visser, L., Shaw, M., Wu, L.J., Errington, J., Marenduzzo, D., and Hamoen, L.W. (2009). Localisation of DivIVA by targeting to negatively curved membranes. EMBO J. *28*, 2272–2282.

Levin, P.A. (2002). Light microscopy techniques for bacterial cell biology. In Methods in Microbiology, (Academic Press Ltd., London), pp. 115–132.

Levin, P.A., Shim, J.J., and Grossman, A.D. (1998). Effect of minCD on FtsZ ring position and polar septation in *Bacillus subtilis*. J. Bacteriol. *180*, 6048–6051.

Li, Y., Hsin, J., Zhao, L., Cheng, Y., Shang, W., Huang, K.C., Wang, H.-W., and Ye, S. (2013). FtsZ protofilaments use a hinge-opening mechanism for constrictive force generation. Science *341*, 392–395.

Liu, G., Draper, G.C., and Donachie, W.D. (1998). FtsK is a bifunctional protein involved in cell division and chromosome localization in *Escherichia coli*. Mol. Microbiol. *29*, 893–903.

Liu, Z., Mukherjee, A., and Lutkenhaus, J. (1999). Recruitment of ZipA to the division site by interaction with FtsZ. Mol. Microbiol. *31*, 1853–1861.

Loose, M., Fischer-Friedrich, E., Herold, C., Kruse, K., and Schwille, P. (2011). Min protein patterns emerge from rapid rebinding and membrane interaction of MinE. Nat. Struct. Mol. Biol. *18*, 577–583.

Loose, M., and Mitchison, T.J. (2014). The bacterial cell division proteins FtsA and FtsZ self-organize into dynamic cytoskeletal patterns. Nat. Cell Biol. *16*, 38–46.

Lu, C., Stricker, J., and Erickson, H.P. (2001). Site-specific mutations of FtsZ-effects on GTPase and *in vitro* assembly. BMC Microbiol. *1*, 7.

Lutkenhaus, J. (2012). The ParA/MinD family puts things in their place. Trends Microbiol. *20*, 411–418.

Lutkenhaus, J., Pichoff, S., and Du, S. (2012). Bacterial cytokinesis: from Z ring to divisome. Cytoskeleton *69*, 778–790.

Ma, L., King, G.F., and Rothfield, L. (2004). Positioning of the MinE binding site on the MinD surface suggests a plausible mechanism for activation of the *Escherichia coli* MinD ATPase during division site selection. Mol. Microbiol. *54*, 99–108.

Ma, X., and Margolin, W. (1999). Genetic and functional analyses of the conserved C-terminal core domain of *Escherichia coli* FtsZ. J. Bacteriol. *181*, 7531–7544.

Marbouty, M., Saguez, C., Cassier-Chauvat, C., and Chauvat, F. (2009). Characterization of the FtsZ-interacting septal proteins SepF and Ftn6 in the spherical-celled Cyanobacterium synechocystis strain PCC 6803. J. Bacteriol. *191*, 6178–6185.

Margolin, W. (2000). Themes and variations in prokaryotic cell division. FEMS Microbiol. Rev. *24*, 531–548.

Margolin, W. (2001). Spatial regulation of cytokinesis in bacteria. Curr. Opin. Microbiol. *4*, 647–652.

Margolin, W. (2005). FtsZ and the division of prokaryotic cells and organelles. Nat. Rev. Mol. Cell Biol. *6*, 862–871.

Marston, A.L., and Errington, J. (1999). Selection of the midcell division site in *Bacillus subtilis* through MinD-dependent polar localization and activation of MinC. Mol. Microbiol. *33*, 84–96.

Marston, A.L., Thomaides, H.B., Edwards, D.H., Sharpe, M.E., and Errington, J. (1998). Polar localization of the MinD protein of *Bacillus subtilis* and its role in selection of the mid-cell division site. Genes Dev. *12*, 3419–3430.

Martos, A., Monterroso, B., Zorrilla, S., Reija, B., Alfonso, C., Mingorance, J., Rivas, G., and Jiménez, M. (2012). Isolation, characterization and lipid-binding properties of the recalcitrant FtsA division protein from *Escherichia coli*. PLoS ONE *7*, e39829.

Mateos-Gil, P., Paez, A., Hörger, I., Rivas, G., Vicente, M., Tarazona, P., and Vélez, M. (2012). Depolymerization dynamics of individual filaments of bacterial cytoskeletal protein FtsZ. Proc. Natl. Acad. Sci. *109*, 8133–8138.

Mazor, S., Regev, T., Mileykovskaya, E., Margolin, W., Dowhan, W., and Fishov, I. (2008). Mutual effects of MinD–membrane interaction: I. Changes in the membrane properties induced by MinD binding. Biochim. Biophys. Acta BBA - Biomembr. *1778*, 2496–2504.

Mierzejewska, J., and Jagura-Burdzy, G. (2012). Prokaryotic ParA–ParB–parS system links bacterial chromosome segregation with the cell cycle. Plasmid *67*, 1–14.

Mileykovskaya, E., and Dowhan, W. (2000). Visualization of phospholipid domains in *Escherichia coli* by using the cardiolipin-specific fluorescent dye 10-N-nonyl acridine orange. J. Bacteriol. *182*, 1172–1175.

Mileykovskaya, E., Fishov, I., Fu, X., Corbin, B.D., Margolin, W., and Dowhan, W. (2003). Effects of phospholipid composition on MinD-membrane interactions *in vitro* and *in vivo*. J. Biol. Chem. *278*, 22193–22198.

Miroux, B., and Walker, J.E. (1996). Over-production of proteins in *Escherichia coli*: Mutant hosts that allow synthesis of some membrane proteins and globular proteins at high levels. J. Mol. Biol. *260*, 289–298.

Mohammadi, T., van Dam, V., Sijbrandi, R., Vernet, T., Zapun, A., Bouhss, A., Diepeveen-de Bruin, M., Nguyen-Distèche, M., de Kruijff, B., and Breukink, E. (2011). Identification of FtsW as a transporter of lipid-linked cell wall precursors across the membrane. EMBO J. *30*, 1425–1432.

Mohl, D.A., and Gober, J.W. (1997). Cell cycle–dependent polar localization of chromosome partitioning proteins in *Caulobacter crescentus*. Cell *88*, 675–684.

Monahan, L.G., Liew, A.T.F., Bottomley, A.L., and Harry, E.J. (2014). Division site positioning in bacteria: one size does not fit all. Front. Microbiol. *5*.

Moreira, I.S., Fernandes, P.A., and Ramos, M.J. (2006). Detailed microscopic study of the full ZipA:FtsZ interface. Proteins Struct. Funct. Bioinforma. *63*, 811–821.

Mosyak, L., Zhang, Y., Glasfeld, E., Haney, S., Stahl, M., Seehra, J., and Somers, W.S. (2000). The bacterial cell-division protein ZipA and its interaction with an FtsZ fragment revealed by X-ray crystallography. EMBO J. *19*, 3179–3191.

Mukherjee, A., and Lutkenhaus, J. (1998). Dynamic assembly of FtsZ regulated by GTP hydrolysis. EMBO J. *17*, 462–469.

Mukherjee, A., Saez, C., and Lutkenhaus, J. (2001). Assembly of an FtsZ mutant deficient in GTPase activity has implications for FtsZ assembly and the role of the Z ring in cell division. J. Bacteriol. *183*, 7190–7197.

Mulder, E., El'Bouhali, M., Pas, E., and Woldringh, C.L. (1990). The Escherichia coli minB mutation resembles gyrB in defective nucleoid segregation and decreased negative supercoiling of plasmids. Mol. Gen. Genet. MGG *221*, 87–93.

Ojima, I., Kumar, K., Awasthi, D., and Vineberg, J.G. (2014). Drug discovery targeting cell division proteins, microtubules and FtsZ. Bioorg. Med. Chem.

Osawa, M., Anderson, D.E., and Erickson, H.P. (2008). Reconstitution of contractile FtsZ rings in liposomes. Science *320*, 792–794.

Osawa, M., Anderson, D.E., and Erickson, H.P. (2009). Curved FtsZ protofilaments generate bending forces on liposome membranes. EMBO J. *28*, 3476–3484.

Osawa, M., and Erickson, H.P. (2011). Inside-out Z rings - constriction with and without GTP hydrolysis. Mol. Microbiol. *81*, 571–579.

Osawa, M., and Erickson, H.P. (2013). Liposome division by a simple bacterial division machinery. Proc. Natl. Acad. Sci. *110*, 11000–11004.

Paradis-Bleau, C., Sanschagrin, F., and Levesque, R.C. (2005). Peptide inhibitors of the essential cell division protein FtsA. Protein Eng. Des. Sel. *18*, 85–91.

Park, K.-T., Wu, W., Battaile, K.P., Lovell, S., Holyoak, T., and Lutkenhaus, J. (2011). The Min oscillator uses MinD-dependent conformational changes in MinE to spatially regulate cytokinesis. Cell *146*, 396–407.

Park, K.-T., Wu, W., Lovell, S., and Lutkenhaus, J. (2012). Mechanism of the asymmetric activation of the MinD ATPase by MinE. Mol. Microbiol. *85*, 271–281.

Patrick, J.E., and Kearns, D.B. (2008). MinJ (YvjD) is a topological determinant of cell division in *Bacillus subtilis*. Mol. Microbiol. *70*, 1166–1179.

Pazos, M., Natale, P., and Vicente, M. (2013). A specific role for the ZipA protein in cell division: Stabilization of the FtsZ protein. J. Biol. Chem. *288*, 3219–3226.

Peters, N.T., Dinh, T., and Bernhardt, T.G. (2011). A fail-safe mechanism in the septal ring assembly pathway generated by the sequential recruitment of cell separation amidases and their activators. J. Bacteriol. *193*, 4973–4983.

Pichoff, S., and Lutkenhaus, J. (2001). *Escherichia coli* division inhibitor MinCD blocks septation by preventing Z-ring formation. J. Bacteriol. *183*, 6630–6635.

Pichoff, S., and Lutkenhaus, J. (2002). Unique and overlapping roles for ZipA and FtsA in septal ring assembly in *Escherichia coli*. EMBO J. *21*, 685–693.

Pichoff, S., and Lutkenhaus, J. (2005). Tethering the Z ring to the membrane through a conserved membrane targeting sequence in FtsA. Mol. Microbiol. *55*, 1722–1734.

Pichoff, S., and Lutkenhaus, J. (2007). Identification of a region of FtsA required for interaction with FtsZ. Mol. Microbiol. *64*, 1129–1138.

Pichoff, S., Shen, B., Sullivan, B., and Lutkenhaus, J. (2012). FtsA mutants impaired for self-interaction bypass ZipA suggesting a model in which FtsA's self-interaction competes with its ability to recruit downstream division proteins. Mol. Microbiol. *83*, 151–167.

Popp, M.W., Antos, J.M., Grotenbreg, G.M., Spooner, E., and Ploegh, H.L. (2007). Sortagging: a versatile method for protein labeling. Nat. Chem. Biol. *3*, 707–708.

Potluri, L.-P., Kannan, S., and Young, K.D. (2012). ZipA is required for FtsZ-dependent preseptal peptidoglycan synthesis prior to invagination during cell division. J. Bacteriol. *194*, 5334–5342.

Ramamurthi, K.S., and Losick, R. (2009). Negative membrane curvature as a cue for subcellular localization of a bacterial protein. Proc. Natl. Acad. Sci. *106*, 13541–13545.

Raskin, D.M., and de Boer, P.A. (1997). The MinE ring: an FtsZ-independent cell structure required for selection of the correct division site in *E. coli*. Cell *91*, 685–694.

Raskin, D.M., and de Boer, P.A. (1999a). Rapid pole-to-pole oscillation of a protein required for directing division to the middle of *Escherichia coli*. Proc. Natl. Acad. Sci. *96*, 4971–4976.

Raskin, D.M., and de Boer, P.A. (1999b). MinDE-dependent pole-to-pole oscillation of division inhibitor MinC in *Escherichia coli*. J. Bacteriol. *181*, 6419–6424.

RayChaudhuri, D. (1999). ZipA is a MAP–Tau homolog and is essential for structural integrity of the cytokinetic FtsZ ring during bacterial cell division. EMBO J. *18*, 2372–2383.

Redick, S.D., Stricker, J., Briscoe, G., and Erickson, H.P. (2005). Mutants of FtsZ targeting the protofilament interface: effects on cell division and GTPase activity. J. Bacteriol. *187*, 2727–2736.

Renner, L.D., and Weibel, D.B. (2011). Cardiolipin microdomains localize to negatively curved regions of *Escherichia coli* membranes. Proc. Natl. Acad. Sci. *108*, 6264–6269.

Renner, L.D., and Weibel, D.B. (2012). MinD and MinE interact with anionic phospholipids and regulate division plane formation in *Escherichia coli*. J. Biol. Chem. *287*, 38835–38844.

Rico, A.I., García-Ovalle, M., Mingorance, J., and Vicente, M. (2004). Role of two essential domains of *Escherichia coli* FtsA in localization and progression of the division ring. Mol. Microbiol. *53*, 1359–1371.

Robinson, A.C., Begg, K.J., and Donachie, W.D. (1988). Mapping and characterization of mutants of the *Escherichia coli* cell division gene, *ftsA*. Mol. Microbiol. *2*, 581–588.

Robinson, A.C., Begg, K.J., and MacArthur, E. (1991). Isolation and characterization of intragenic suppressors of an *Escherichia coli ftsA* mutation. Res. Microbiol. *142*, 623–631.

Rodrigues, C.D.A., and Harry, E.J. (2012). The Min system and nucleoid occlusion are not required for identifying the division site in *Bacillus subtilis* but ensure its efficient utilization. PLoS Genet. *8*, e1002561.

Romantsov, T., Battle, A.R., Hendel, J.L., Martinac, B., and Wood, J.M. (2010). Protein localization in *Escherichia coli* cells: comparison of the cytoplasmic membrane proteins ProP, LacY, ProW, AqpZ, MscS, and MscL. J. Bacteriol. *192*, 912–924.

Romberg, L., and Levin, P.A. (2003). Assembly dynamics of the bacterial cell division protein FtsZ: poised at the edge of stability. Annu. Rev. Microbiol. *57*, 125–154.

Rothfield, L. (2003). New insights into the developmental history of the bacterial cell division site. J. Bacteriol. *185*, 1125–1127.

Rothfield, L., Taghbalout, A., and Shih, Y.-L. (2005). Spatial control of bacterial division-site placement. Nat. Rev. Microbiol. *3*, 959–968.

Sanchez, M., Dopazo, A., Pla, J., Robinson, A.C., and Vicente, M. (1994). Characterization of mutant alleles of the cell division protein FtsA, a regulator and structural component of the *Escherichia coli* septator. Biochimie *76*, 1071–1074.

Sass, P., and Brötz-Oesterhelt, H. (2013). Bacterial cell division as a target for new antibiotics. Curr. Opin. Microbiol. *16*, 522–530.

Sass, P., Josten, M., Famulla, K., Schiffer, G., Sahl, H.-G., Hamoen, L., and Brotz-Oesterhelt, H. (2011). Antibiotic acyldepsipeptides activate ClpP peptidase to degrade the cell division protein FtsZ. Proc. Natl. Acad. Sci. *108*, 17474–17479.

Schiefer, A., Vollmer, J., Lammer, C., Specht, S., Lentz, C., Ruebsamen-Schaeff, H., Brotz-Oesterhelt, H., Hoerauf, A., and Pfarr, K. (2013). The ClpP peptidase of *Wolbachia* endobacteria is a novel target for drug development against filarial infections. J. Antimicrob. Chemother. *68*, 1790–1800.

Sengupta, S., and Rutenberg, A. (2007). Modeling partitioning of Min proteins between daughter cells after septation in *Escherichia coli*. Phys. Biol. *4*, 145–153.

Shen, B., and Lutkenhaus, J. (2009). The conserved C-terminal tail of FtsZ is required for the septal localization and division inhibitory activity of MinCC/MinD. Mol. Microbiol. *72*, 410–424.

Shen, B., and Lutkenhaus, J. (2010). Examination of the interaction between FtsZ and MinC ^{N} in *E. coli* suggests how MinC disrupts Z rings. Mol. Microbiol. *75*, 1285–1298.

Shiomi, D., and Margolin, W. (2007a). The C-terminal domain of MinC inhibits assembly of the Z ring in *Escherichia coli*. J. Bacteriol. *189*, 236–243.

Shiomi, D., and Margolin, W. (2007b). Dimerization or oligomerization of the actin-like FtsA protein enhances the integrity of the cytokinetic Z ring. Mol. Microbiol. *66*, 1396–1415.

Shiomi, D., and Margolin, W. (2008). Compensation for the loss of the conserved membrane targeting sequence of FtsA provides new insights into its function. Mol. Microbiol. *67*, 558–569.

Strahl, H., and Hamoen, L.W. (2010). Membrane potential is important for bacterial cell division. Proc. Natl. Acad. Sci. *107*, 12281–12286.

Strauss, M.P., Liew, A.T.F., Turnbull, L., Whitchurch, C.B., Monahan, L.G., and Harry, E.J. (2012). 3D-SIM super resolution microscopy reveals a bead-like arrangement for FtsZ and the division machinery: implications for triggering cytokinesis. PLoS Biol. *10*, e1001389.

Stricker, J., Maddox, P., Salmon, E.D., and Erickson, H.P. (2002). Rapid assembly dynamics of the *Escherichia coli* FtsZ-ring demonstrated by fluorescence recovery after photobleaching. Proc. Natl. Acad. Sci. *99*, 3171–3175.

Suefuji, K., Valluzzi, R., and RayChaudhuri, D. (2002). Dynamic assembly of MinD into filament bundles modulated by ATP, phospholipids, and MinE. Proc. Natl. Acad. Sci. *99*, 16776–16781.

Sugimoto, S., Yamanaka, K., Nishikori, S., Miyagi, A., Ando, T., and Ogura, T. (2010). AAA+ chaperone ClpX regulates dynamics of prokaryotic cytoskeletal protein FtsZ. J. Biol. Chem. *285*, 6648–6657.

Szeto, T.H., Rowland, S.L., Habrukowich, C.L., and King, G.F. (2003). The MinD membrane targeting sequence is a transplantable lipid-binding helix. J. Biol. Chem. *278*, 40050–40056.

Szwedziak, P., Wang, Q., Freund, S., and Löwe, J. (2012). FtsA forms actin-like protofilaments. EMBO J. *31*, 2249–2260.

Thanbichler, M., and Shapiro, L. (2006). MipZ, a spatial regulator coordinating chromosome segregation with cell division in *Caulobacter*. Cell *126*, 147–162.

Thanedar, S., and Margolin, W. (2004). FtsZ exhibits rapid movement and oscillation waves in helix-like patterns in *Escherichia coli*. Curr. Biol. *14*, 1167–1173.

Thomaides, H.B., Freeman, M., El Karoui, M., and Errington, J. (2001). Division site selection protein DivIVA of Bacillus subtilis has a second distinct function in chromosome segregation during sporulation. Genes Dev. *15*, 1662–1673.

Tonthat, N.K., Arold, S.T., Pickering, B.F., Van Dyke, M.W., Liang, S., Lu, Y., Beuria, T.K., Margolin, W., and Schumacher, M.A. (2011). Molecular mechanism by which the nucleoid occlusion factor, SlmA, keeps cytokinesis in check. EMBO J. *30*, 154–164.

Tonthat, N.K., Milam, S.L., Chinnam, N., Whitfill, T., Margolin, W., and Schumacher, M.A. (2013). SlmA forms a higher-order structure on DNA that inhibits cytokinetic Z-ring formation over the nucleoid. Proc. Natl. Acad. Sci. U. S. A. *110*, 10586–10591.

Tormo, A., Martínez-Salas, E., and Vicente, M. (1980). Involvement of the *ftsA* gene product in late stages of the *Escherichia coli* cell cycle. J. Bacteriol. *141*, 806–813.

Touhami, A., Jericho, M., and Rutenberg, A.D. (2006). Temperature dependence of MinD oscillation in *Escherichia coli*: running hot and fast. J. Bacteriol. *188*, 7661–7667.

Treuner-Lange, A., Aguiluz, K., van der Does, C., Gómez-Santos, N., Harms, A., Schumacher, D., Lenz, P., Hoppert, M., Kahnt, J., Muñoz-Dorado, J., et al. (2013). PomZ, a ParA-like protein, regulates Z-ring formation and cell division in *Myxococcus xanthus*. Mol. Microbiol. *87*, 235–253.

Varley, A.W., and Stewart, G.C. (1992). The divIVB region of the *Bacillus subtilis* chromosome encodes homologs of *Escherichia coli* septum placement (*minCD*) and cell shape (*mreBCD*) determinants. J. Bacteriol. *174*, 6729–6742.

Varma, A., Huang, K.C., and Young, K.D. (2008). The Min system as a general cell geometry detection mechanism: branch lengths in Y-shaped *Escherichia coli* cells affect Min oscillation patterns and division dynamics. J. Bacteriol. *190*, 2106–2117.

Vecchiarelli, A.G., Havey, J.C., Ing, L.L., Wong, E.O.Y., Waples, W.G., and Funnell, B.E. (2013). Dissection of the ATPase active site of P1 ParA reveals multiple active forms essential for plasmid partition. J. Biol. Chem. *288*, 17823–17831.

Vicente, M., and Rico, A.I. (2006). The order of the ring: assembly of *Escherichia coli* cell division components. Mol. Microbiol. *61*, 5–8.

Wang, L., and Lutkenhaus, J. (1998). FtsK is an essential cell division protein that is localized to the septum and induced as part of the SOS response. Mol. Microbiol. *29*, 731–740.

Ward Jr, J.E., and Lutkenhaus, J. (1985). Overproduction of FtsZ induces minicell formation in E. coli. Cell *42*, 941–949.

Weart, R.B., Nakano, S., Lane, B.E., Zuber, P., and Levin, P.A. (2005). The ClpX chaperone modulates assembly of the tubulin-like protein FtsZ. Mol. Microbiol. *57*, 238–249.

van Wezel, G.P., van der Meulen, J., Kawamoto, S., Luiten, R.G.M., Koerten, H.K., and Kraal, B. (2000). *ssgA* is essential for sporulation of *Streptomyces coelicolor* A3(2) and affects hyphal development by stimulating septum formation. J. Bacteriol. *182*, 5653–5662.

Wang, J., Galgoci, A., Kodali, S., Herath, K.B., Jayasuriya, H., Dorso, K., Vicente, F., Gonzalez, A., Cully, D., Bramhill, D., et al. (2003). Discovery of a small molecule that inhibits cell division by blocking FtsZ, a novel therapeutic target of antibiotics. J. Biol. Chem. *278*, 44424–44428.

Wickstead, B., and Gull, K. (2011). Evolution: The evolution of the cytoskeleton. J. Cell Biol. *194*, 513–525.

Willemse, J., Borst, J.W., de Waal, E., Bisseling, T., and van Wezel, G.P. (2011). Positive control of cell division: FtsZ is recruited by SsgB during sporulation of *Streptomyces*. Genes Dev. *25*, 89–99.

Wloka, C., and Bi, E. (2012). Mechanisms of cytokinesis in budding yeast. Cytoskeleton *69*, 710–726.

Wu, L.J., and Errington, J. (2004). Coordination of cell division and chromosome segregation by a nucleoid occlusion protein in *Bacillus subtilis*. Cell *117*, 915–925.

Wu, L.J., Ishikawa, S., Kawai, Y., Oshima, T., Ogasawara, N., and Errington, J. (2009). Noc protein binds to specific DNA sequences to coordinate cell division with chromosome segregation. EMBO J. *28*, 1940–1952.

Yu, X.-C., and Margolin, W. (1999). FtsZ ring clusters in min and partition mutants: role of both the Min system and the nucleoid in regulating FtsZ ring localization. Mol. Microbiol. *32*, 315–326.

Yu, X.-C., Weihe, E.K., and Margolin, W. (1998). Role of the C terminus of FtsK in *Escherichia coli* chromosome segregation. J. Bacteriol. *180*, 6424–6428.

Zhou, H., and Lutkenhaus, J. (2003). Membrane binding by MinD involves insertion of hydrophobic residues within the C-terminal amphipathic helix into the bilayer. J. Bacteriol. *185*, 4326–4335.

VITA

Jennifer Renee Juarez Herricks was born in Baton Rouge, Louisiana. After graduating from Runnels High School in 2003, she attended Louisiana State University and earned a Bachelor of Science in 2007 with a major in biology and a minor in anthropology. In the fall of 2007 Jennifer entered the Ph.D. program at the University of Texas Graduate School of Biomedical Sciences at Houston. In May of 2008 she officially joined the Microbiology and Molecular Genetics Program and the laboratory of William Margolin, Ph.D.

In July of 2014, Jennifer will begin a career in science policy as a postdoctoral fellow at the James A. Baker III Institute for Public Policy at Rice University, where she will be working with the National School of Tropical Medicine at Baylor College of Medicine to promote and influence policy initiatives as part of an effort to advance treatment and prevention strategies for neglected tropical diseases.